

AMERICAN UNIVERSITY OF BEIRUT

ROBUST SIGNAL PROCESSING
ALGORITHMS FOR RF COMPLEXITY
REDUCTION IN COGNITIVE RADIO
SYSTEMS

by
LISE EMILE SAFATLY

A dissertation
submitted in partial fulfillment of the requirements
for the degree of Doctor of Philosophy
to the Department of Electrical and Computer Engineering
of the Faculty of Engineering and Architecture
at the American University of Beirut

Beirut, Lebanon
May 2014

AMERICAN UNIVERSITY OF BEIRUT

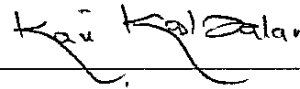
ROBUST SIGNAL PROCESSING
ALGORITHMS FOR RF COMPLEXITY
REDUCTION IN COGNITIVE RADIO
SYSTEMS

by
LISE EMILE SAFATLY

Approved by:

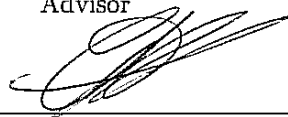
Dr. Karim Kabalan, Professor
Electrical and Computer Engineering

Chair of Committee



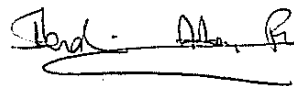
Dr. Ali El Hajj, Professor
Electrical and Computer Engineering

Advisor



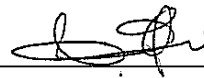
Dr. Ibrahim Abou Fayçal, Associate Professor
Electrical and Computer Engineering

Member of Committee



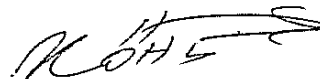
Dr. Youssef Nasser, Senior Lecturer
Electrical and Computer Engineering

Member of Committee



Dr. Mohammed Al Hussein, Senior Researcher
Beirut Research and Innovation Center, Lebanon

Member of Committee



Dr. Jean François Diouris, Professor
Polytech Nantes, Nantes, France

Member of Committee



Dr. Yves Louët, Professor
SUPELEC, Rennes, France

Member of Committee



Date of dissertation defense: May 5th, 2014

“The fear of the Lord is the beginning of wisdom” *Proverbs 1:7*

Acknowledgements

First of all, I thank God for the blessing and perseverance that He has been bestowed upon me during this thesis, and indeed, throughout my life.

I would like to thank my thesis advisor, Prof. Ali El Hajj, for appreciating my research strengths and patiently encouraging me to improve my weaker areas. Without his strong support of my ideas and research directions, and confidence in my abilities, this dissertation could not have come to fruition. The doors to Prof. El Hajj's office were always open since the first email I sent asking about the PhD program till the submission of this manuscript.

I would also like to express my deepest appreciation to Prof. Karim Y. Kabalan, who has the attitude and the caring of a father. He continuously conveyed a spirit of encouragement and support. I thank him for being a supportive and strong guiding force as a co-advisor and chair of my thesis committee. His support, guidance, and advices throughout the dissertation, as well as his painstaking effort in proof reading my work, are greatly appreciated.

It is also a great pleasure for me to thank the rest of my thesis committee, Dr. Ibrahim Abou Fayçal for his insightful suggestions and comments, Dr. Youssef Nasser for offering many precious ideas and opportunities and managing my research visit to France, Prof. Yves Louët for hosting this visit and helping in every way he can to achieve my goals, and my former advisor Prof. Jean-François Diouris, for his continuous encouragement and guidance. I am also grateful to Dr. Mohammed Al Husseini, a talented and passionate researcher. With his strong background, expertise, and research skills, he helped me establish the overall direction of my dissertation.

The PhD journey can be a difficult and draining experience. I am proud to say that my experience in the EMRF group, guided by Prof. Kabalan and Prof. El Hajj, was intellectually exciting and fun, and has energized me to continue in this area. I thank all my group-mates especially my best friend Nadeen for improving my presentation skills and making the scientific conferences the best memories of my life, and Dr. Ali Ramadan for many beneficial discussions

and suggestions.

To Mrs. Rabab Abi Chakra and Mr. Khaled Joujou, thank you not only for your time and extreme patience, but also for your assistance during my PhD studies.

To my lab-mates, thanks for the fun and support. My experience in the lab was greatly enhanced as it filled out from Dima, Manal, Sara, Rawad, Ahmad, and Jihad. Your love, laughter and food have kept me powerful, smiling, and inspired. You are and always will be my best friends.

The deepest gratitude goes towards my parents and my big family who supported me through the years and were aspiring to this moment. In particular, I am blessed to be surrounded by the patience, love, and understanding of my mother Najah and my father Emile, my hard-working parents that have sacrificed their lives for my brothers and myself and provided unconditional love and care. Special thanks to my brothers Elias, Mario and Abboud, my sisters Hanane and Layal, my nephews Youhanna, Anis and Emile, my aunts Zakiya and Klova, and my beloved grand mother. I hope I was able to make them all proud.

This work couldn't be accomplished without the prayers and blessings of Father Younan, Father Nicolas Malek, Father Nicolas Remlawi, and Mother Fevronia. I am really grateful for all what you have done for me.

Last but not least, I want to give the most heartfelt thanks and dedicate this dissertation to my best friend, soul-mate, and husband Zareh. Four years ago, we decided together to sacrifice and make this come true and with his care, support, late-night proof readings, and cheering up techniques, he showed continuously an endless encouragement.

An Abstract of the Dissertation of

Lise Emile Safatly for Doctor of Philosophy
Major: Electrical and Computer Engineering

Title: Robust Signal Processing Algorithms for RF Complexity Reduction
in Cognitive Radio Systems

The need for an efficient spectrum usage policy is becoming more pressing due to the rapid growth of wireless communications applications and the under-utilization of most licensed bands. Cognitive Radio arises to be a novel solution to this spectrum wastage problem by allowing the dynamic allocation of unused bands. In these scenarios, a secondary or unlicensed user detects, exploits and utilizes an unoccupied spectrum band, called a white space, reserved for primary users. Thus, two major functions of a cognitive radio transceiver are scanning the spectrum for a potential white space and transmitting a suitable adaptive signal. In real-world dynamic scenarios, this highly adaptive radio technology presents unique signal processing challenges and requires specific algorithms for spectrum sensing and spectrum sculpting.

In an Ultra-Wide Band (UWB) scenario, secondary users are required to scan bands that are of hundreds of megahertz in width. This puts strict hardware requirements on the RF front-end, relating to the linearity, dynamic range and sensitivity of the circuitry. On the other hand, RF impairments could dramatically degrade the performance of the secondary user. These imperfections result from the large spectrum to be sensed and from the low-cost implementations of the analog RF front-ends. In such scenarios, advanced signal processing algorithms are required not only to sense the incumbent spectrum but also to improve the radio sensitivity by mitigating the RF impairments effects to relax the hardware requirements.

In this dissertation, we investigate and propose signal processing algorithms to build a highly adaptive, fully functional cognitive radio transceiver working in the UWB range. At first, we start by studying basic spectrum sensing algorithms, we then move to assess the performance of these algorithms against RF impairments. A blind algorithm is selected, improved and implemented in real-world scenarios. A mitigation stage is devised and added to the sensing scheme in order to obtain a robust and blind detector capable of mitigating RF impairments and enhancing RF front-end sensitivity. On the other hand, spectrum sculpting techniques are also studied and their performance is compared to the filter-based solutions. Signal processing techniques are therefore implemented to obtain a reconfigurable, intelligent and adaptive CR terminal working in the UWB range, where these algorithms are required to mitigate the hardware imperfections effects and solve the circuitry limitations.

Contents

Acknowledgment	vii
Abstract	ix
Contents	x
1 Introduction	1
1.1 Software-Defined Radio	1
1.1.1 Overview	1
1.1.2 SDR platform	2
1.2 Cognitive Radio	3
1.2.1 Overview	3
1.2.2 Hardware Challenges in Cognitive Radio	5
1.3 Dissertation Objectives	8
1.4 Organization of the Dissertation	9
2 Spectrum Sculpting	10
2.1 Ultra Wide Band Cognitive Radio	10
2.2 Parks-McClellan Algorithm	12
2.2.1 Simulation Details	12
2.2.2 Generated Pulses	12
2.3 Neural Network	12
2.3.1 Description of the Technique	12
2.3.2 Simulations Results	15
2.4 Filter Antenna Design	16
2.4.1 Filter Design and Stop-Band Control	16
2.4.2 Measured and Simulated Characteristics of the Filter	17
2.4.3 Generated Pulses	19
2.4.4 Antenna Configuration	21
2.5 Conclusion	24
3 An Overview of Spectrum Sensing	25
3.1 Introduction	25

3.2	Primary signal detection	25
3.2.1	Introduction	25
3.2.2	Energy Detector	28
	Introduction	28
	Mathematical Formulation of ϵ and δ	28
	Results and Discussions	29
3.2.3	Cyclostationary Feature Detector	30
	Feature Detection	30
	Cyclostationarity-Based Algorithm	31
	Results and Discussions	33
3.3	Challenges in Spectrum Sensing	34
3.3.1	Blind Detectors	35
	Blind Eigenvalue-Based Detector	36
	The CAF Symmetry-Based Detector	37
3.3.2	Wideband Spectrum Sensing	37
	Wavelet Transform Based Technique	38
	Compressive Sensing Technique	39
3.4	Conclusion	40
4	Theoretical and Experimental Study of the Blind SPCAF Detector	41
4.1	Introduction	41
4.2	Theoretical Formulation of the SPCAF	42
4.3	Experimental Implementation	48
4.4	Experimental Results	50
4.4.1	SNR Estimation	52
4.4.2	Scenario 1: USRP Signals	52
4.4.3	Scenario 2: 3G Network and DVB-T	53
4.4.4	Scenario 3: 802.11ac Indoor Channel	53
4.5	Results and Discussions	54
4.5.1	Scenario 1: USRP Signals	55
4.5.2	Scenario 2: 3G Network and DVB-T	55
4.5.3	Scenario 3: 802.11ac Indoor Channel	58
4.5.4	Detection Performance of SPCAF with Different Parameters	59
4.6	Conclusion	61
5	RF Impairments Effects on Spectrum Sensing	63
5.1	Introduction	63
5.2	RF Impairments Impact on ED and SPCAF	66
5.2.1	Carrier Frequency Offset Impact	67
5.2.2	Phase Noise Impact	68
5.2.3	I/Q Imbalance Impact	70
5.2.4	Nonlinearities Impact	74

5.3	DSP Algorithms for In-Band RF Impairments Compensation . . .	76
5.3.1	Phase Noise Impact Compensation	76
5.3.2	I/Q Imbalance Impact Compensation	77
5.4	RF Impairments Impact on Wide Band Sensing	77
5.4.1	RF Impairments Analysis in Wide Band Receivers	77
5.4.2	Analysis of the ED and SPCAF Degradation	80
5.5	Mitigation algorithms for Wide Band Sensing	80
5.5.1	The AIC Algorithm	80
5.5.2	The Improved Adaptive Mitigation Algorithm	83
5.6	Conclusion	83
6	A Robust, Blind and Wide Band Sensing Algorithm for Practical CR Receivers	85
6.1	Introduction	85
6.2	The Dual Stage Algorithm	86
6.2.1	Stages of the Algorithm	86
6.2.2	Results and Discussions	87
6.3	The Proposed Algorithm	90
6.3.1	Sensing Scheme	90
6.3.2	Mitigation Algorithm	93
6.3.3	The Combined Algorithm	96
6.3.4	Results and Discussions	98
6.3.5	Computational Complexity	100
6.4	Conclusion	101
7	Conclusion	103
7.1	Contributions	103
7.2	Other Related Research Work	105
7.3	Future Research	106
7.4	Publications	107
7.4.1	Book Chapters	107
7.4.2	Journal papers	107
7.4.3	Conference papers	108
7.4.4	Presentations	108
	List of Figures	114
	List of Tables	117
	Bibliography	118

Chapter 1

Introduction

1.1 Software-Defined Radio

1.1.1 Overview

In this era of increasing demand on data communication networks, a modern society relies on diverse services such as social interactions, financial transactions, e-commerce, national security, and others. Consequently, electronic devices are urged to perform advanced functions to support numerous applications including voice telephony, data transfer, multimedia streaming, web browsing, etc. Employing the latest achievements in microelectronics, new wireless transceivers are becoming more versatile, powerful, and portable.

Given this rapid growth in telecommunications, the development of software defined radio (SDR) technology is enabled as a prime candidate for several advanced wireless applications and services that were unrealizable only few years ago. The key feature of an SDR platform is that the functionalities of a transceiver are at least partially controlled or implemented in software. Therefore, any digital waveform designed in the memory of an SDR platform can be employed on any frequency [1]. To do so, high speed conversion process between the analog and digital signaling domains is required. An ideal SDR concept is becoming attainable with the emergence of inexpensive and high speed digital-to-analog converters (DACs) and analog-to-digital converters (ADCs).

An SDR platform designed to reconfigure operating parameters in regard to the changing environment and conditions to best exploit capacity is known as cognitive radio (CR) [2]. Obviously, SDR goes hand in hand with CR to deliver functionalities considered unachievable not long ago. Consequently, before elaborating on CR analysis, we first highlight the fundamentals of the SDR technology.

1.1.2 SDR platform

As depicted in Figure 1.1, the communication chain of a conventional digital radio consists of five sections [3]:

1. **Antenna:** transmits/receives information encoded in radio waves.
2. **RF front-end:** transmits/receives radio frequency signals from the antenna and converts them to an intermediate frequency (IF) signal.
3. **Analog-to-digital converter ADC/Digital-to-analog converter DAC:** performs analog to digital/digital to analog conversion.
4. **Digital up converter DUC/ digital down converter DDC:** performs modulation/demodulation between pass band and base band signals.
5. **Baseband operations:** performs coding/decoding, interleaving, frequency hopping, equalization, and compression.

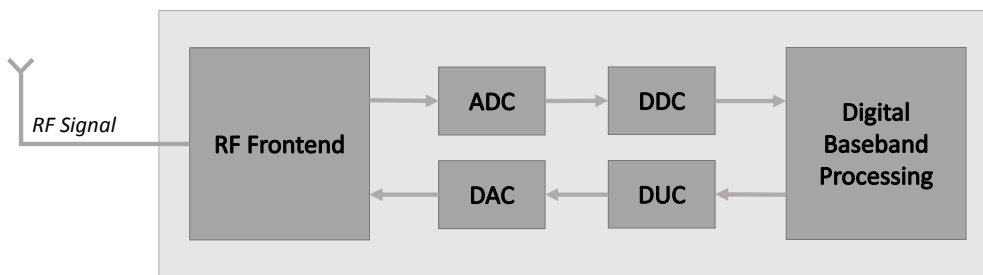


Figure 1.1: Schematic block diagram of a digital radio

In an SDR platform, baseband operations are performed by software modules running on digital signal processors (DSP), field programmable gate arrays (FPGA) or general purpose processors (GPP). The programmability of these blocks allows a simple modification of any operation characteristic of the radio such as coding, frequency band, and modulation type. Consequently, multiple radio devices using different modulations are replaceable by a single SDR device that can achieve the same functions. The ultimate goal for software radio is to digitize all signal processing thus to move the ADC/DAC as close as possible to the antenna. However, the feasibility of such radios is limited by several constraints:

- Digitization of the incoming RF signal requires a sampling rate higher than the Nyquist frequency. This rate is currently very hard to attain with an acceptable linearity especially when dealing with high-frequency signals in the gigahertz range.

- Replacing hardware-based radio by software-defined radio necessitates an increase in computation, which in return results in increasing the power consumption. This will put severe constraints on the battery life of a wireless terminal.

Nowadays, SDR platforms are built to support multiple interface technologies such as Wi-Fi, GSM, CDMA, and WiMAX by simply configuring the software. They are expensive due to the incorporated high performance programmable devices. They are widely used in military applications, because high costs are acceptable in such applications. In addition to the commercial and military expensive platforms, low quality SDR platforms are accessible for research and academia. The universal software radio peripheral (USRP), shown in Figure 1.2, is an affordable SDR mother board. An RF front-end daughter board and an antenna could be coupled to the USRP to form an SDR platform widely used in universities and research communities.



Figure 1.2: The universal software radio peripheral (USRP)

1.2 Cognitive Radio

1.2.1 Overview

Cognitive Radio is considered an encouraging approach to solve the spectrum shortage problem by allowing smart and dynamic spectrum management in future wireless communication systems. Defined by J. Mitola III [4], CR technology is “*a really smart radio that would be self-aware, RF-aware, user-aware, and that would include language technology and machine vision along with a lot of high-fidelity knowledge of the radio environment*”. Being “*a software defined radio with a cognitive engine brain*”, CR has the adaptability, the reconfigurability and the capability to sense its wireless environment and take action in the most intelligent manner [5].

CR arises as the adequate alternative of the current inefficient spectrum allocation based on assigning a specific band to a particular service. The Federal

Communication Committee (FCC) frequency allocation chart shown in Figure 1.3 seems to indicate a high degree of spectrum utilization. However, the FCC Spectrum Policy Task Force [6] reported that spectrum utilization in the bands below 3 GHz varies from 15 to 85%. It is even more poorly utilized in the frequency range above 3 GHz. Several other measurement studies have shown that much of the licensed spectrum is relatively unused across time, space and frequency [7–11]. A solution to this inefficiency, which has been highly successful in the ISM (2.4 GHz), the U-NII (5-6 GHz), and microwave (57-64 GHz) bands, is to make spectra available on an unlicensed basis. With recent developments in CR technology, it is now possible for unlicensed or secondary users to access the spectrum while respecting the rights of license holders.

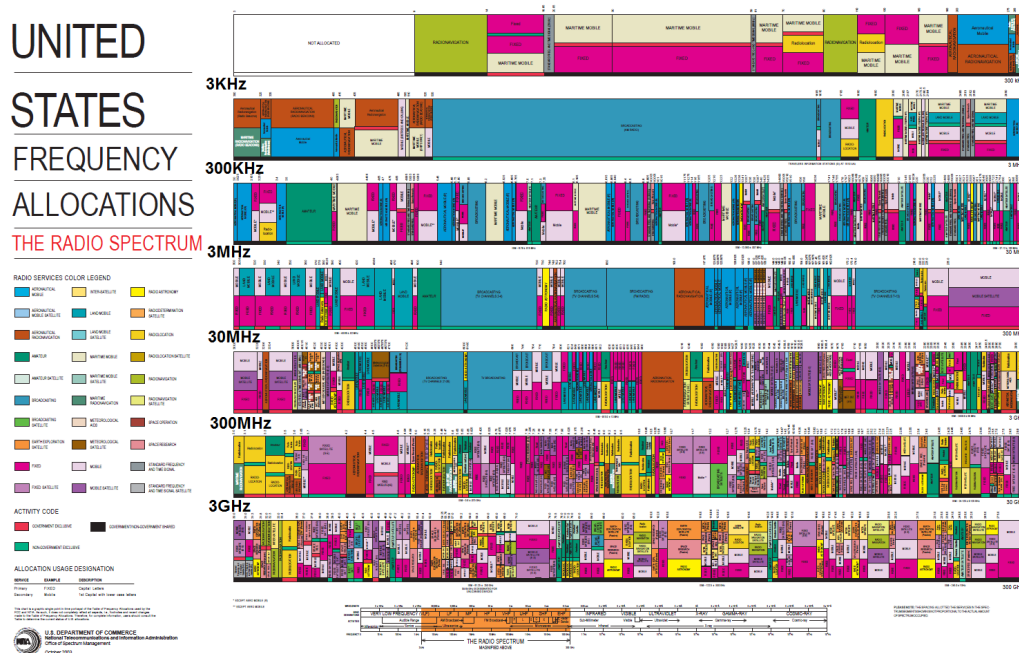


Figure 1.3: The US spectrum allocation chart [11]

In practice, the secondary users are urged to monitor the spectrum activities continuously to find a suitable spectrum band for possible utilization and to avoid potential interference with the licensed users. A highly adaptive radio technology needs to have the following minimal features [12]:

- Efficient spectrum sensing techniques at the receiver that provide continuous monitoring of the spectrum activities.
- Dynamic spectrum access methods that adapt to the CR network and suitably allocate bandwidth.
- Adaptive spectrum sculpting at the transmitter end that causes minimal or no interference to the primary users occupying adjacent bands.

To build a fully functional cognitive radio network, novel signal processing techniques need to be developed. In this dissertation, we focus on the signal processing aspects needed to meet the requirements of CR networks. More precisely, we investigate *spectrum sensing* and *spectrum sculpting* in cognitive radio applications.

1.2.2 Hardware Challenges in Cognitive Radio

In the design of a cognitive radio system, severe requirements are indispensable since the radio environment is highly variable with the presence of different types of primary user systems, propagation losses, and interferences. Meticulous specifications are desired in each block of a cognitive terminal, illustrated in Figure 1.4. The main design challenge is to define RF and analog architecture with suitable linearity, accuracy, power, and sampling rate, in addition to the implementation of digital signal processing techniques for spectrum sensing, cognition, and adaptation. These algorithms could also be employed for relaxing challenges of analog front-ends, specifically wideband amplification, mixing and A/D conversion of over one GHz or more of bandwidth, and for enhancing overall radio sensitivity.

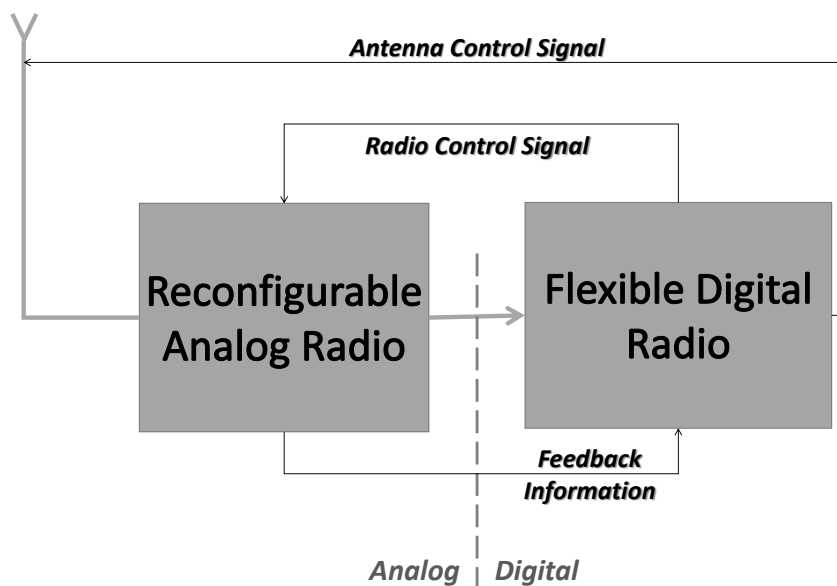


Figure 1.4: Analog and digital blocks of a CR transceiver

Mainly, two radio bands are open to cognitive radio operations: the UHF TV band (400 to 800 MHz) and the UWB band (3 to 10 GHz). Several channels of the lower UHF bands are unoccupied in different geographical regions. This encouraged the FCC to permit the sharing of spectrum resources by unlicensed

users especially because of the good propagation properties in this band and the static TV channel allocation which makes the time requirements for adaptivity very relaxed [13]. FCC also opened the UWB band for opportunistic use due to its very low spectral utilization illustrated in Figure 1.5.

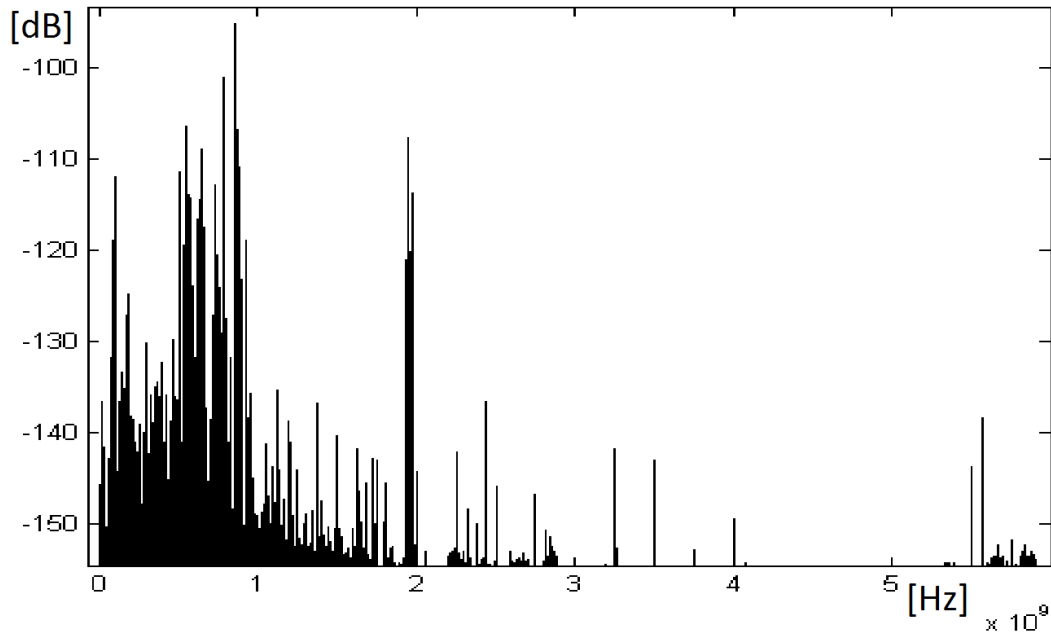


Figure 1.5: Measurement of 0-6 GHz spectrum utilization [14]

In UWB scenarios, the antenna of the secondary user's receiver collects a wideband RF waveform generated by close and widely separated primary transmitters. Each licensed transmitter is operating at a specific power level and bandwidth. Accordingly, unlike conventional wireless transceivers, which operate in only certain pre-allocated frequency bands, CR transceivers are required to operate in any unoccupied channel of a wide frequency range [15]. Thus, the design of the RF components shown in Figure 1.6, such as the antenna, filter, duplexer, power amplifier, and oscillator is delicate. In other words, their design should obey strict requirements such as operating over a wide frequency range while preserving linearity and accuracy.

The ability to design linear components and architectures for a wideband RF front-end is considered a primary technological concern in cognitive radio architectures. A tutorial on highly integrated and tunable RF front-ends for reconfigurable multi-band transceivers is presented in [16]. In [17] and [18], a software-defined cognitive radio prototype is proposed. Composed of broadband and tunable antennas, multi-band amplifiers, RF filters, broadband direct conversion mixers, baseband filters, and ADCs/DACs, the equipment's tunable and multi-band front-end operates over 400 MHz - 6 GHz band. On the digital side,

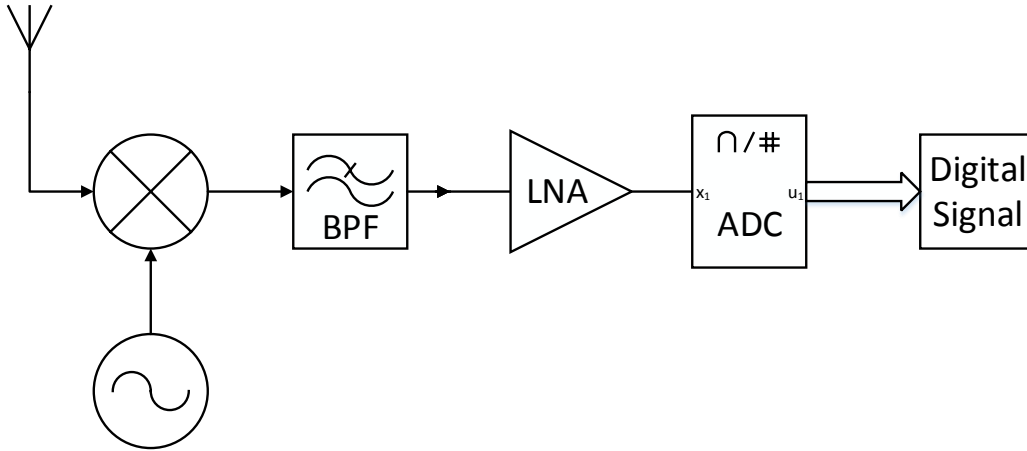


Figure 1.6: RF/analog front-end architecture for CR receivers

the software platform is an FPGA-based signal processing unit that manages the spectrum sensing task and reconfigures the communications schemes adaptively.

In [19], the authors have studied four RF architectures for wideband cognitive front-ends in terms of performance, power consumption, cost and size. Multiple narrowband, tunable, wideband, and wideband with few medium bands RF front-end architectures are compared. It was demonstrated that wideband architecture has a very poor linearity, while tunable front-ends suffer from high insertion loss and large size, and multiple narrowband architecture can support a limited number of standards. Therefore, the proposed wideband architecture implemented via few medium bands is well suited for commercial applications since it guarantees a good linearity and a low insertion loss with reduced size and cost. In [20], it is stated that the design of a multi-band cognitive radio system needs significant analog and RF processing, which is an unavoidable cause of nonlinearities, regardless of the carefully designed circuit techniques. Therefore, different design approaches, including digitized RF front-ends, have been reported to address those impairments.

A key advantage of the emergence of high performance programmable devices is that digital signal processing can be used to assist the analog circuits. In case of spectrum sensing, signal processing techniques are needed to improve the RF front-end sensitivity by processing gain and relaxing the circuitry design challenges in addition to the identification of primary users. In case of spectrum sculpting, signal processing techniques could replace and outperform the integration of RF filters.

1.3 Dissertation Objectives

Emerging wireless systems push towards designing flexible and reconfigurable receivers able to operate over multiple frequency bands and supporting various standards. A fundamental key in building such cognitive radios is the integration of sophisticated digital signal processing (DSP) techniques. In fact, the nonlinear characteristics of the transceiver analog front-end were proved to be a critical source of degradation of the cognitive behavior of secondary users. Recently, an extensive research work focused on the analog improvement of the front-end stages to enhance the terminal performance.

However, compensating the RF impairments via advanced DSP techniques, by benefiting from the software reconfigurability of the device, has not been studied efficiently. Since the design of a reconfigurable RF front-end is considered nowadays the bottleneck of the synthesis of a fully adaptive engine, linearizing the hardware in dynamic scenarios is currently beyond of the state-of-the-art in electronics. Thus, an assistance by using DSP techniques is proposed to relax the delicate conception of the cognitive reconfigurable hardware. This is the main target of the thesis where signal processing techniques are implemented in the cognitive transceiver to perform spectrum sculpting and sensing while taking into account the limitations of the circuitry. Therefore, the dissertation objectives and main contributions are summarized below:

1. Studying and verifying techniques used for spectrum sculpting in the UWB range. Generating a UWB adaptive pulse by using the main two techniques in the literature; Parks McClellan algorithm and Neural Networks-based algorithm, is implemented and tested.
2. Proposing an RF filter design to perform the pulse shaping. The role of such reconfigurable band stop filter is to generate adaptive UWB pulses. It uses specific RF components to cause frequency notches and switches to achieve the dynamic characteristic of cognitive radios. A prototype of the designed filter is fabricated to obtain measurements of its functionality. Comparative analysis on using hardware or software-based solution for spectrum sculpting is highlighted.
3. Investigating and practically implementing spectrum sensing techniques for cognitive radio applications. Techniques already implemented and used in CR receivers are studied. Energy detection and cyclostationarity based algorithms are tested. The robustness of these algorithms against RF impairments is assessed.
4. Selecting and improving a blind algorithm based on the detection of the cyclostationarity feature. The blindness of this scheme leads to accurate decisions in real-world scenarios where dynamic signals are present, and

models of noise and channel are variant. This makes the detector adequate to be deployed in practical CR receivers.

5. Combining the selected algorithm and a well-known mitigation technique to obtain a robust and blind spectrum sensing technique with the capability to mitigate RF impairments effects on a cognitive terminal. A dual-stage algorithm is obtained. The first stage consists of the blind sensing algorithm selected and improved in step 3. Its mission is to identify the presence of a licensed user and its main criterion is its efficiency in real-world environments. The second stage is a complementary algorithm that mitigates the non-linearly induced interference.
6. Proposing a new optimized detector with a fast mitigation algorithm devised to rapidly cleanse the received signal from distortions. The detection is based on a hybrid sensing technique. The complexity of the proposed algorithm is assessed to highlight the improved performance.
7. Implementing all studied signal processing techniques on a real time physical test-bed, i.e. the universal software radio peripheral USRP, and measuring their performance to verify their proper functioning and demonstrate the simulated efficiency.

1.4 Organization of the Dissertation

In this manuscript, the thesis work is presented in several chapters organized as follows: Chapter 2 studies the spectrum sculpting approach in UWB-CR, gives examples of the use of Neural Networks and the Parks-McClellan algorithm to generate the adaptive UWB pulses, and treats the design of reconfigurable bandstop filters and their employment in pulse shaping. Chapter 3 reviews the fundamentals and challenges of spectrum sensing algorithms in CR receivers. Chapter 4 presents a practical study of a blind cyclostationarity based spectrum sensing technique on the USRP platform. Models of RF impairments and their effects on the detectors' performance are assessed in Chapter 5. In Chapter 6, a dual stage algorithm composed of a recently proposed mitigation technique and the selected detector is presented with measured results. An improved version of this algorithm with a devised fast mitigation technique is proposed and described in this chapter. Several tests and measurements are performed and shown in this chapter to demonstrate the efficiency of the devised and optimized scheme. Finally, a conclusion and a list of the thesis-related publications are given in Chapter 7.

Chapter 2

Spectrum Sculpting

2.1 Ultra Wide Band Cognitive Radio

With the increasing use of communication technologies, spectrum resources have become scarcer and more valuable [21]. The combination of UWB technology and cognitive radio is an encouraging approach to ease this urgent situation [22].

UWB is characterized by a unique potential in short-range high-data-rate wireless communications. It is mainly utilized in military applications, such as high precision radar, life search after natural disaster, positioning, and homeland security [23]. Carried out by transmitting extremely short pulses, UWB is limited at very low energy levels. Therefore, the FCC has released the spectral mask on UWB emission power in 2002 [6]. UWB systems are allowed to operate in the 3.1-10.6 GHz band without a license requirement, but under very strict transmission power limits: the equivalent isotropically radiated power (EIRP) of UWB should be below -41.3 dBm/MHz to avoid the degradation of the legal wireless systems performance.

With CR technology, unlicensed users are allowed to access spectrum bands licensed to primary users, while avoiding interference with them. This can be achieved by the use of adaptive UWB pulses characterized by the ability to form, in their spectral masks, nulls in the bands used by existing narrow-band wireless services. This is the concept of spectrum sculpting that can be achieved using two UWB signal design techniques: UWB pulse shaping filter design (hardware solution) and UWB waveform optimization (software solution).

Although the UWB shaping filters can achieve relatively high spectrum efficiency, they require a much higher sampling rate and filter orders, thus considerably complicating the hardware structure [24]. The UWB waveform optimization found in the literature, such as genetic algorithm, is simple to implement but it remains difficult to achieve satisfactory spectrum efficiency and meet the deep frequency null at primary users' locations [25]. Consequently, this flexible solution is limited by the attenuation depth of the spectrum notches [26]. Thus,

having multiple UWB secondary users can cause a serious degradation of the legal signal due to the cumulated interferences. Yang presented in [27] a pulse based on Hermit Gaussian functions but the need of a deep frequency null is not solved in this thesis. In [28], a novel antenna is designed to attenuate the transmitted signal in the primary user bands. However, the large size of the UWB antenna has limited its benefits and applications.

Most of these techniques can only handle a fixed environment and not achieve dynamic interference cancellation, or they are complex to implement and slow to adapt to a changing environment. On the other hand, the fundamental feature of a cognitive radio is to instantly adapt to the active environment. Motivated by these requirements, we study three different techniques that generate a smart, dynamic and adaptive UWB waveform:

- The first technique relies on an advanced signal processing algorithm, Parks-McClellan (PM), which is combined with CR technology to generate an adaptive UWB pulse for multiple narrow interference suppression bands. Results confirm the robustness of the generated pulse in that it closely meets the FCC mask and achieves the desired spectrum nulls.
- Second, a novel pulse generator based on a neural network (NN) is studied. The designed NN can adaptively modify its parameters to adjust its output spectrum according to the state of primary users. The obtained UWB pulse can maximize the spectrum utilization, and can also dynamically perform spectrum avoidance.
- Last, the hardware solution is studied. The design of a reconfigurable band stop filter is proposed. The filter is characterized by two basic elements: Split-ring slots to introduce frequency notches and electronic switches to enable the control of these notches. One of the switching conditions guarantees the all-pass behavior of the filter. The remaining switching combinations result in band-stops at unauthorized frequencies. The filter was integrated in the feed line of an UWB antenna which could be used to transmit the resulting adaptive pulse. Simulations and measurements illustrate the dynamic response of the designed filter and the characteristics of the antenna.

This chapter is organized as follows. The PM algorithm is implemented in section 2.2, the design of the neural network is detailed in section 2.3, and the reconfigurable filter and antenna are presented in section 2.4. Finally in the conclusion, the performance of these three techniques are compared and contrasted.

2.2 Parks-McClellan Algorithm

2.2.1 Simulation Details

In this section, we are going to show a first method to generate an Adaptive UWB pulse for multiple narrow-band interference suppression: the Parks-McClellan Algorithm combined with the Cognitive Radio (CR) technology. Parks McClellan algorithm is generally utilized to design and implement efficient and optimal FIR filters [29]. In fact, the CR technology will detect the bandwidth and the central frequency of narrow-band primary users. In [30], Parks-McClellan Algorithm is used to generate an adaptive pulse ensuring an interference avoidance between users. For the simulation, the Matlab function *firpm* is used. After several iterations, an optimum pulse and its corresponding spectrum is illustrated, this shows clearly the multiple notches at some frequencies. The inputs of the *firpm* function should respect the locations of the frequency notches and the FCC spectral mask. The *firpmord* function is used to obtain these inputs and to specify the order of the filter.

2.2.2 Generated Pulses

Figure 2.1 shows the pulse obtained by simulating the Parks-McClellan Algorithm in Matlab, considering two frequency nulls at 3.5 GHz and 5.2 GHz, which are the famous bands of WiMAX and WLAN. The needed filter order is 546. Consequently, the designed filter has a delay of $546/2 = 273$ samples. In Figure 2.2, the corresponding spectrum is illustrated, showing the notches.

With the help of spectrum detection technology, Parks-McClellan algorithm can generate adaptive pulses that meet the FCC spectral mask and avoid narrow-band interferences. Despite the high filter order, PM algorithm is providing excellent spectrum utilization and a depth of -45 dB at undesired bands.

2.3 Neural Network

2.3.1 Description of the Technique

The second proposed method for UWB pulse shaping is the usage of Neural Networks. They are composed of simple elements operating in parallel which are inspired by biological nervous systems [31]. As in nature, the network function is determined largely by the connections between elements. A neural network could be designed to perform a particular function by adjusting the values of the connection (weights) between elements. In this section, this method is used to generate the dynamic UWB pulse. Commonly a neural network is adjusted, or trained so that a particular input leads to a specific target output. The network will then adjust its parameters, based on a comparison of the output and the

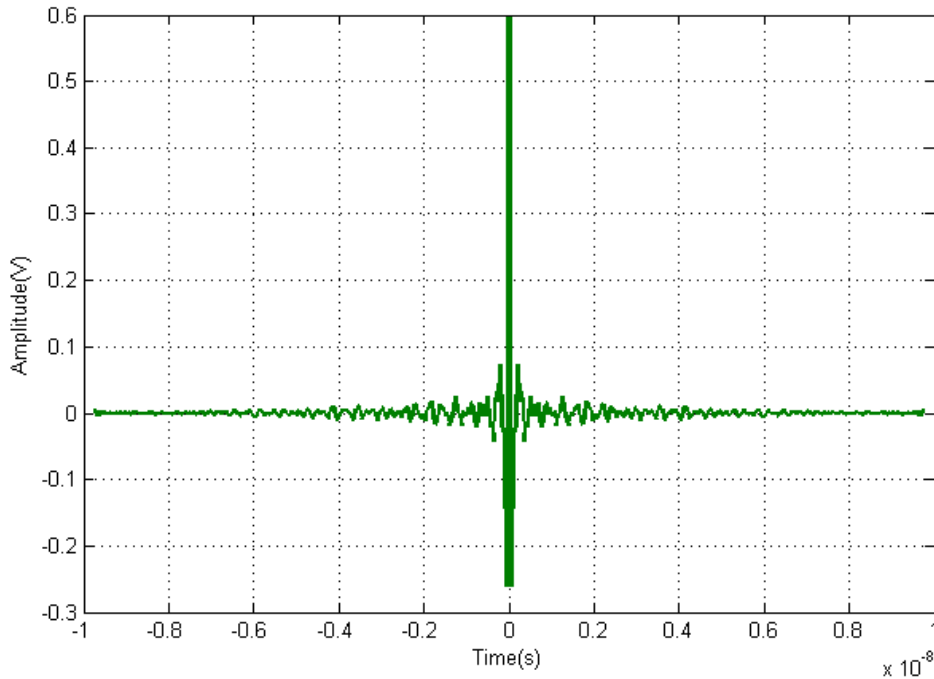


Figure 2.1: The pulse generated by the PM algorithm

target, until the output matches the target. The target signal is a result of spectrum sensing, which will be determined by the current frequency bands of the primary users. Then, by adjusting the network weight according to specific learning rules, the actual output can trace the target signal after a very limited number of iterations. The radial basis function (RBF) network will be selected in this work because it has the capability to ensure the requirements suggested previously. It is shown that RBF network can approximate any function at any precision by altering its basis functions [32]. Figure 2.3 shows a simplified block diagram to explain our model.

The RBF network needs an input matrix P based on a basis function $p(n)$ that is supposed to meet two requirements:

1. The basis function should be even symmetry around its center.
2. The energy of the basis function should be finite.

Based on the above restrictions, a famous candidate for the basis waveform is the Gaussian function [33]. In this case, the total network input P can be written as:

$$P = [p_0 p_1 p_2 \dots p_N] \quad (2.1)$$

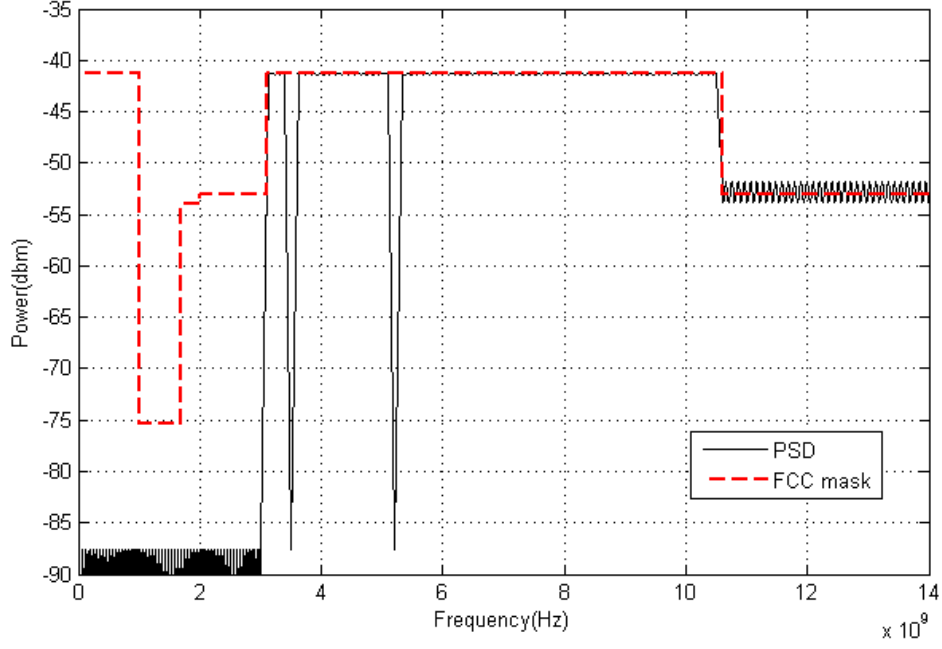


Figure 2.2: PSD of the pulse generated by the PM algorithm

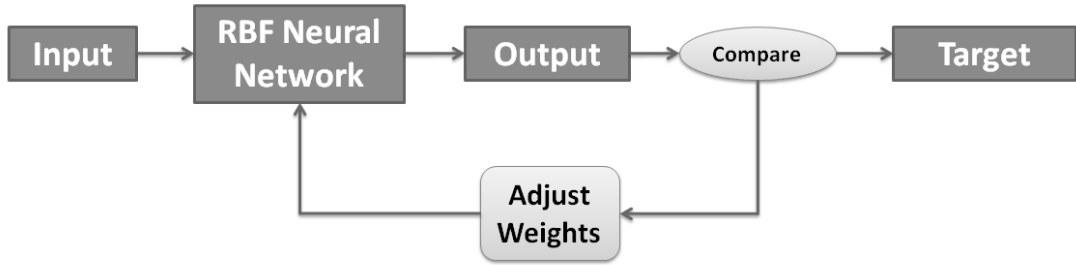


Figure 2.3: RBF Neural Network model

The basic Gaussian function is given by:

$$\begin{cases} p_0(k) = 1 & \text{if } k = 0, 1, \dots, N - 1 \\ p_i(k) = \frac{1}{\sqrt{2\pi s_i}} \exp\left(-\frac{f_s^2}{2s_i^2}(k - \lambda_i)^2\right) & \text{if } i > 1 \text{ and } k = 0, 1, \dots, N - 1 \end{cases} \quad (2.2)$$

2.3.2 Simulations Results

The input matrix is formed using the basis waveform $p(n)$. Each input vector p_i is generated using Matlab. The target signal of the neural network can be dynamically determined by the result of spectrum sensing, which decides the licensed bands to be avoided. In the simulation, the target signal is set to the FCC mask with two notches at WiMAX and WLAN frequency locations.

To build two different networks and compare their results, two softwares are used in this work. First, the Neural Network Toolbox in Matlab is utilized. During the learning step, the network weight vector is updated. After the network weight achieved its convergence, the learning process is terminated and the network output is fed to the transmitting antenna. Our goal is to optimize the learning time to ensure a dynamic system. The Power Spectral Density (PSD) of the obtained pulse using the Neural Network training tool in Matlab with 31 iterations is shown in Figure 2.4.

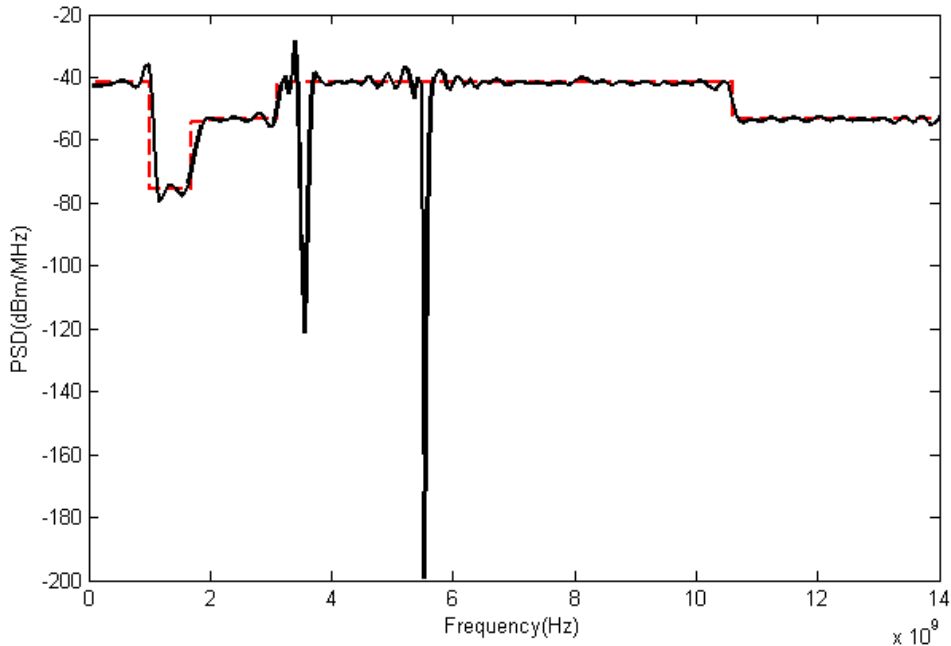


Figure 2.4: PSD of the pulse generated by the neural network in Matlab

Second, the same simulation parameters are used in “NeuroSolutions”: the premier Neural Network Development Environment. The same input (based on Gaussian functions) and the same target signal (FCC mask with 2 frequency nulls at 3.5 GHz and 5.2 GHz) are given. The PSD of the obtained results using NeuroSolutions is shown in Figure 2.5 with a number of iterations equal to 120.

The proposed UWB pulse generation using neural networks provides much safer protection to the primary users. When the number of iterations

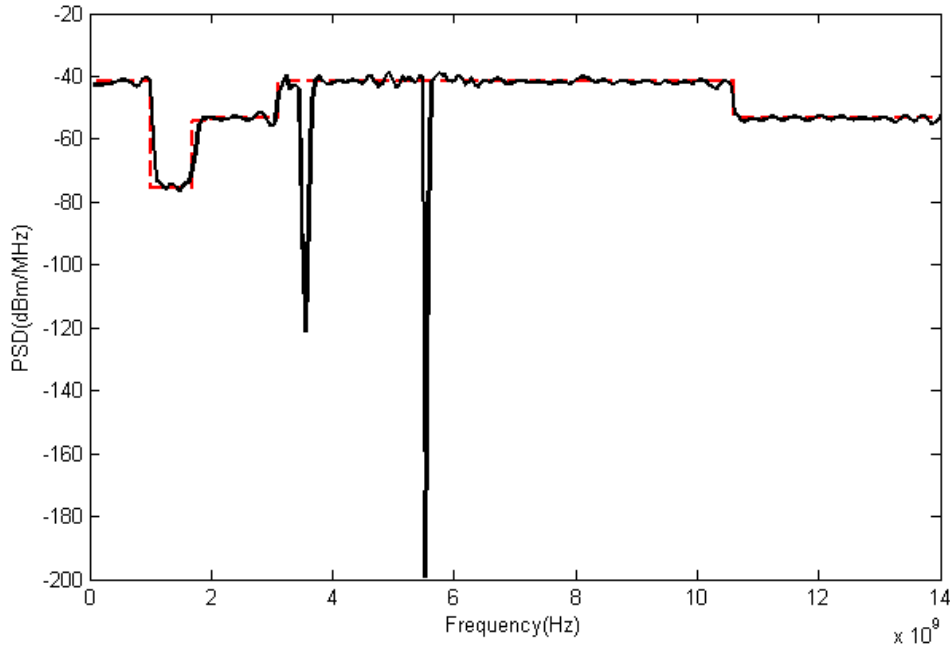


Figure 2.5: PSD of the pulse generated by NeuroSolution

of the learning step is increasing, the generated pulse becomes more efficient ensuring perfect frequency utilization and spectrum avoidance since it provides the deepest frequency notch.

2.4 Filter Antenna Design

The hardware technique investigated in this chapter is based on a filter-antenna design. A reconfigurable stop band filter is firstly designed, and then it is incorporated on the feed of a UWB antenna to ensure pulse shaping and interference avoidance with licensed users.

2.4.1 Filter Design and Stop-Band Control

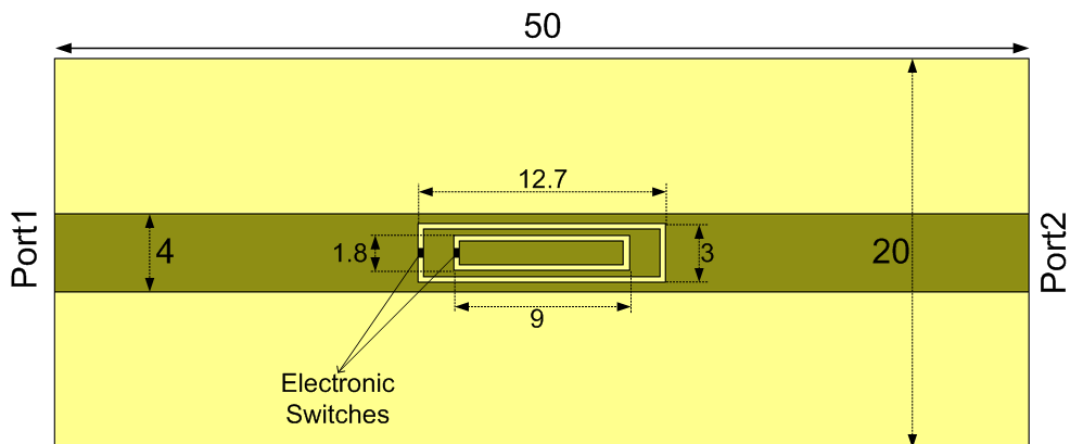
To shape the output pulse of the antenna, a dual stop-band filter is designed, as shown in Figure 2.6. The filter is a 50Ω microstrip line, printed on a 1.6mm-thick Rogers RO3203 substrate with a relative permittivity $\epsilon_r = 3.02$, on which two rectangular split-ring slots have been incorporated with two electronic switches mounted across each ring slot. The split-ring slot is a single-ring complementary split-ring resonator (CSR). CSRs and their dual-counterparts, the SRRs introduced in [34], have been employed in [35] for the design of UWB antennas with fixed notched bands, and in [36] for the design of UWB antennas with multiple

controllable band notches.



Figure 2.6: Photo of the designed dual stop-band filter

The dimensions of the CSRRs are indicated in Figure 2.7. If one of the electronic switches is ON, the corresponding CSRR will resonate inducing a bandstop on the primary user's location. In our designed filter, CSRRs are parameterized to cause nulls at 3.5 GHz and 5.2 GHz. To avoid other wireless systems, further bandstops could be generated by adding other CSRRs. If no primary users are active, the filter should re-establish its all-pass behavior by turning OFF all the switches.



Units: mm

Figure 2.7: Configuration of the designed dual stop-band filter

2.4.2 Measured and Simulated Characteristics of the Filter

The filter is simulated using Ansoft HFSS [37] and a prototype of the filter is fabricated, as shown before. The reflection coefficient (S11), and transmission

(S21), were simulated and measured respectively. Although the structure of the filter is not perfectly symmetrical, the simulations and measurements have shown that S11 and S22 are very close since the mismatch is negligible. The same property applies to S21 and S12. Figures 2.8 and 2.9 respectively show the computed and measured S11 and S21 plots. Two of four switching cases are illustrated: the all-pass behavior and the dual stop bands. It is shown that when both switches are ON, two stop-bands occur at 3.5 and 5.2 GHz. Generating only one bandstop is also possible by turning OFF one of the switches. The plots show good analogy between simulated and measured results.

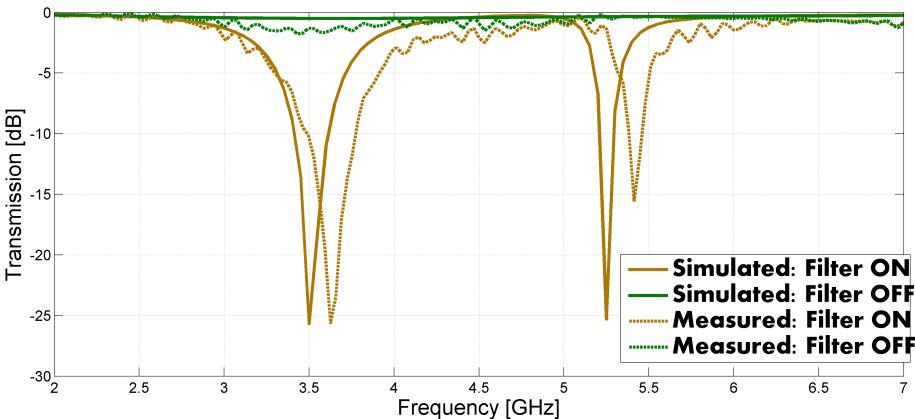


Figure 2.8: Simulated and Measured S11

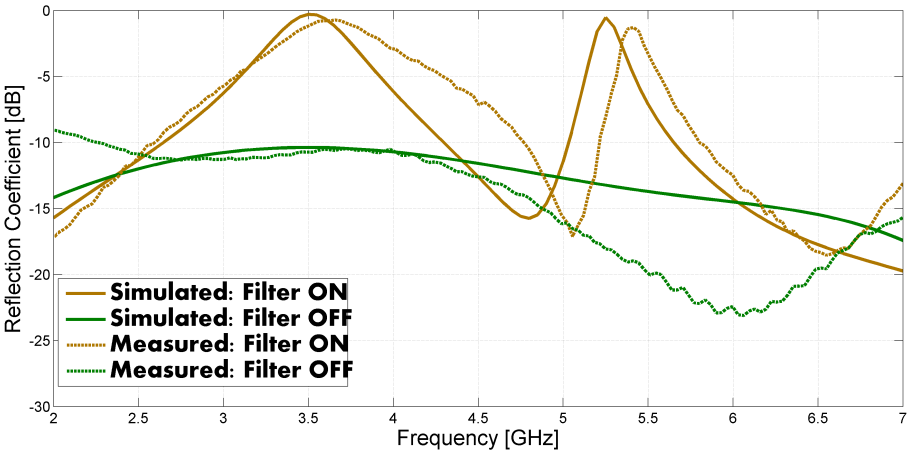


Figure 2.9: Simulated and Measured S21

2.4.3 Generated Pulses

A UWB pulse is fed to the filter, the output from the other filter port is also a UWB pulse, with very similar shape, except in bandstops, where the pulse has nulls. These nulls help to avoid interference to primary users or services operated in these bands. In UWB communications, information is contained in narrow pulses (monocycles). Several possible pulses are investigated in the literature such as the derivatives of the Gaussian pulses especially the fifth derivative. In [38], an algorithm is used to design a UWB pulse that meets the FCC spectral mask requirements. In this work, two types of UWB pulses are tested with the filter: Gaussian and Scholtz's monocycles. The Gaussian monocycle is similar to the first derivative of the Gaussian pulse and is given by [39]:

$$w(k) = 2\frac{A}{T_{au}}\sqrt{e}(t - T_c) \exp\left(-2\left(\frac{t - T_c}{\tau}\right)^2(k - \lambda_i)^2\right) \quad (2.3)$$

In Equation 2.3, A is the amplitude, T_{au} the pulse shape parameter, and T_c the time duration of the pulse. On the other hand, the Scholtz's monocycle is an attractive waveform because of its flat power spectrum density, which best suits the designed filter. This monocycle is similar to the second derivative of the Gaussian pulse and can be represented as in [40] by:

$$w(k) = A\left(1 - 4\pi\left(\frac{t - T_c}{\tau}\right)^2\right) \exp -2\pi\left(\frac{t - T_c}{\tau}\right)^2 \quad (2.4)$$

Figure 2.10 shows the simulated PSD of the inputted Gaussian monocycle and its corresponding output pulse. The simulation is done in Matlab using filter parameters exported from HFSS. Similarly, Figure 2.11 shows that for the Scholtz's monocycle. Both figures reveal an attenuation of about 15 dB in the filter's stop-bands.

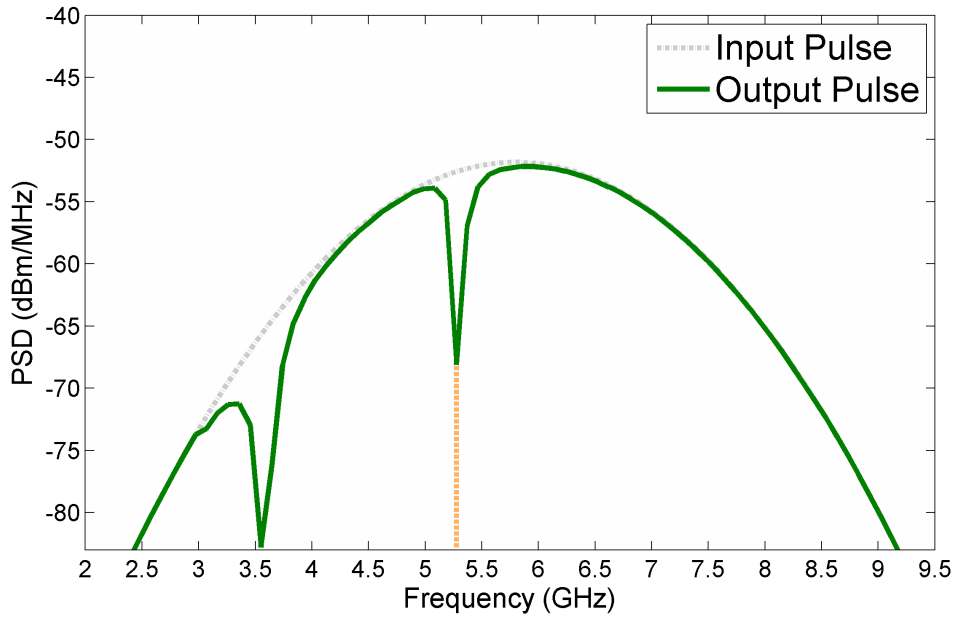


Figure 2.10: Input Gaussian monocycle and corresponding output

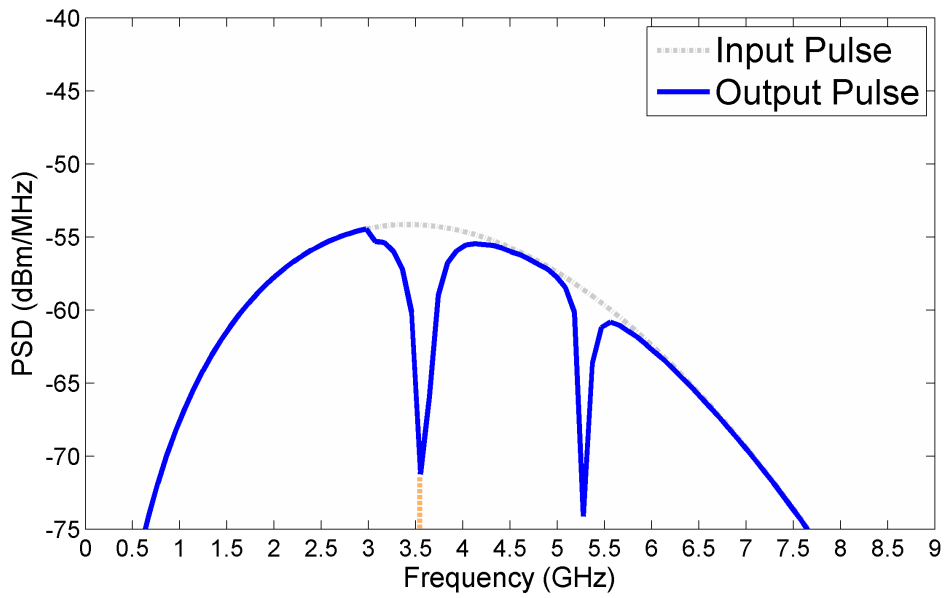


Figure 2.11: Input Scholtz's monocycle and corresponding output

2.4.4 Antenna Configuration

In this section, an antenna suitable for UWB-CR is proposed. Having our designed filter integrated on its feed line, the proposed antenna is reconfigurable and has band stops in the WLAN and WiMAX bands.

Depicted in Figure 2.12, the antenna is a monopole printed on a 1.6mm-thick Rogers RO3203 substrate with $\epsilon_r = 3.02$, and features a partial rectangular ground plane. The patch is almost circular in shape. The dimensions of the different parts are optimized for an impedance bandwidth covering the UWB range (starting 3 GHz). To induce band notches, the reconfigurable stop band filter is integrated in the feed line. Switching cases studied in Section 4.2 are also applicable on this antenna.

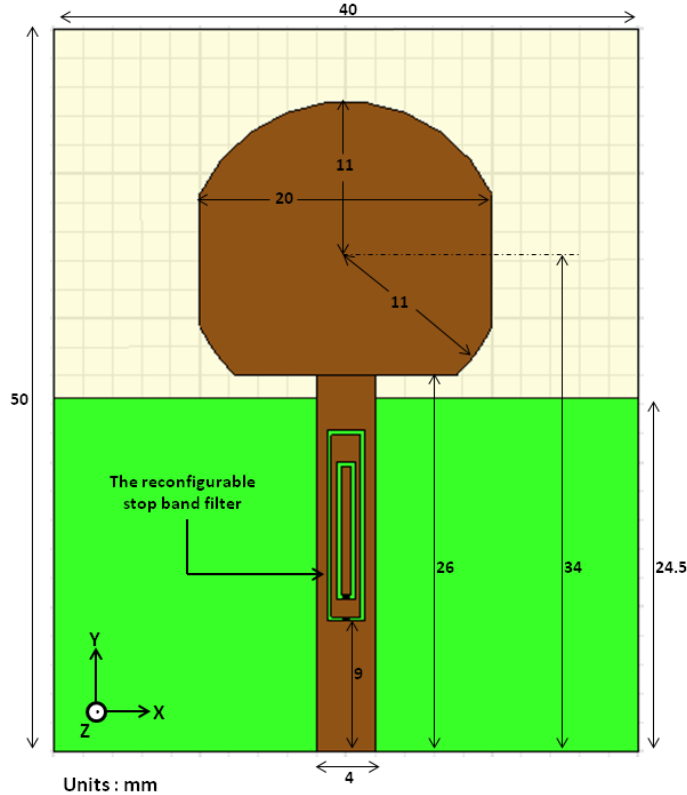


Figure 2.12: Antenna geometry

The antenna was designed and simulated using Ansoft HFSS [37]. A prototype was fabricated and illustrated in Figure 2.13, and the reflection coefficient was measured for two operation scenarios. The all-pass behavior is shown in Figure 2.14 and two bandstops at 3.5 GHz and 5.2 GHz are added in Figure 2.15 by turning ON the switches. The HFSS-computed normalized gain patterns in the X-Z and Y-Z planes, for each case, are shown in Figure 2.16. All cases result in

omni-directional patterns. The patterns are unchanged for the Switches-ON and Switches-OFF cases. This means that outside the rejected bands, the patterns are independent of the filter state.



Figure 2.13: Antenna photo

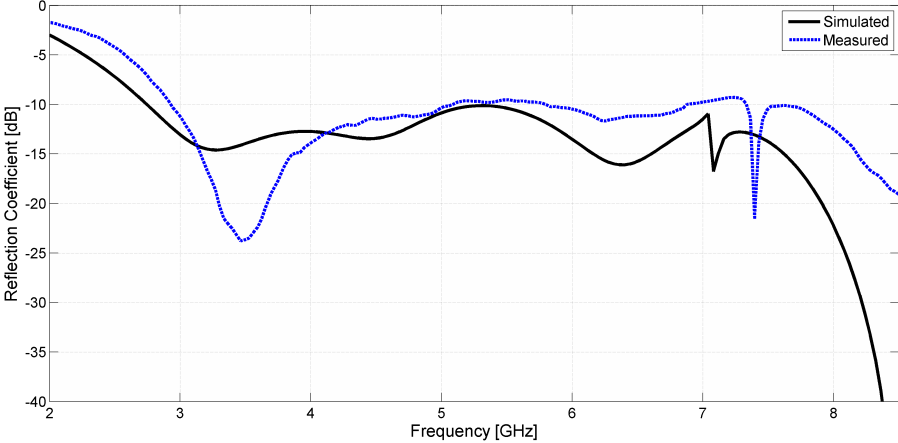


Figure 2.14: Reflection coefficient when all switches are tuned OFF

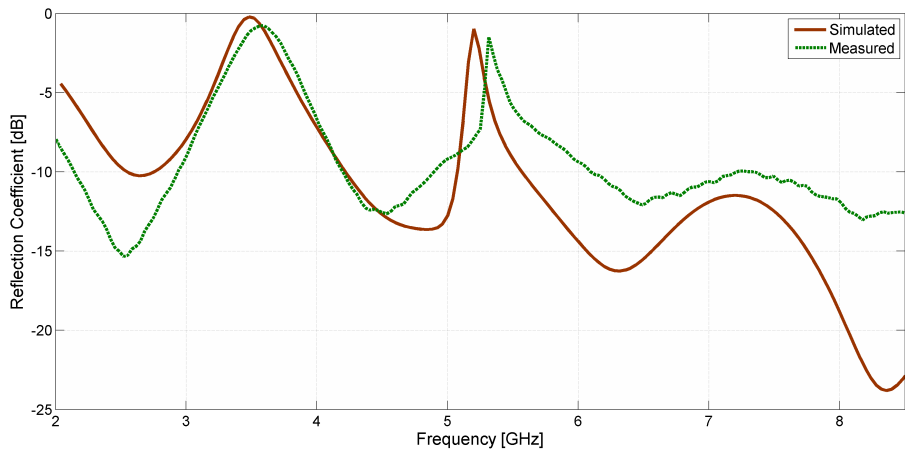


Figure 2.15: Reflection coefficient when all switches are tuned ON

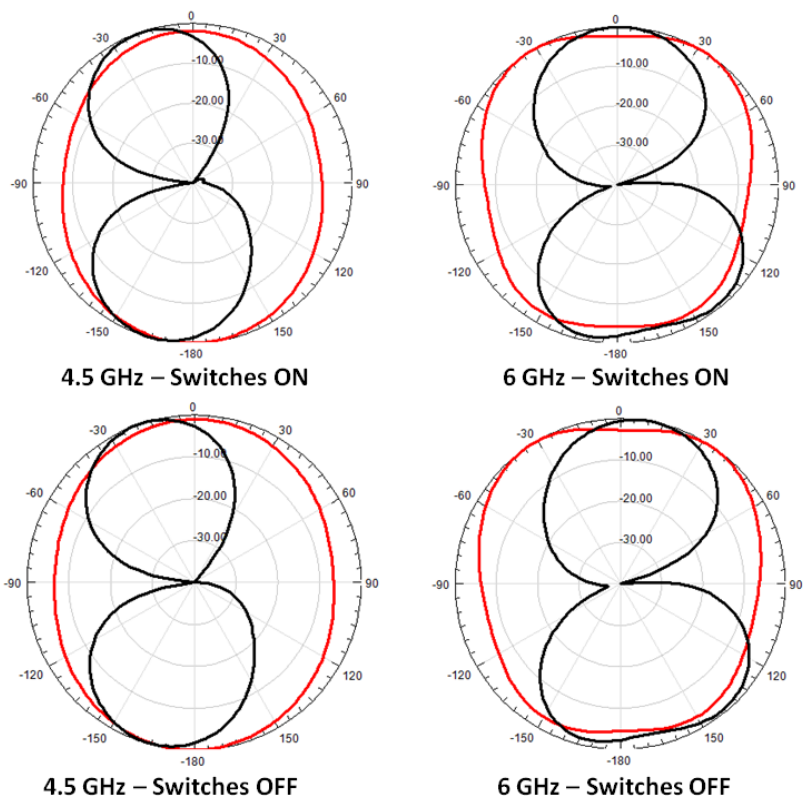


Figure 2.16: Radiation pattern at 4 or 6 GHz when switches are turned ON or OFF

2.5 Conclusion

In this chapter, we studied three different techniques to generate adaptive UWB waveforms for application in UWB-CR. Two of these techniques, Parks-McClellan and neural network, are based on advanced signal processing algorithms. The third relies on the design of reconfigurable RF filters. Matlab simulations showed that the PM algorithm can achieve high spectrum utilization. The main drawback of this technique is its heavy computation resulting from the high filter order. This will increase the adaptation time of the cognitive transceiver. On the other hand, Neural Networks, which are easier to implement to fit any practical function, can be used as a UWB adaptive pulse generator. Our designed neural network provided a UWB waveform overcoming all the challenges of UWB-CR after a limited number of iterations thus ensuring a rapid adaptive response.

In the proposed hardware solution, the reconfigurable stop band filter was easy to implement and had the advantage of simple integration in the feed line of a UWB antenna. Simulated and measured results for the filter and the antenna were presented. Despite its advantages, the nulls generated by this technique were not as deep as those of the first two techniques. On the other hand, the filter rejects two preselected band notches based on famous license holders. Consequently, in the presence of other primary users, the hardware should be entirely modified to ensure a suitable frequency rejection. In the case of signal processing based algorithms, only few parameters will be altered in the software to perform the interference avoidance against the added primary user.

Chapter 3

An Overview of Spectrum Sensing

3.1 Introduction

In a CR scenario, secondary users are allowed to detect, exploit, and use underutilized spectral resources licensed to primary users. Such opportunistic behavior urges CR transceivers to scan the spectrum in order to find white spaces and transmit adaptive signals. Thus, spectrum sensing is the key function of smart receivers since it enables the cognitive cycle proposed by Mitola in [2, 4]. This functionality creates unique signal processing challenges and requires sophisticated algorithms to overcome practical imperfections such as model uncertainty and hardware imperfections.

To address these challenges, CR researchers proposed in the last decade implementing various detectors that have different complexity levels, performance results, and requirements. This chapter investigates spectrum sensing methodologies for cognitive radio to ensure reliable identification of white spaces. The classical energy detector and the well-known cyclostationarity based detector are studied in Section 3.2 as basic detectors. Furthermore, major trade-offs involved in the design and optimization of these signal processing techniques are characterized. A literature review on the main challenges in the design and the practical implementation of sensing schemes is presented in Section 3.3.

3.2 Primary signal detection

3.2.1 Introduction

The spectrum sensor essentially performs a binary hypothesis test on whether or not there are Primary Users (PU) in a particular channel. The channel is idle under the hypothesis H_0 and busy under the hypothesis H_1 . It is obvious that

under H_0 the received signal is only the ambient noise while it consists of the PU's signal and the ambient noise under H_1 .

$$\begin{cases} y(k) = w(k) & H_0 \\ y(k) = w(k) + s(k) & H_1 \end{cases} \quad (3.1)$$

for $k = 1, \dots, n$ where n is the number of received samples, $w(k)$ represents ambient noise, and $s(k)$ is the PU signal. It is evident that the received signal will have more energy when the channel is busy than when it is idle. An energy detector is based on this concept in order to detect the presence of a PU. When aspects of the PU signal are known, one can exploit the feature of the received signal and identify the PU; a special case leads to the cyclostationarity detector. When the PU's signal $s(n)$ is fully known, the matched filter based detector could be used [13, 41].

Regardless of the used sensing algorithm, sensing errors are inevitable due to additive noise, limited observations, and the inherent randomness of the observed data. False alarms (or Type I errors) occur if an idle channel is detected as busy, and missed detections (or a Type II error) occur when a busy channel is detected as idle.

A false alarm leads to a wasted opportunity for the SU to transmit but a missed detection leads to a collision with the PU, thus a wasted transmission for both PU and SU. A clear compromise lies between ensuring the protection of the PU and providing service to the SU. A given level of protection of PU is ensured by placing a threshold on the allowed probability of missed detection. A good detector is an algorithm that minimizes the probability of false alarm, subject to a constraint on the probability of missed detection. Thus, the performance of a detector is characterized by two parameters, the probability of Missed Detection P_{MD} and the probability of False Alarm P_{FA} , which are defined as in Figure 3.1:

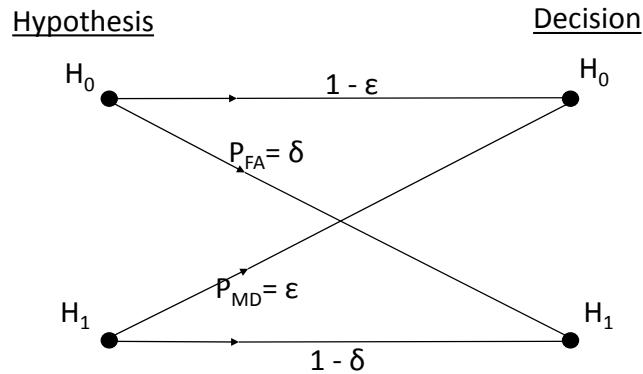


Figure 3.1: Possible scenarios of detection

The performance of a detector could be observed by drawing its receiver operating characteristic (ROC) curve. ROC is a plot of $1 - P_{MD} = 1 - \delta$, the probability of detection (P_D), versus $\epsilon = P_{FA}$. For example, the ROC curve of the energy detector is illustrated in Figure 3.2. Choosing different detection algorithms or sensing parameters leads to different ROCs.

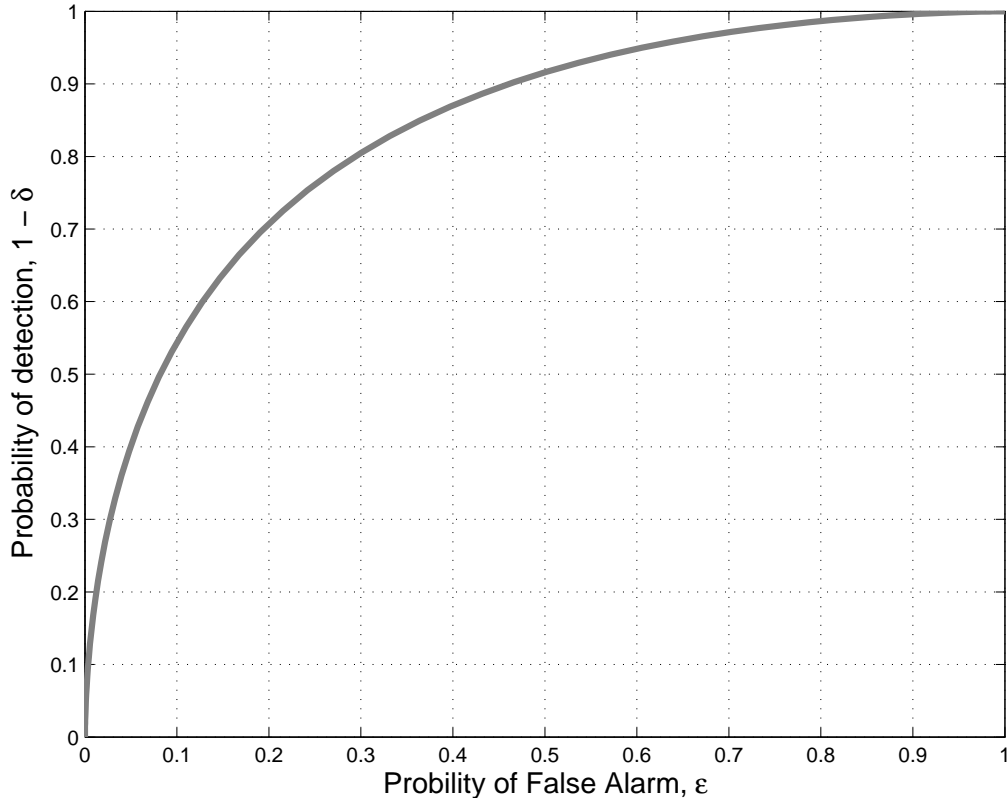


Figure 3.2: ROC of the energy detector

Several review papers listed the spectrum sensing methods devised in the last decade [41–43]. In summary, well-known spectrum sensing algorithms, sorted in an ascending order of complexity are: energy detection (ED) [44–46], matched filter (MF) based detection [45, 47], cyclostationarity based detection (CSD) [48–52], covariance based sensing [53, 54], and eigenvalue based sensing [55–57].

Some of these methods require a priori knowledge of noise and/or signal power information, these include MF, CSD (relying on the full or partial knowledge of signal and noise levels), and ED (having a threshold dependent of the estimated noise power level). For example, MF is demonstrated as the best detector since the a priori information about the primary user’s characteristics is utilized for deterministic detection. To benefit from this advantage, primary

users should transmit known patterns or pilots which is not practical in real-world scenarios since the SU should be able to detect any unknown PU signal.

In the next paragraph, we present an overview of the classical ED and CSD detectors.

3.2.2 Energy Detector

Introduction

In many cases, the signaling scheme of the PU may be unknown to the SU. The energy detector is based on the idea that with the presence of a signal in the channel, there would be significantly more energy than if there was no signal present. This concept is applicable for any PU without knowing any of its characteristics. Energy detection simply involves the application of a threshold on the collected energy from the channel. The threshold is used to decide whether a licensed transmission is occurring or not. Consequently, the block diagram of the energy detector, illustrated in 3.3, shows its simple detection mechanism.



Figure 3.3: Block diagram of the energy detector

Mathematical Formulation of ϵ and δ

Since the detection is only based on the received amount of energy, the signal can be simply modeled as a zero-mean stationary white Gaussian process, independent of the white Gaussian noise. The spectrum sensing problem is distinguishing between two mutually independent Gaussian sequences:

$$\begin{cases} y(k) = w(k) & H_0 \\ y(k) = w(k) + s(k) & H_1 \end{cases} \quad (3.2)$$

for $k = 1, \dots, n$. Here $w(k)$ and $s(k)$ are zero-mean complex Gaussian random variables with variances σ_w^2 and σ_s^2 , respectively. Let $y = [y(1), \dots, y(n)]^T$ denote the vector of the n observed samples and $\sigma_0^2 = \sigma_w^2$, and $\sigma_1^2 = \sigma_w^2 + \sigma_s^2$.

A simple formulation of the ED detector is given in [58] as:

$$z = \frac{1}{2n\sigma_0^2} \sum_{k=1}^n |y(k)|^2 > \tau \quad (3.3)$$

where τ is the threshold chosen respecting a given P_{FA} and P_{MD} . Each operating point on the ROC depends on the selected threshold of the ED detector. Points

on the lower part of a ROC curve corresponds to low P_{FA} thus to a low threshold. Contrarily, a high threshold minimizes the P_{MD} and thus maximizes the probability of detection P_D leading to an operating point in the upper part of a ROC curve. It is obvious that the choice of the threshold controls the performance and the efficiency of the ED [46].

To formulate the mathematical equation of the ROC for the ED, the statistic z should be investigated [59]. z is a scaled version of a standard χ^2 random variable with $2n$ degrees of freedom. If x_i s are independent real Gaussian variables with zero means and unit variances, then $x = \sum_{i=1}^{2n} x_i^2$ is χ^2 distributed with $2n$ degrees of freedom. Thus, the Probability Density Function PDF of x is given by:

$$p(x) = \frac{1}{2^n(n-1)!} x^{n-1} \exp\left(-\frac{x}{2}\right) \quad x > 0 \quad (3.4)$$

In this case, the tail probability is:

$$\begin{aligned} p(x > \tau) &= \int_{\tau}^{\infty} \frac{1}{2^n(n-1)!} x^{n-1} \exp\left(-\frac{x}{2}\right) dx \\ &= \Gamma_u\left(\frac{\tau}{2}, n\right) \end{aligned} \quad (3.5)$$

where $\Gamma_u(\cdot, \cdot)$ is the upper incomplete gamma function defined by

$$\Gamma_u(a, n) = \frac{1}{\Gamma(n)} \int_a^{\infty} x^{n-1} \exp(-x) dx \quad (3.6)$$

Since the statistic $z \times 2n$ has the same PDF as a χ^2 variable with $2n$ degrees of freedom. Hence, P_{FA} and P_{MD} for the ED are theoretically given by:

$$\epsilon = P_{FA} = \Gamma_u(n\tau, n) \quad (3.7)$$

$$\delta = P_{MD} = 1 - \Gamma_u\left(\frac{n\tau}{1 + SNR}, n\right) \quad (3.8)$$

where $SNR = \frac{\sigma_s^2}{\sigma_w^2}$

Results and Discussions

In Figure 3.4, the ROC of the ED is illustrated. The first curve is based on the calculated formulas. On the other hand, ϵ and δ are estimated in Matlab using a Monte Carlo simulation and based on the block diagram in Figure 3.3.

Although simple to implement, a drawback of the ED is that its performance is highly susceptible to dramatical degradations especially in low SNR scenarios. In the presence of noise uncertainty, there exists an SNR wall for energy detection. An SNR wall is an SNR value below which reliable detection is not possible even if the sensing duration is increased indefinitely [60]. On the other hand, since different transmitters employ different signal power levels and

transmission ranges, one of the major concerns of energy detection is the selection of an appropriate threshold. A threshold that may work for one transmission may not be sufficient for another. All these drawbacks are the motivation behind studying blind detectors that can exploit additional signal features.

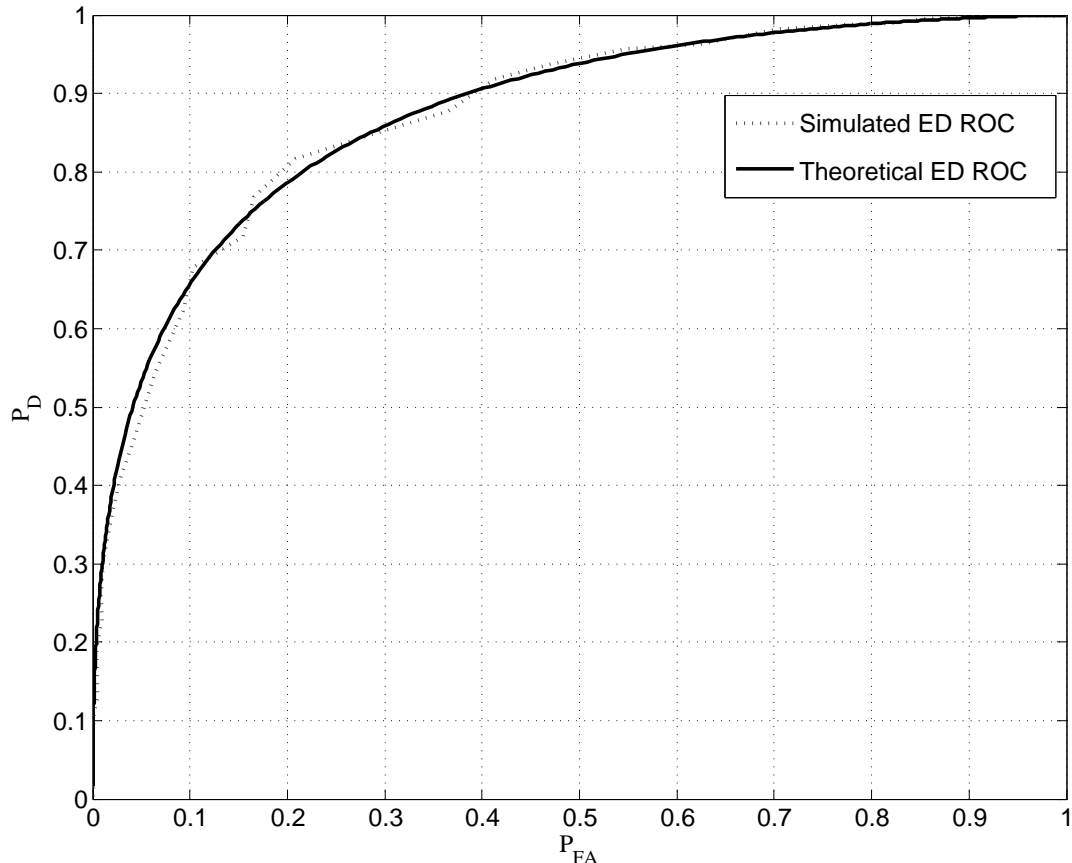


Figure 3.4: Simulated and theoretical ROC of the ED for $n = 80$ and $SNR = -7dB$

3.2.3 Cyclostationary Feature Detector

Feature Detection

In practice, little is known about the primary users signal structure at the SU. Transmitted signals are to some extent determined by standards and regulations. Thus, some features of the signal to be detected, like data rates, the modulation type, and the carrier frequency, are usually known. In the following, we will describe one of the widely used detectors exploiting known features of the signal, the cyclostationarity feature detector.

Cyclostationarity-Based Algorithm

To modulate signals, transmitters multiply base band signals with sine wave carriers, pulse trains, repeated spreading, hopping sequences, or cyclic prefixes which result in built-in periodicity. Thus, a modulated signal is characterized as cyclostationary since its statistics, mean and autocorrelation, exhibit periodicity. This feature can be extracted and analysed using Fourier analysis. In communications, this periodicity is introduced intentionally so a receiver can estimate several parameters such as carrier phase, pulse timing, or direction of arrival [49, 50, 61]. In CR networks, this periodicity is the feature for detecting a random signal with a particular modulation type in a background of noise and other modulated signals [13, 48].

The signal $x(t)$ is said to be (second-order) cyclostationary if its autocorrelation function $r_{xx}(t, \tau)$ is periodic with period T :

$$r_{xx}(t, \tau) = r_{xx}(t + T, \tau) \quad (3.9)$$

These periodicities are examined using the cyclic autocorrelation function (CAF)

$$R_{xx}(\alpha, \tau) = \frac{1}{T} \int_T r_{xx}(t, \tau) \exp(-j2\pi\alpha t) dt \quad (3.10)$$

In other words, $R_{xx}(\alpha, \tau)$ measures the spectral correlation between the signal $x(t)$ and a frequency shifted version of the signal. For man-made signals, CAF is nonzero for few values of the shift in frequency (α). It should be noted that $R_{xx}(\alpha, \tau)$ is discrete in α and continuous in τ . A theoretical plot of the CAF of a linearly modulated signal, shaped with a rectangular window is shown in Figure 3.5.

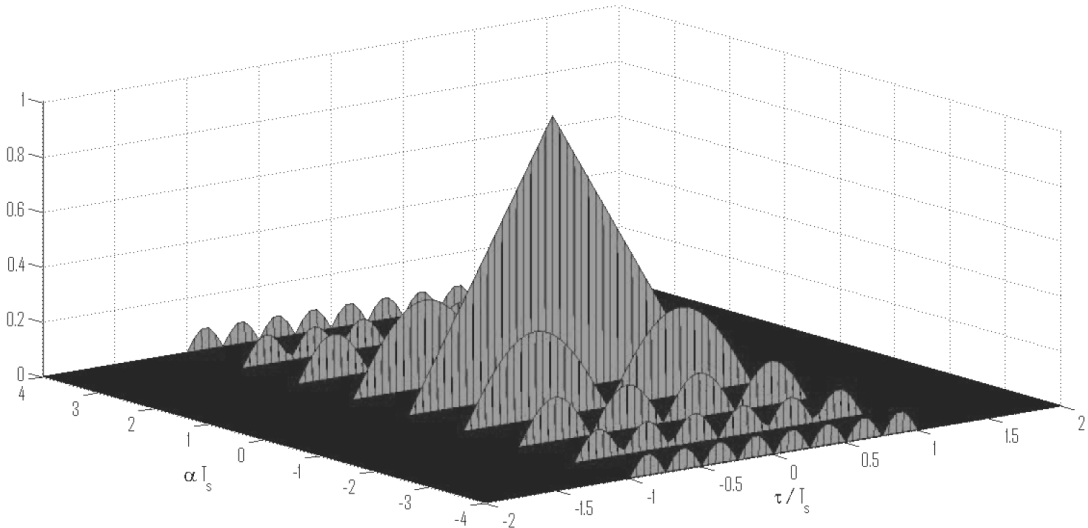


Figure 3.5: Theoretical 3D plot of a CAF

Taking the Fourier transform with respect to τ results in the cyclic spectrum density function (CSD) or the cyclic spectrum:

$$S_{xx}(\alpha, f) = \lim_{\Delta T \rightarrow \infty} \lim_{T \rightarrow \infty} \int_{-\Delta T/2}^{\Delta T/2} X_T\left(t, f + \frac{\alpha}{2}\right) X_T^*\left(t, f - \frac{\alpha}{2}\right) dt \quad (3.11)$$

where $X(f)$ is the Fourier transform of the time signal $x(t)$.

In summary, the CAF $R_{xx}(\alpha, \tau)$ is the Fourier transform of the autocorrelation function $r_{xx}(t, \tau)$ with respect to t . The CSD $S_{xx}(\alpha, f)$ is the Fourier transform of the CAF with respect to the delay τ . Unlike PSD, which is one dimensional transform, CSD depends on two dimensions: the frequency f and the cycle frequency α . PSD is a special case of CSD for $\alpha = 0$. The distinctive character of spectral redundancy appears in CSD and makes the PU signal recognizable in presence of noise because overlapping features in PSD are non overlapping features in CSD. In a scenario where different PUs with different modulations coexist, cyclostationarity based detector could easily detect the difference between signals. In fact, different types of modulations can have highly distinct cyclic spectrum. At the same time, different signals using these modulations can have the same PSD. An example is illustrated in Figure 3.6, where the CSD of a linearly modulated signal with rectangular shaping is illustrated.

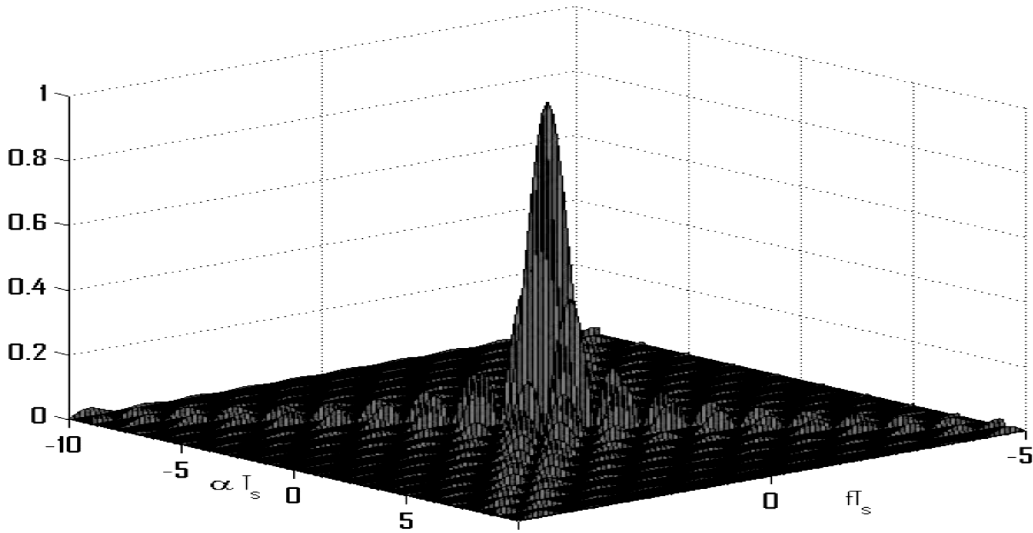


Figure 3.6: Theoretical 3D plot of a CSD

In addition, stationary noise and interference do not exhibit any spectral correlation. Consequently, the cyclostationarity feature of the signal could be detected in the presence of noise even in very low SNR scenarios. Based on the calculation of the CSD, the block diagram of the cyclostationarity feature based detector depends on the correlation of the Fourier transform of the transmitted

signal, as shown in Figure 3.7. The feature detection depends on the knowledge of some parameters of the PU, especially the modulation type.

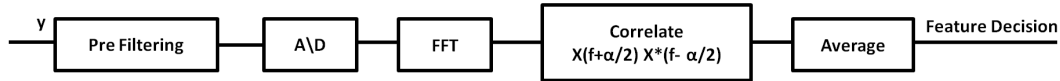


Figure 3.7: Block diagram of the cyclostationarity feature based detector

Results and Discussions

In Figure 3.8, the ROC of the cyclostationarity feature based detector is compared with ED detector. On the efficiency versus complexity level, the higher-order statistics based spectrum sensing in [62] can effectively separate noise from received signals even in very low SNR regimes. However, it often requires a large number of samples to obtain the accurate estimations of the relevant statistics. The ED approach has been widely studied and deployed for primary user's signal detection since it has a very low computational complexity [13, 63]. Unfortunately, its detection efficiency degrades heavily under low SNR and noise uncertainty conditions [60, 64, 65], which can restrict its efficiency for cognitive radio systems. Moreover, other ED drawbacks are highlighted in the literature such as filter effects and spurious tones [66]. On the other hand, cyclostationary features may be completely lost due to channel fading. It is also shown in [60] that model uncertainties cause an SNR wall for cyclostationary based feature detectors too.

In this thesis, the main concern is to devise signal processing techniques suitable for real-world applications. Unfortunately, the basic sensing schemes described above are not suitable for such applications. For that, the main challenges faced in practical implementations of efficient detectors in CR scenarios are highlighted and addressed in the next section.

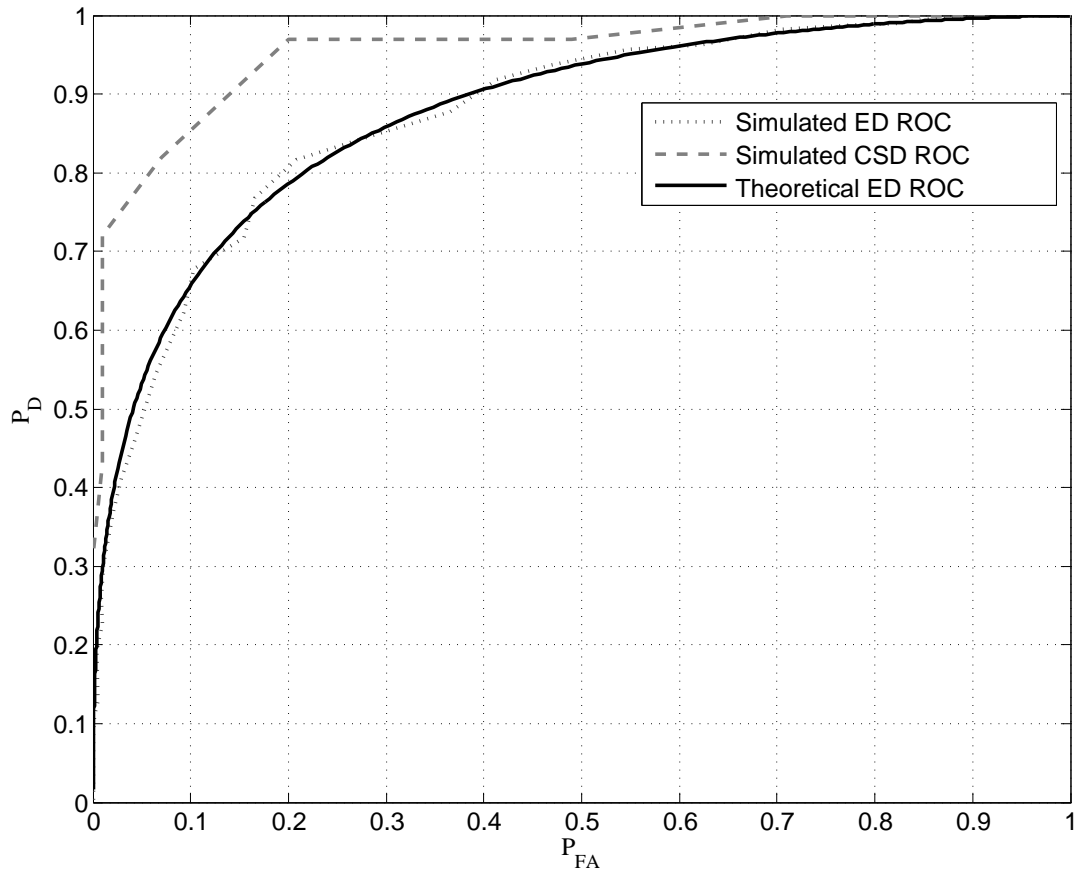


Figure 3.8: ROC Curves for comparison between spectrum sensing algorithms

3.3 Challenges in Spectrum Sensing

CR receivers are required to sense and avoid various licensed users having a dynamic power range. In low SNR scenarios, weak signal levels could mislead the detector, which increases the probability of missed detection and enables a harmful transmission in busy bands. This phenomenon occurs mainly for sensing schemes that rely on the estimation of the noise and/or signal models, where low SNR values could deteriorate the calculation of sensing parameters. Several solutions were suggested in the literature to overcome this issue. Being less complex and power efficient, blind sensing schemes are developed to achieve a comparable performance with other knowledge-based techniques.

In a cognitive receiver, RF impairments could harm the performance of the spectrum sensing algorithm by inducing unwanted frequency components in the collected signal spectrum. To mitigate the effects of such impairments, “Dirty RF” is applied on the SU receiver inducing a post-processing of the signal,

thus compensating for analog imperfections [67–69]. A robust detector, based on smart digital signal processing, should be able to digitally lower the effects of RF impairments and guarantee a high sensing accuracy. This challenge is thoroughly discussed in Chapter 5 since it is one of the main concerns of this dissertation.

The early-designed spectrum sensing algorithms aimed to detect a white space from narrow frequency bands where many emerging wireless applications require an opportunistic usage of a wideband spectrum [70–73]. Consequently, SUs are forced to scan a wide range of potential spectrum and detect available holes to be able to transmit. One of the main concern of the CR community is to conceive wideband spectrum sensing methods to replace the complicated implementation of high sampling rate ADCs, capable of down-converting wideband signals.

The selection of signal processing algorithms and their parameters reflects the speed and sensing time of the cognitive receiver. A complex signal processing algorithm should respect an optimum sensing value depending on the capabilities of the radio and its temporal characteristics in the environment. On the other hand, the ADC is considered as the primary bottle-neck of the DSP architecture speed since it controls the clock of the system. Moreover, the selection of the digital signal processing platform affects the speed of the front-end. All these parameters influence the sensing frequency and speed of cognitive radio receivers. For that, researchers focus on implementing sensing algorithms with low complexity, high speed, and flexibility in order to conceive an adaptive CR terminal.

In the following subsections, we will describe two main practical spectrum sensing challenges and recently proposed solutions. Model uncertainty and wideband sensing are studied while recent blind detectors and wideband techniques are presented. Accordingly, in the rest of this chapter, we provide an overview of the state-of-the-art of spectrum sensing algorithms that have been proposed to answer these major research challenges.

3.3.1 Blind Detectors

As per regulation specifications, secondary users are required to detect very weak licensed users in order to protect primary transmissions [74, 75]. Any missed detection will enable an unlicensed transmission on a busy channel harming the incumbent primary signal. Unfortunately, many detectors reveal a performance degradation at low SNR due to inappropriate estimation of the signal or noise models. For the ED, an estimation of the noise variance is required to select a suitable threshold. Imperfect knowledge of the noise model, especially in low SNR scenarios, will consequently deteriorate the efficiency of this algorithm. The SNR wall phenomenon also harms any detector based on the received signal's moments. Using cooperative spectrum sensing techniques or relying on calibration and compensation algorithms are possible solutions to the model uncertainty

problem [60, 76]. However, using totally blind detectors, that detect the presence of a signal without any knowledge of signal or noise parameters, is considered the ideal alternative. Two recently proposed blind detectors are described below.

Blind Eigenvalue-Based Detector

Zeng et al. [56] devised a blind detector algorithm based on the computation of the minimum and maximum eigenvalues λ_{min} and λ_{max} of the sample covariance matrix $\mathbf{R}(N_S)$. The test statistics of this maximum-minimum eigenvalue (MME) detection is simply given by:

$$\frac{\lambda_{max}}{\lambda_{min}} \underset{H_0}{\overset{H_1}{\gtrless}} \nu \quad (3.12)$$

where ν is the threshold calculated by using the number of acquired samples, the smoothing factor used for the calculation of $\mathbf{R}(N_S)$, and a selected probability of false alarm. The algorithm's steps are summarized in Table 3.1.

Table 3.1: Steps of the MME detector

Initialize: Acquire L consecutive data samples and assume that there are ($M \geq 1$) receivers (antennas), and (N_S) is the total number of collected samples.

a). Define the received vector x_n given by:

$$\mathbf{x}(n) = [x_1(n), x_2(n), \dots, x_M(n)]^T$$

b). The collection of L consecutive outputs $\hat{\mathbf{x}}_n$ is defined as:

$$\hat{\mathbf{x}}_n = [\mathbf{x}^T(n), \mathbf{x}^T(n-1), \dots, \mathbf{x}^T(n-L+1)]^T$$

c). Compute the sample covariance matrix $\mathbf{R}(N_S)$:

$$\mathbf{R}(N_S) = \frac{1}{N_S} \sum_{n=L}^{L-1+N_S} \hat{\mathbf{x}}_n \hat{\mathbf{x}}_n^H$$

d). Compute λ_{max} and λ_{min} the maximum and minimum eigenvalues of the matrix $\mathbf{R}(N_S)$.

e). Compute the threshold ν for the test statistics:

$$\nu = \frac{(\sqrt{N_S} + \sqrt{ML})^2}{(\sqrt{N_S} - \sqrt{ML})^2} \left(1 + \frac{(\sqrt{N_S} + \sqrt{ML})^{-2/3}}{(N_S ML)^{1/6}} F_1^{-1}(1 - P_{FA}) \right)$$

Where F_1 is the Tracy-Widom distribution of order 1 [77].

The decision test:

f). Decide on H_0 or H_1 by computing the ratio between λ_{max} and λ_{min} :

$$\frac{\lambda_{max}}{\lambda_{min}} \underset{H_0}{\overset{H_1}{\gtrless}} \nu$$

It is expected that noise produces small eigenvalues where as the correlation inherited in modulated signals increases the eigenvalues. The proposed test statistic does not depend on any knowledge of noise, signal or channel models, thus it is not sensitive to the model uncertainty problem. The main disadvantage of this detector is that several receiving antennas are required to achieve a good sensing performance comparable to the CSD scheme which increase the cost of a CR receiver.

The CAF Symmetry-Based Detector

This blind spectrum sensing detector is based on the symmetry property of the cyclic autocorrelation function (CAF). Benefiting from the sparsity property of CAF, the compressed sensing tool is adopted in this algorithm to reduce the computational complexity of calculating the CAF function and make it deployable in real scenarios. A test statistic is defined, without the computation of any threshold, offering a blind decision rule independent from any model estimation. Thus, the CAF symmetry-based detector proposed in [78] is selected as a first step in designing a fast, blind, wideband and robust detector. A theoretical and practical study and optimization of this detector is presented in the next chapter.

3.3.2 Wideband Spectrum Sensing

Several emerging wireless applications and regulation encourage cognitive receivers to scan a wideband spectrum to find potential spectrum holes. In contrast to the narrowband techniques mentioned above, wideband spectrum sensing methods aim to sense a frequency bandwidth exceeding the coherence bandwidth of the channel. A frequent example deals with the design of an algorithm capable of sensing the whole ultra-high-frequency (UHF) TV band (between 300 MHz and 3 GHz). Practically, wideband scanning could be performed via two different methods:

1. By using a filter bank formed by preset multiple narrowband pass filters BPFs [75]. This hardware-based solution requires more hardware components thus increasing the cost and the RF impairments harmful effect, and limiting the flexibility of the radio by fixing the number of filters. After each filter, a narrowband state-of-the-art technique is implemented. A relaxed solution was proposed and discussed in [19]. It was shown that the proposed wideband architecture implemented via few medium bands is well suited for commercial applications since it guarantees a good linearity and a low insertion loss with reduced size and cost.
2. By using sophisticated signal processing techniques. In fact, narrowband sensing techniques cannot be directly applied to scan a wideband since they are based on single binary decision for the whole spectrum. Thus,

they cannot simultaneously identify vacant channels that lie within the wideband spectrum. Recently proposed wideband spectrum sensing can be broadly categorized into two types:

- Nyquist wideband sensing processes digital signals taken at or above the Nyquist rate, e.g. the wavelet transform based technique.
- Sub-Nyquist wideband sensing acquires signals using a sampling rate lower than the Nyquist rate, e.g. the compressive sensing technique

In the following sections, two approaches to perform wideband spectrum sensing are discussed.

Wavelet Transform Based Technique

In this method, the SU transceiver scans a wideband without using a bank of narrow BPFs. Alternatively, a wideband receiver will be based on high-speed digital signal processing to search over multiple frequency bands in an adaptive manner. The obtained digital signal will be modeled as a train of consecutive narrow frequency bands as shown in Figure 3.9. To identify these bands and search for potential spectrum holes, the wavelet transform will be used to locate edges between different narrow sub-bands. The corresponding block diagram is depicted in Figure 3.10. Wavelet transform is used in mathematics to locate irregularities [71]. Consequently, it will be a good candidate to differentiate the narrow sub-bands of wideband signal [73, 79]. A wavelet edge detector is able to identify the average power level within each identified sub-band which will lead to the localization of the spectrum holes.

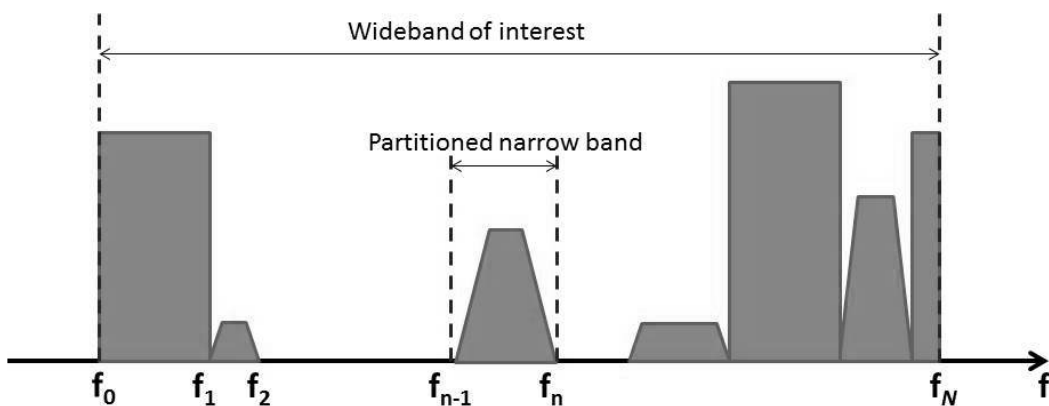


Figure 3.9: A wideband spectrum seen as a train of narrowband signals and presenting frequency irregularities

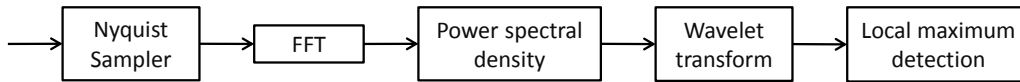


Figure 3.10: Block diagram of Wavelet transform based technique.

The analysis using wavelet transform is based on a function known as the principal wavelet ψ which has a finite energy. Wavelets are used to transform a given signal into another representation that models the information related to the signal in a more utile way. Wavelets could be manipulated in two different ways: moved along the frequency axis or stretched with a variable energy. A Wavelet transform, obtained by summing the product of the signal multiplied by the wavelet, is calculated at different spots of the signal and for different combinations of the wavelet. This calculation could be monitored to detect the irregularities of the signal by observing the different values of the wavelet transform. Unfortunately, the fast processing is not blind and requires channel and noise informations.

Compressive Sensing Technique

A major implementation challenge lies in the very high sampling rates required by conventional spectral estimation methods which have to operate at or above the Nyquist rate. However, to solve this issue, the compressive sampling CS technique is used for the acquisition of sparse signals at rates significantly lower than the Nyquist rate. Signal reconstruction is no more based on old reconstruction techniques but will be a solution to an optimization problem. Several schemes were suggested in the literature for the reconstruction of the signal: by using wavelet transforms [73], the autocorrelation of the signal [80], or advanced algorithms for sparse approximation methods [81, 82]. It is shown that such methods could preserve the adaptive response of the algorithm by offering a relatively small processing time.

Sparse approximation consists of finding a signal or a vector with sparseness property, i.e. it has a small number of nonzero elements that satisfies (approximately) a system of equations. For example, consider a linear system of equations $y = \mathbf{A}x$, where \mathbf{A} is an $n - by - M$ matrix with $n < M$. Since \mathbf{A} is over complete ($n < M$), this problem does not have a unique solution. Among all the possible solutions, if the true one is known a priori to be sparse then it happens that the sparsest, i.e. the solution x containing as many as possible zero components and satisfying $y \cong Ax$, is close to the true solution. Reducing the problem complexity to n instead of M increases the adaptation time of the

reconstruction algorithm thus provides better processing time. Relying on the sparsity assumption, this technique could not be implemented in various wide bands where several PUs can occupy the spectrum.

3.4 Conclusion

While selecting a sensing method, some trade-offs should be considered. First, the available knowledge of the characteristics of primary users are the main factor. Then, several other criteria should be investigated: cyclostationary features contained in the waveform, existence of regularly transmitted pilots, and time/frequency characteristics are all important. Other general factors such as required accuracy, sensing duration requirements, computational complexity, and network requirements are preliminary before selecting a suitable spectrum sensing algorithm.

In the thesis, we will be focusing on practical detectors characterized by the robustness against RF imperfections degradations, the blindness, the fast decision making, and the accuracy. For that, the next chapter describes the blind CAF symmetry-based detector and its practical optimized implementation on the USRP N210. Later chapters focus on the sensitivity of this detector against RF impairments and propose a combined sensing and mitigation scheme.

Chapter 4

Theoretical and Experimental Study of the Blind SPCAF Detector

4.1 Introduction

The enabler stage of the cognitive behavior in smart receivers is the spectrum sensing stage that should deliver accurate results independently from the possible practical imperfections. In the literature, most famous sensing algorithms require full or partial knowledge of the channel or noise models [41]. The energy detector, which is the classical and widely used detector, estimates the noise model for the calculation of its basic parameter [60]. The ED is simply based on capturing the power of the received signal and comparing it to a threshold, calculated from the estimation of the noise level. Thus, in low signal-to-noise ratio (SNR) environments, the calculation of the threshold could be harmed by faulty values which delivers detection errors. Other detectors are sensitive to the channel model and their performance are deteriorated in fast fading scenarios [83].

Due to its low computational complexity, it is common to deploy the ED, also known as radiometer, in most practical cognitive terminals. However, it was proved theoretically that the cyclostationarity feature based detectors can deliver more accurate decisions but have a more complex architecture and require more knowledge of the channel and noise models [50]. To enhance the sensing efficiency in real-world CR receivers, we propose to implement and test the blind detector based on the symmetry property of the cyclic autocorrelation function (SPCAF) [78]. This algorithm was selected because of its reduced complexity, complete blindness, and accurate results since it is based on extracting the cyclostationarity feature of the received signal.

In this chapter, several setups were built to compare the performance of the ED and the SPCAF detectors. The test-beds are composed of a Universal

Software Radio Peripheral (USRP N210) [84], a Software Defined Radio (SDR) transceiver platform, acting as the cognitive receiver, where all the intelligent process is implemented through a host computer. At the transmitter side, various scenarios were adopted to test and compare these detectors. Accordingly, experimental results are measured in various bands such as the 802.11ac bands, the 3G network band, DVB-T bands, and bands selected by a transmitting USRP.

To validate the simulated performance and complexity of the SPCAF, we present in this chapter a practical study characterized by real time measurements, code optimization and thorough testing. Unfortunately, theoretical work tested with simulations is not sufficient in CR scenarios and needs to be validated considering the real physical limitations of the hardware. For that, the blind spectrum sensing detector based on the symmetry property of the CAF function is implemented to exploit its high performance and low sensing time. The complexity of this algorithm, which influences its sensing time, was monitored throughout the experiments and reduced by applying code optimization techniques. A different set of parameters is chosen in each experiment to describe the algorithm sensitivity.

This chapter is organized as follows. Section 4.2 introduces the system model of the blind SPCAF sensing method. After describing the experimental setup in Section 4.3, we show the various test-beds in Section 4.4 and the measured results and corresponding discussions in Section 4.5 followed by the chapter's conclusion.

4.2 Theoretical Formulation of the SPCAF

In CR networks, the cyclostationarity is the feature for detecting a random signal with a particular modulation type in a background of noise and other modulated signals [48].

The signal $y(t)$ is said to be cyclostationary if its autocorrelation function $r_{yy}(t, \tau)$ is periodic with period T_0 , with respect to t . Accordingly,

$$r_{yy}(t, \tau) = r_{yy}(t + T_0, \tau) \quad (4.1)$$

These periodicities are examined using the cyclic autocorrelation function (CAF)

$$R_{yy}^{\alpha}(\tau) = \lim_{T \rightarrow \infty} \frac{1}{T} \sum_{t=0}^{T-1} r_{yy}(t, \tau) \exp(-j2\pi\alpha t) \quad (4.2)$$

In [78], Khalaf et al. recommended using the sparse property of the CAF to reduce the complexity of the cyclostationarity feature detector. An estimation method that utilizes the sparseness constraint is applied to estimate the CAF. Finally, to ensure the blindness of the algorithm, a symmetry test is checked on the estimated version of the CAF.

Firstly, it is shown from equation 4.2 that the cyclic autocorrelation vector \mathbf{R}_{yy}^α for a given delay τ_0 could be estimated as a scaled version of the Discrete Fourier Transform (DFT) of the autocorrelation vector \mathbf{f}_{τ_0} :

$$\mathbf{f}_\tau = [f_\tau(0), f_\tau(1), \dots, f_\tau(N-1)]^T \text{ where } f_\tau(t) = y(t)y(t+\tau) \quad (4.3)$$

$$\mathbf{R}_{yy}^\alpha(\tau_0) = \frac{1}{N} DFT(\mathbf{f}_{\tau_0}) \quad (4.4)$$

To reduce the complexity of the calculation of the cyclic autocorrelation vector, its reconstruction over $\alpha \in [-\alpha_{max}, \alpha_{max}]$ will be done using n data samples with $n \ll N$, and applying compressed sensing. The key idea of compressed sensing is to recover a sparse signal, i.e. CAF in our case, from a small number of samples by optimization. Thus, the problem is to compute the sparse coefficient vector \mathbf{R}_{yy}^α with respect to an over-complete system. The system representing our problem is shown below:

$$A\mathbf{r}^{(\tau_0)} = \mathbf{b}^{(\tau_0)} \quad (4.5)$$

where A is an n by N matrix representing the Inverse Discrete Fourier Transform (IDFT) having the (p, q) element equal to $e^{2i\pi(p-1)(q-1)/N}$, and $\mathbf{b}^{(\tau_0)}$ is an n -dimension vector formed by the n^{th} first elements of \mathbf{f}_{τ_0} . The solution $\mathbf{r}^{(\tau_0)}$ is an N -dimensional vector, and is the solution of the problem that estimates the cyclic autocorrelation vector.

A sparse representation of such problem is:

$$\hat{\mathbf{r}}^{(\tau_0)} = \min \|\mathbf{r}^{(\tau_0)}\|_0, \text{ s. t. } A\mathbf{r}^{(\tau_0)} = \mathbf{b}^{(\tau_0)} \quad (4.6)$$

where $\|\cdot\|_0$ is the l_0 -norm defined as the number of non zero elements in the vector. To solve this sparse problem, the SPCAF algorithm uses an iterative optimization technique called Orthogonal Matching Pursuit (OMP) [82] that delivers an approximated solution of the following problem:

$$\hat{\mathbf{r}}^{(\tau_0)} = \min \|\mathbf{r}^{(\tau_0)}\|_0, \text{ s. t. } \|A\mathbf{r}^{(\tau_0)} - \mathbf{b}^{(\tau_0)}\|_2 \leq \rho \quad (4.7)$$

OMP is based on an iterative procedure that calculates the least mean square in order to minimize the error and update the residual. It uses a new atom after each iteration to guarantee a fast convergence of the algorithm. The steps of OMP are presented thoroughly in Table 4.1.

The last step of the algorithm is to check the symmetry of the estimated cyclic autocorrelation vector. A limited number of non-zero elements are selected and their symmetry in terms of α is observed. To model the symmetry test, a symmetry index $IND_{sym}^{(\tau_0)}$ is calculated by ignoring the first amplitude that

corresponds to $\alpha = 0$, and measuring the mean value of the abscissa of the remaining L non zero elements. The corresponding formula is shown below:

$$IND_{sym}^{(\tau_0)} = \frac{1}{L} \sum_{i=1}^L \alpha_i \quad (4.8)$$

It is shown that only modulated signals that have some inherited redundancy have a symmetric CAF and succeed in the symmetry test having $IND_{sym}^{(\tau_0)} = 0$. To achieve an efficient decision, the OMP algorithm will be repeated for several values of τ and then an equivalent index will be used to make the final decision. The equivalent index, shown below, is calculated by making a soft decision that combines all the indexes.

$$IND_{sym}^{(equ)} = \frac{1}{M} \sum_{i=1}^M |IND_{sym}^{(\tau_i)}| \quad (4.9)$$

To control the probability of false alarm and missed detection, a positive threshold ξ could be used to decide between hypothesis H_0 or H_1 , by applying:

$$IND_{sym}^{(equ)} < \xi \quad (4.10)$$

Varying ξ leads to the ROC curve of the SPCAF algorithm illustrated in Figure 4.1 for two values of the number n of samples and at $SNR = 0dB$. The detailed SPCAF algorithm is given in Table 4.1.

Table 4.1: Steps of the SPCAF detector

Initialize: Acquire n data samples of the received signal y
Set L the number of OMP iterations
Set M the number of delays τ s to calculate the autocorrelation vector

For M different values of τ ,

a). Calculate the autocorrelation vector \mathbf{f}_{τ_0} given by:

$$\mathbf{f}_{\tau} = [f_{\tau}(0), f_{\tau}(1), \dots, f_{\tau}(N - 1)]^T$$
where $f_{\tau}(t) = y(t)y(t + \tau)$

b). Calculate the elements of the reduced matrix A :

$$a_{(p,q)} e^{2i\pi(p-1)(q-1)/N}$$

For L iterations

The OMP algorithm

c). Run an iteration of the OMP algorithm to solve the following system of equations: $A\mathbf{r}_{\tau} = \mathbf{f}_{\tau}$

d). Each iteration estimates one sample of the vector $\hat{\mathbf{r}}_{\tau}$ (estimated of the CAF) as follows:

- 1). Let $v_t = i$, where a_i gives the solution of $\langle r_t, a_t \rangle$, where a_k are the row vectors of A .
- 2). Update the set V_t with v_t : $V_t = V_{t-1} \cup \{v_t\}$.
- 3). Solve the least-squares problem: $\min \|\mathbf{b} - \sum_{j=1}^t c(v_j)a_{v_j}\|_2$
- 4). Calculate the new residual using c : $res_t = res_{t-1} - \sum_{j=1}^t c(v_j)a_{v_j}$

End For

Symmetry check

e). Check the symmetry of the vector $\hat{\mathbf{r}}_{\tau}$ by observing the index $IND_{sym}^{(\tau_0)}$ in 4.8

End For

Equivalent symmetry check :
Calculate the equivalent index and decide H_1 if:

$$IND_{sym}^{(equ)} = \sum_{i=1}^M |IND_{sym}^{(\tau_i)}| > \xi.$$

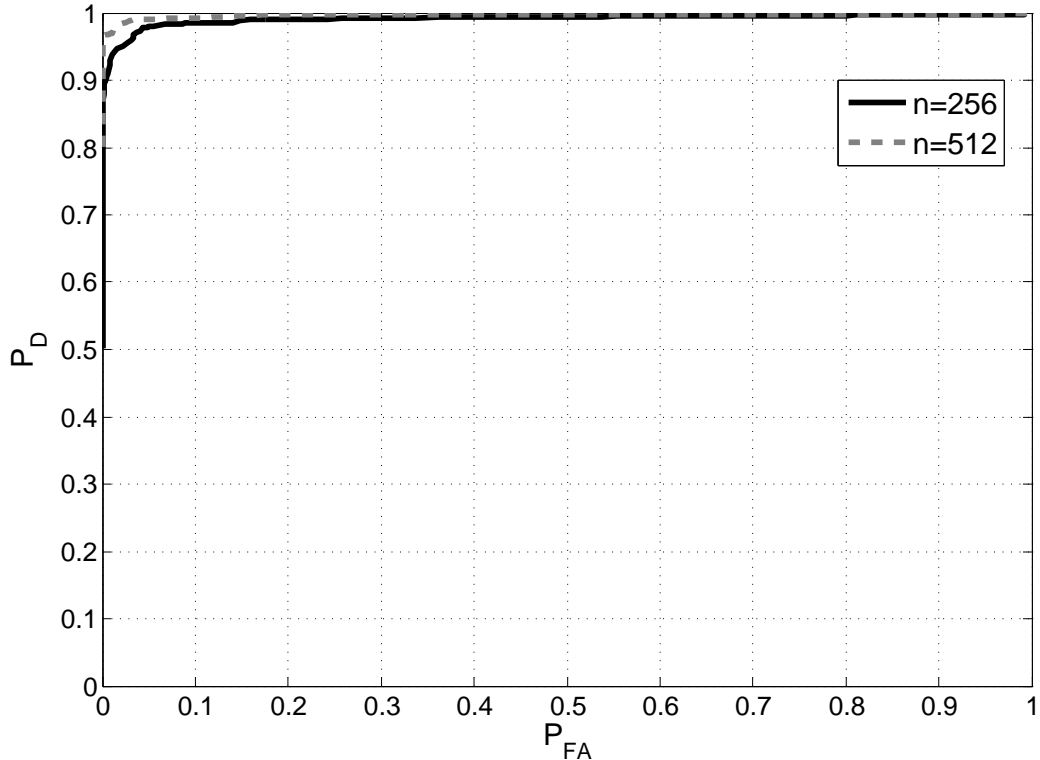


Figure 4.1: ROC of the SPCAF detector for a BPSK signal at SNR = 0dB

In summary, the adopted algorithm is based on observing the symmetry property of the cyclic autocorrelation function (CAF). To avoid the complexity in the calculation of the CAF of the received signal, the compressed sensing tool is used to construct an estimate of the function. Accordingly, a cyclic autocorrelation vector is calculated by solving an under-determined system of equations. Such estimation is possible since the CAF is theoretically sparse and symmetric. A theoretical plot of the norm of the CAF of a BPSK signal is shown in Figure 4.2. Thus, to decrease the complexity of the calculation, a reduced dictionary matrix is constructed with the minimal number of elements. Finally, an iterative algorithm is used to compute the cyclic autocorrelation vector by performing few iterations. In this algorithm, the orthogonal matching pursuit (OMP) is utilized. It is shown that only 3 iterations of OMP are sufficient to perform the symmetry check. The obtained cyclic autocorrelation vector is composed of only 3 non-zero elements as shown in the estimated CAF plotted in Figure 4.3 where their indexes are observed to check if the CAF is symmetric. A positive decision corresponds to a symmetric CAF, thus to a cyclostationary signal. In the measurements, we set $\xi = 0$ since it delivers adequate decisions and it optimizes the complexity of the algorithm. $\xi = 0$ means that if the CAF estimated for one value of τ is symmetric, the signal is directly considered cyclostationary. We summarize these

steps in Figure 4.4.

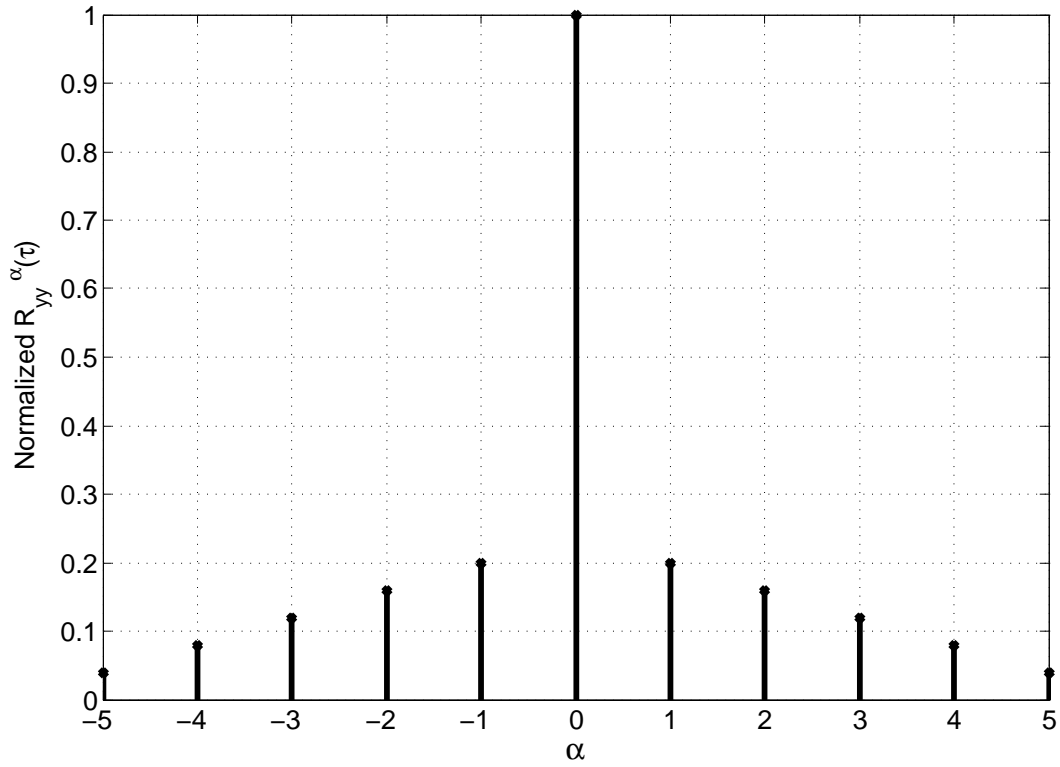


Figure 4.2: Theoretical plot of the norm of the CAF of a BPSK signal

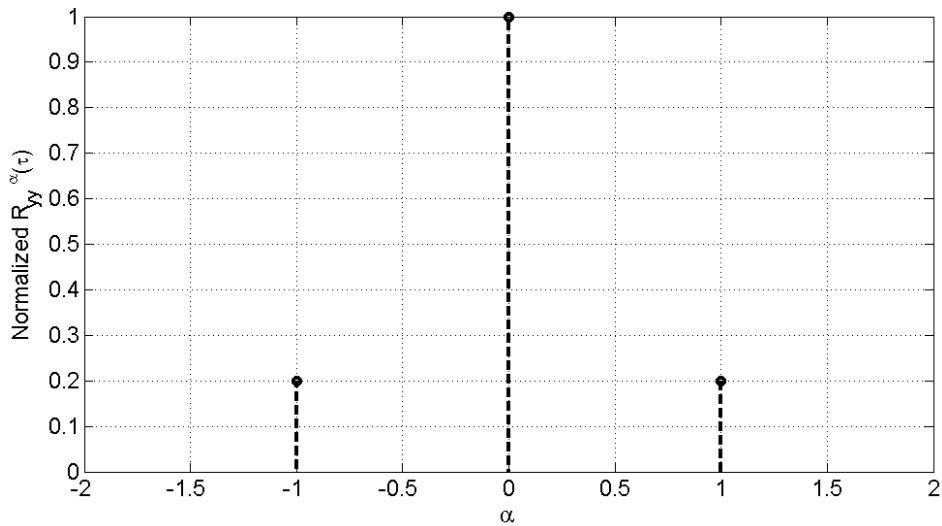


Figure 4.3: Estimated plot of the norm of the CAF of a BPSK signal

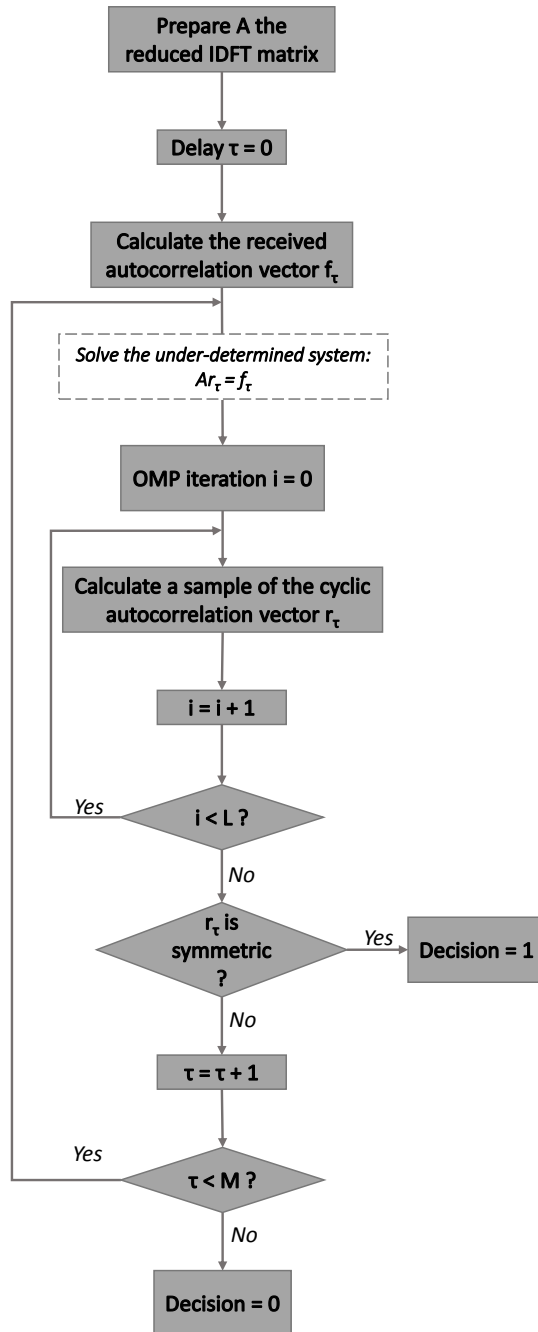


Figure 4.4: Block Diagram of the SPCAF algorithm

4.3 Experimental Implementation

In this section, we present the main components of our test-bed. The test-bed can be divided into two main parts i.e. software and hardware parts. The hardware

part is in charge of the RF and sampling processing while the radio transceivers physical layer is software driven, running on a computer.

In this work, our software part is comprised of GNU Radio to implement both ED and SPCAF spectrum sensing algorithms. The GNU Radio is an open source software toolkit for software defined radio. This toolkit provides a number of radio components, pre-written in Python or C++ programming languages, which can communicate with each others using various data types. Moreover, GNU Radio offers a simple and sophisticated graphical design environment, known as GNU Radio Companion (GRC), which enables users to create signal flow graphs and automatically generates Python source code. Designers can write their own signal processing blocks if needed and integrate them in GRC. Python is an object-oriented scripting language that runs on Linux/windows and has great support for interfacing with C++ code. This feature is often used in GNU Radio, where the signal processing blocks are written in C++, and Python is used to glue them together and control the digital data flow. This is done using Simplified Wrapper and Interface Generator (SWIG) by creating shared libraries common for both Python and C++. In other words, SWIG is an interface compiler that connects programs written in C++ with Python as shown in Figure 4.5. GNU Radio can work as a simulation environment but it can also

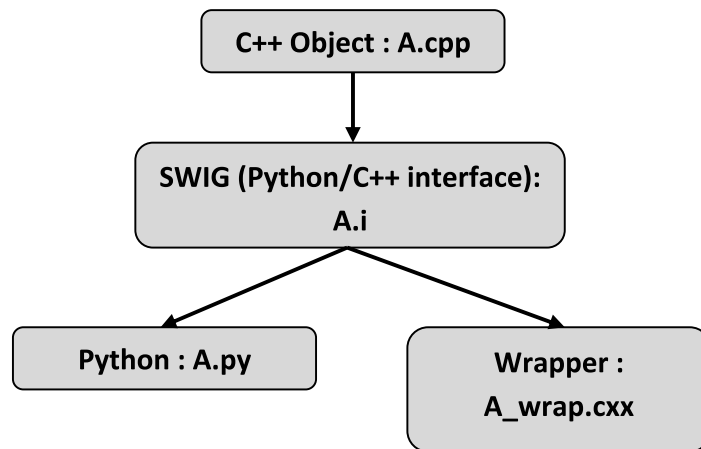


Figure 4.5: GNU Radio interface through SWIG

create a real radio system using SDR platforms. A snapshot of the receiver model designed in GNU radio is shown in Figure 4.6.

For the hardware part, we use USRP N210 (Universal Software Radio Peripheral) motherboard as the radio frequency interface with a selected daughterboard and a wide band antenna to perform spectrum sensing tests. On host processors, where all signal processing blocks take place, the GRC or GNU Radio

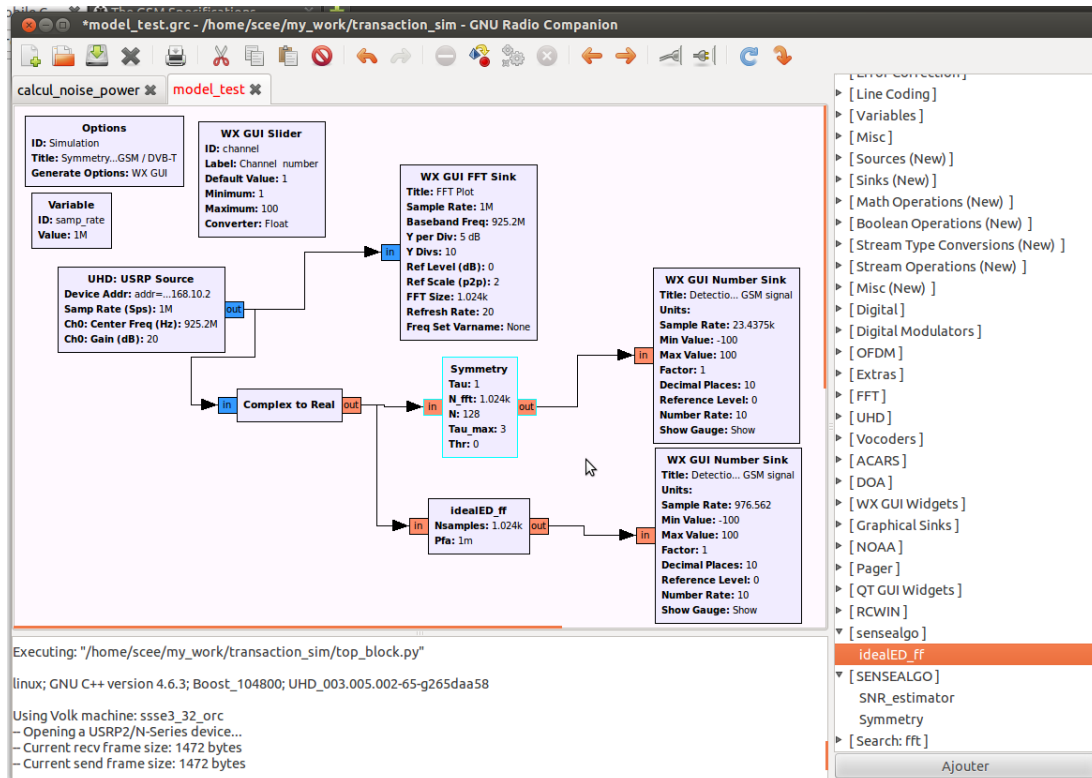


Figure 4.6: A snapshot of the GNU radio receiver model with ED and SPCAF detectors blocks.

use Universal Hardware Drivers (UHD) to send and receive signals to/from the USRP N210 board via Gigabit Ethernet link as shown in Figure 4.7. Figure 4.8 shows a photo of the implemented test-bed.

To minimize the complexity of this algorithm, code optimization is applied on the C++ code level. The main complex node of the code was the generation of the IDFT matrix A (see Equation 4.5), as concluded from the complexity tracking tool in GNU Radio. For this reason, look up tables are created and stored before running the experiments. These modifications provided fast decisions of the detector. Another major improvement of the computational complexity of this algorithm is discussed in Chapter 6.

4.4 Experimental Results

To record and analyze real-world measurements, the platform used in academia and research, i.e. USRP, is acting as the cognitive receiver. On the computer host, the open source software toolkit GNU Radio is installed [85]. Using the graphical interface GNU Radio Companion (GRC), a user can use a built-in block to communicate with the USRP by setting receiving parameters and acquiring

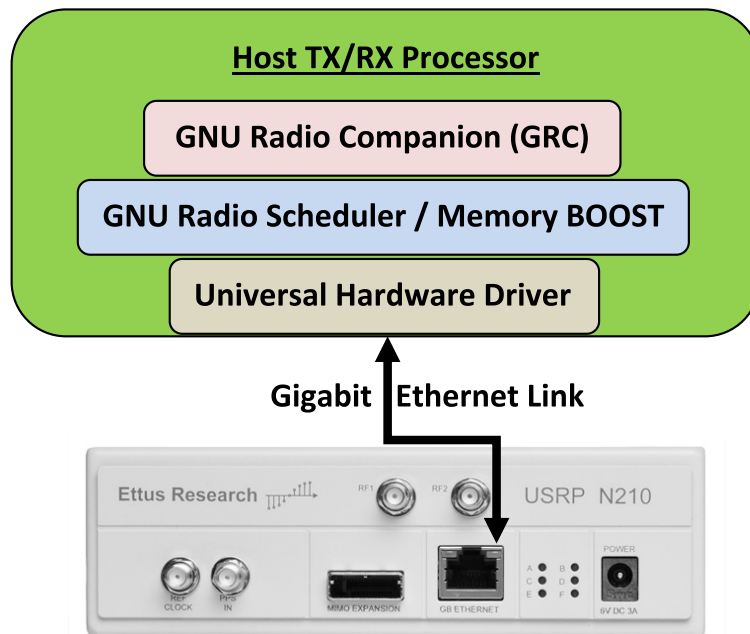


Figure 4.7: Hardware/Software platform

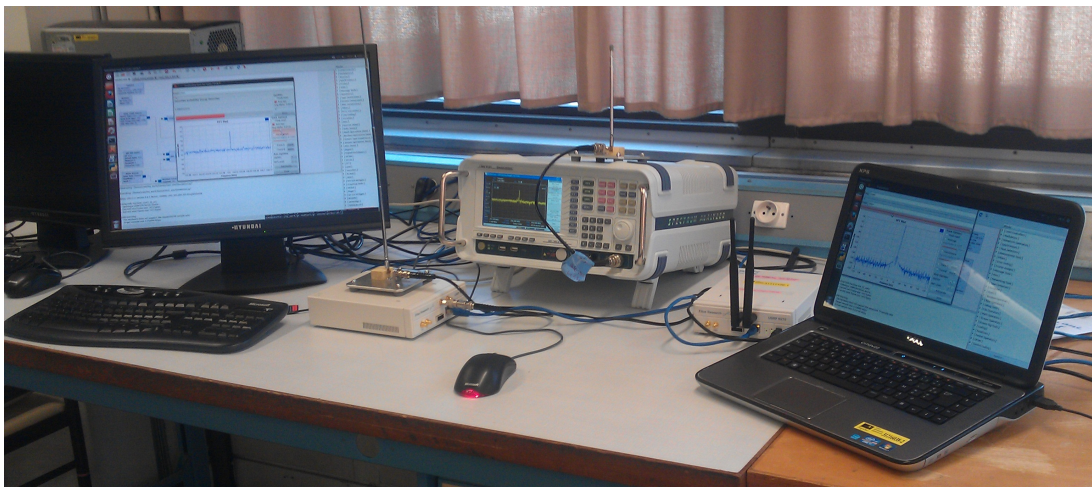


Figure 4.8: Photo of the implemented testbed to test the performance of SPCAF

received data. A library of communication blocks is available to process the data and the capability to create specific blocks is also ensured via C++ programming. The algorithms of the SPCAF and the ED are implemented as out-of-tree modules blocks and embedded in the GRC to process the received signals from the USRP and deliver binary decisions.

Firstly, measurements were recorded to estimate the signal-to-noise ratio SNR of the test-bed environment. Next, three different scenarios deployed to compare the SPCAF and the ED are tested. The idea behind these various

setups is to test the efficiency of these detectors in multiple environments and at different frequencies. This will demonstrate the efficiency of the SPCAF, making it suitable for practical implementations. The last experiments focus on testing the SPCAF detector while varying its parameters.

4.4.1 SNR Estimation

To properly present the detection performance at different signal to noise ratio (SNR) levels, we conducted measurements to estimate SNR following the steps below:

- STEP1: Turn the transmitter OFF and measure the power of the received signal and set it to the noise power (σ_n^2).
- STEP2: Turn the transmitter ON and measure the power of the received signal and set it to $\sigma_{s(A)}^2$ where A represents the transmission power level. Repeat the measurement several times in order to obtain a better estimate.
- STEP3: Once the noise power and the received power are computed, the SNR at the receiver is calculated as follows:

$$SNR_{(A)dB} = 10 \log_{10} \left(\frac{\sigma_{s(A)}^2 - \sigma_n^2}{\sigma_n^2} \right) \quad (4.11)$$

Unfortunately, the noise power at the receiver may vary for several reasons, such as the thermal noise of the different operational stages in the receiver and another interfering transmitter in the same or an adjacent frequency band. Additional care was taken to keep the received noise power as constant as possible in order to focus on the performance of the algorithm. Therefore, the measurements have been conducted in an environment where the interference has been limited, and the carrier frequency and the receiver gain were kept constant.

4.4.2 Scenario 1: USRP Signals

In this scenario, we totally control the transmission parameters by using another USRP as the primary user. As illustrated in Figure 4.9, the transmitting USRP N210, with the SBX daughter-board operating from 0.4 to 4.4 GHz is the primary user transmitting over the 2.45 GHz band. The receiving USRP is attached with the daughter-board XCVR2450 operating at 2.4-2.5 GHz and 4.9-5.9 GHz. A BPSK signal is transmitted and SNR values are controlled by varying the power level of the transmitted signal at the GRC of the computer host connected to the transmitting USRP.

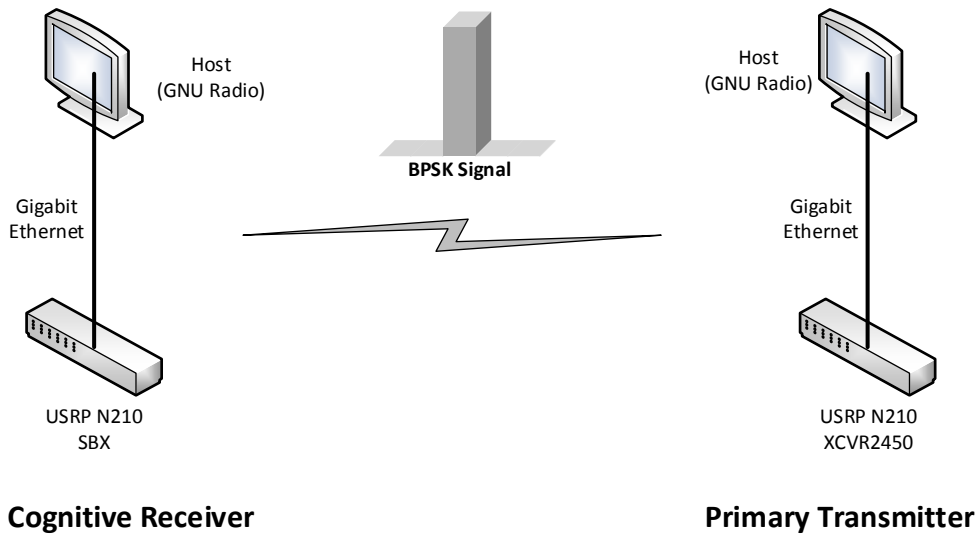


Figure 4.9: Sketch of scenario 1: USRP Signals

4.4.3 Scenario 2: 3G Network and DVB-T

Unlike the previous scenario where the transmitter is one we control, in this section we use the test-bed to sense for externally-transmitted signals. As sketched in Figure 4.10, the 2.122 GHz 3G band is sensed in different locations. This carrier was set as the downlink frequency used in the laboratory area by many measurements recorded in this field. To capture this signal, the SBX daughter-board operating at 0.4-4.4 GHz is mounted in the receiving USRP. Another similar experiment was conducted in Supelec, France to observe the SPCAF performance in DVB-T scenarios on the UHF band.

4.4.4 Scenario 3: 802.11ac Indoor Channel

In this scenario, we shift to a higher frequency range by recording measurements at 5.24 GHz. The dual band wireless access point (WAP) Linksys N300 [86] is considered as the primary transmitter. The receiving USRP is targeting the 802.11ac indoor channel number 48 by using the XCVR2450 daughter-board operating at 2.4-2.5 GHz and 4.9-5.9 GHz. On the other hand, a Galaxy S4 smart-phone [87] compatible with the newly deployed 802.11ac standard is used as a secondary receiver. In fact, a communication is needed between the smart-phone and the access point to ensure that the channel is always occupied. In the different experiments conducted in this scenario, the wireless meter of the Galaxy S4 is observed to evaluate the signal strength. The experiments described in Table 4.2 and Fig-

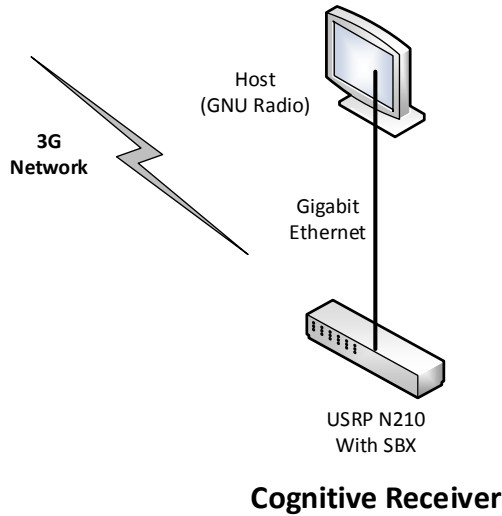


Figure 4.10: Sketch of scenario 2: 3G Network

Figure 4.11 are adopted to compare the decisions of the algorithms at several SNR values.

Experiment	(a)	(b)	(c)	(d)	(e)
Distance between WAP and USRP in m	1	2	2	3	4
Number of walls between WAP and USRP	0	0	1	1	2
Number of bars in S4 wireless meter	4	3	2	1	0
Connection quality in S4	Excellent	Good	Low	Very Low	Not Connected
Estimated SNR value in dB	40	30	20	10	5

Table 4.2: Parameters of the experiments at 802.11ac indoor channel

4.5 Results and Discussions

In this section, results of the described scenarios are presented to compare the performance of the algorithms. The main advantage of blind detectors is their sustainability in low SNR scenarios. To highlight this advantage, the detectors are tested with different SNR values by varying the power level of the transmitter. At very low power levels, the ED loses its performance because of the bad estimation of the SNR which leads to wrong threshold calculations. This could be observed by measuring the probability of detection P_D , a metric commonly used to evaluate the performance of a sensing scheme. In each scenario, P_D versus SNR is recorded via several measurements conducted in our labs.

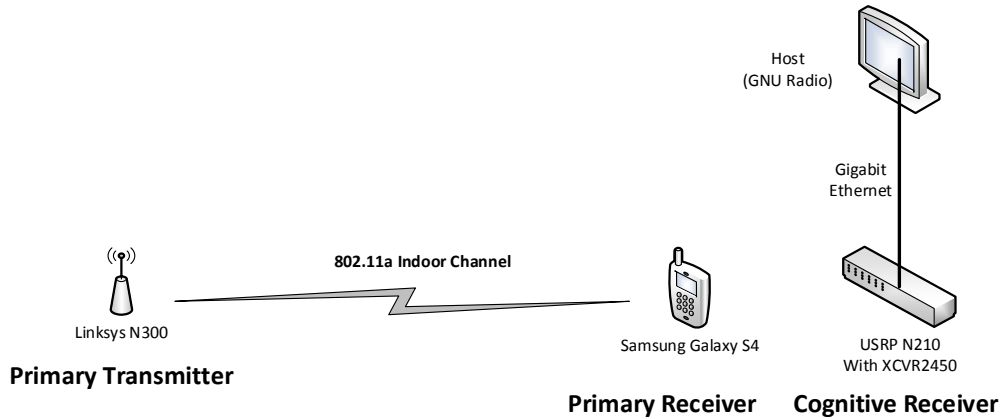


Figure 4.11: Sketch of scenario 3: 802.11ac indoor channel

The measurements are processed for a sufficient time to record more than 1000 decisions for each setup. The probability of detection is then calculated according to the collected binary decisions. Obtained results are presented and discussed in the following sections.

4.5.1 Scenario 1: USRP Signals

The generated BPSK signal is successfully captured at the receiving USRP and communicated to the detection blocks. Figure 4.12 shows the obtained plot of detection probability versus SNR. This demonstrates the efficiency of the SPCAF and the high sensitivity of ED in low SNR scenarios. It is also concluded from the measurements that the probability of false alarm (P_{FA}) is approximately equal to 0.0078 for both detectors. This estimate value is measured while monitoring the decisions of the detectors when our transmitter is turned OFF. P_{FA} is approximately the ratio between the positive decisions and the total number of decisions. Another important point to note is that the SPCAF uses far less samples to perform detection compared to the ED.

4.5.2 Scenario 2: 3G Network and DVB-T

For this scenario, comparing the algorithms with a large range of SNR is not feasible since the primary transmitter is an uncontrollable incumbent signal. The sensing was performed at different spots where the SNR varied from -2 to -20 dB. The probability of detection is computed in the different experiments. The results show that both ED and SPCAF detectors successfully detect the signal's presence in an occupied channel with a probability of detection of 1.

Another similar experiment was built in Supelec Labs, France where we performed sensing for DVB-T signals in the UHF band while the receiver's

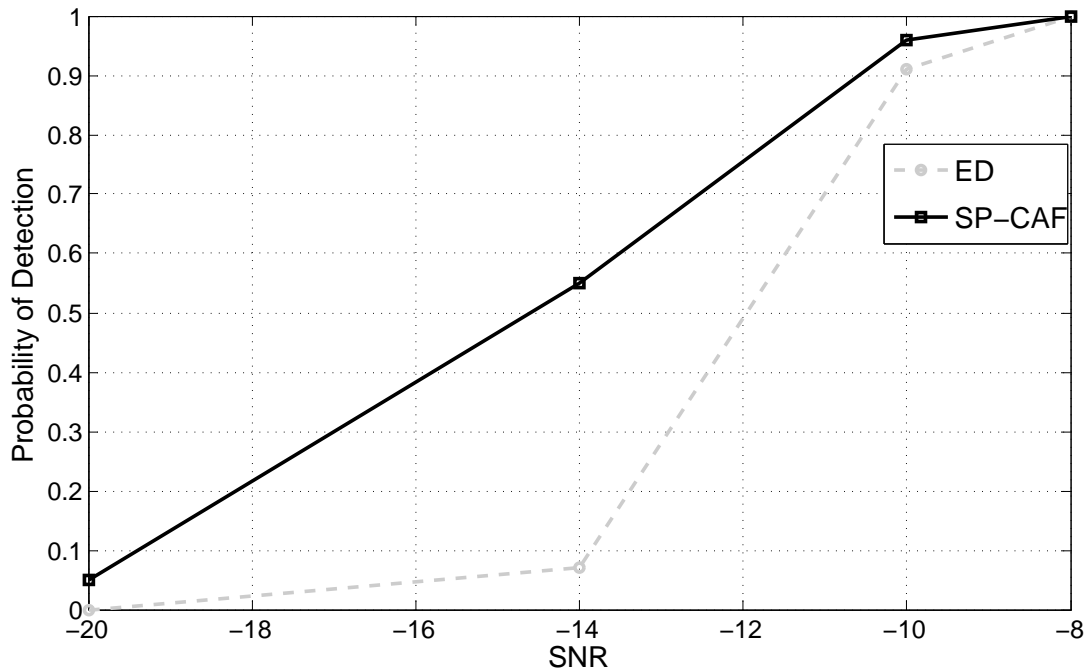


Figure 4.12: Probability of Detection versus SNR for scenario 1

carrier frequency is adjusted over the UHF band according to $306.188MHz + (ChannelNumber) * 8MHz$ using the USRPs in Supelec Labs. Note that in France the channel number varies from 21 to 69, and each DVB-T channel has a bandwidth of 8MHz. Figure 4.13 shows that the SPCAF detector successfully detects the signal present in channel number 21.

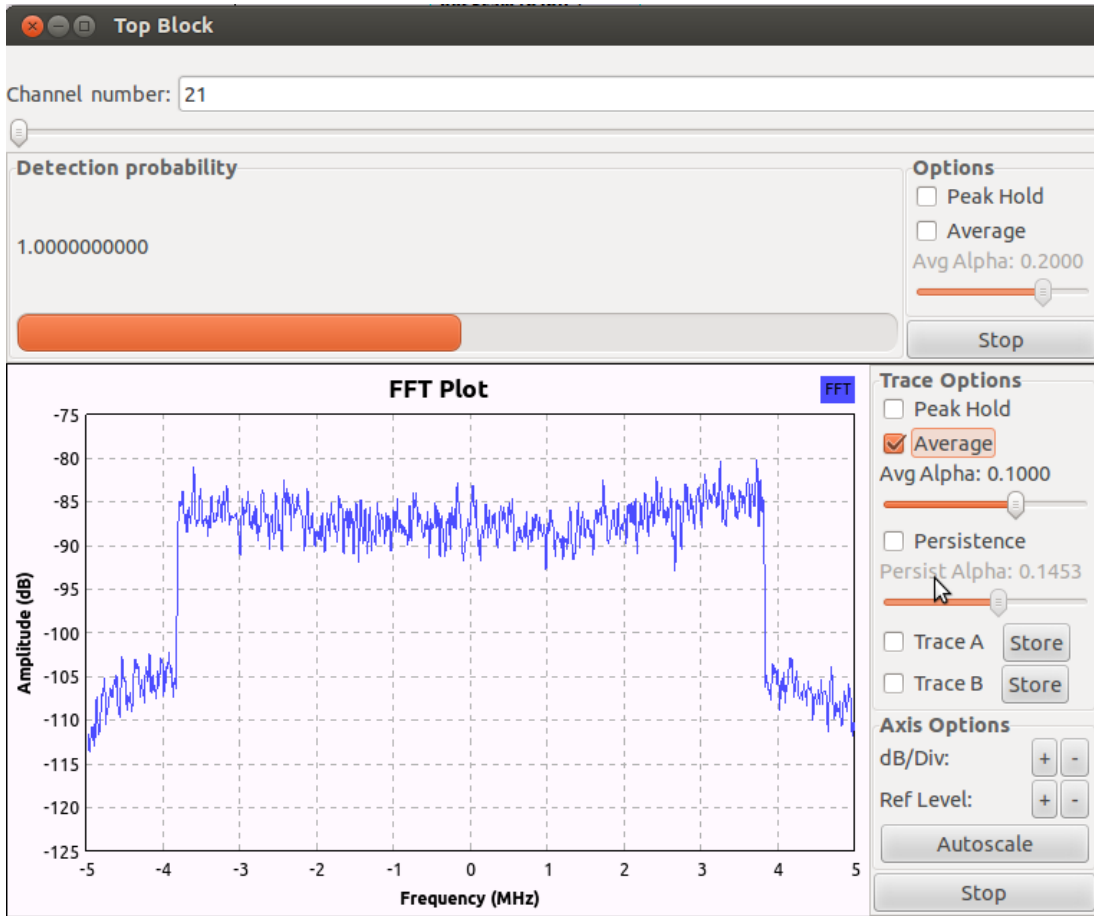


Figure 4.13: Probability of detection of the SPCAF detector in DVB-T scenarios.

The results presented in Figure 4.13 highlight the performance of SPCAF detector in terms of detection probability for real signals. On the other hand, to efficiently compare different detectors, the (P_{FA}) should be considered. In order to compute the P_{FA} for SPCAF detector, we perform the sensing of DVB-T signal in channel number 40 since it has no DVB-T signal. However, Figure 4.14 shows that the SPCAF detects a DVB-T signal with an approximate probability $P_{FA} = 0.0078$.

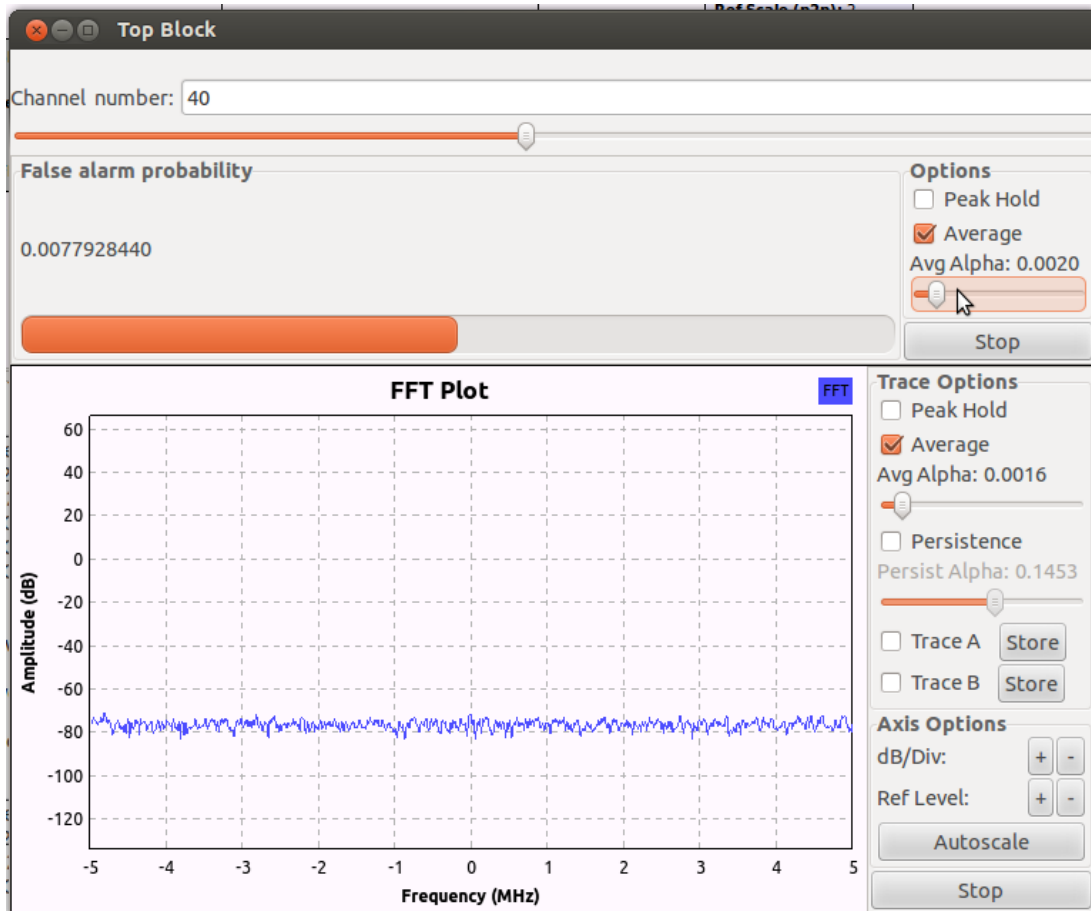


Figure 4.14: Probability of false alarm of the SPCAF detector in DVB-T scenarios.

It is very important to note that the probability of false detection for the SPCAF is very small compared to the DVB-T signals detectors presented in [88]. From the above listed experimental results, it can be concluded that the performance of the SPCAF detector is efficient for real signals, confirmed by its high detection probability and low probability of false alarm.

4.5.3 Scenario 3: 802.11ac Indoor Channel

When the communication between the smart-phone and the WAP begins, the communicated signal is received by the USRP. Afterwards, the detection blocks deliver binary decisions collected to compute the P_D . After performing all the experiments described in Section 4.4.4, the results in Figure 4.15 prove the efficiency of the blind detector. It is clear that SPCAF outperforms the classical ED in all the experiments.

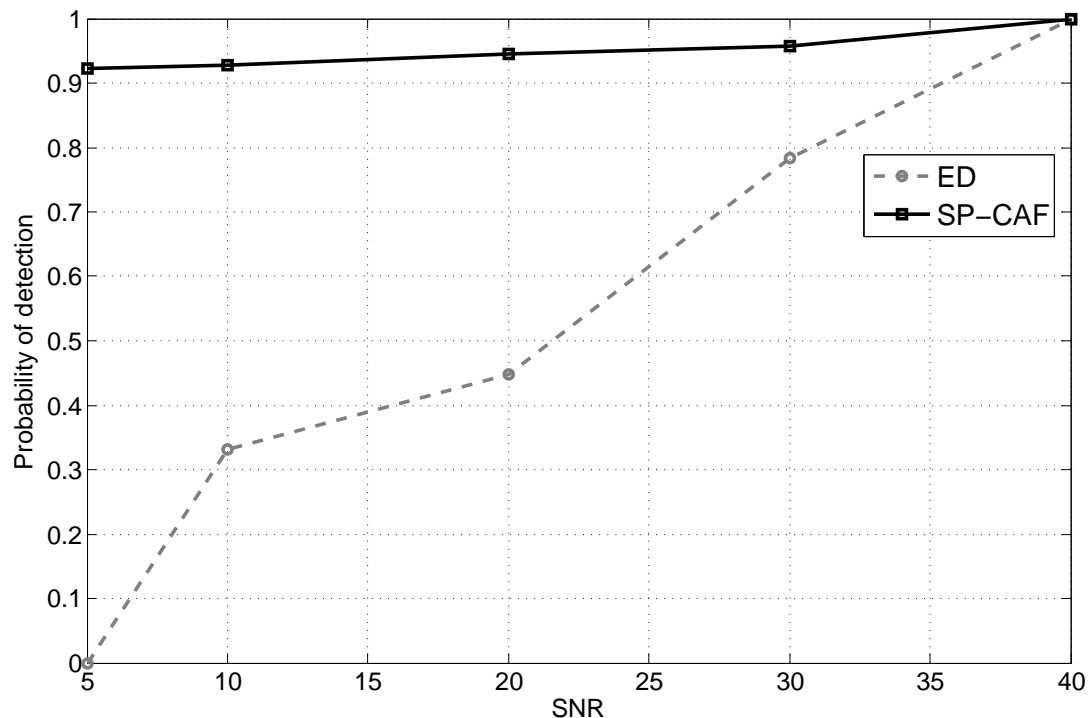


Figure 4.15: Probability of Detection versus SNR for scenario 3

4.5.4 Detection Performance of SPCAF with Different Parameters

In this section, we only focus on the SPCAF detector performance by showing the impact of its different parameters. Mainly, three parameters have an important effect on our detector's efficiency, namely:

- The number of received samples used for detection (n)
- The FFT length ($N_{fft} = N$)
- The maximum value of the delay τ (Equation 4.1) denoted as τ_{max}

In these test scenarios, the transmitted signal is sinusoidal and different parameters are changed successively. The measured probability of false alarm (P_{FA}) is equal to 0.119. First, increasing the number of received samples (n) leads to a better detection probability, as shown in Figure 4.16. In this test scenario, the FFT length is $N_{fft} = 1024$ and τ_{max} is set equal to 3. However, the curves are plotted for $n = 128$ and $n = 256$.

This behavior is quite obvious and self-explanatory since increasing the number of samples requires more sensing time and provides more information, thus a better performance. In Figure 4.17, the detection probability P_d is plotted

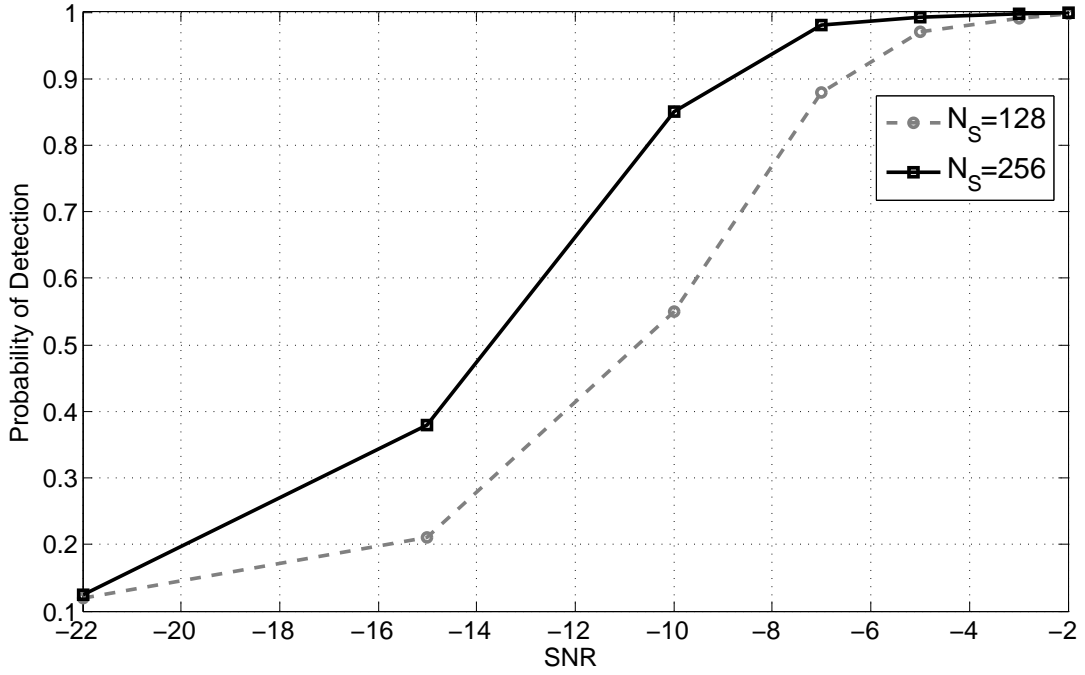


Figure 4.16: Effect of number of received samples on detection performance of SPCAF.

for different FFT lengths i.e. $N_{fft} = 512$ and 1024 . In this case, n is constant and is equal to 256 and τ_{max} remains equal to 3. This Figure shows that the detection probability ameliorates with increased FFT length. As mentioned in section 4.2, the size of the IDFT matrix is $n \times N_{fft}$. Therefore, increasing N_{fft} increases the resolution of the estimated cyclic autocorrelation vector whose symmetry will be checked. Consequently, the detection of the symmetry property of the cyclic autocorrelation function is improved with a more accurate estimation of the CAF.

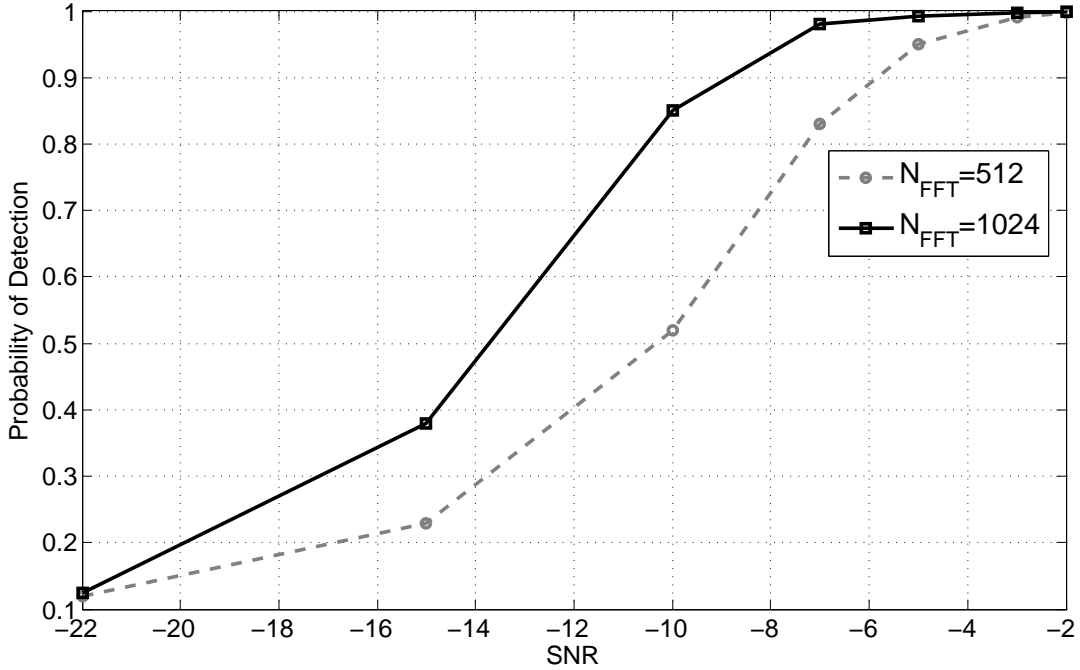


Figure 4.17: Effect of FFT length on the detection performance of SPCAF.

Finally, in Figure 4.18 the impact of τ_{max} on the SPCAF performance is shown. In this case, $n = 256$ and $N_{fft} = 1024$. The probability of detection is plotted for $\tau_{max} = 3$ and 5. For $\tau_{max} = 3$, the cyclic autocorrelation vector is estimated with three values of delay τ , where as for $\tau_{max} = 5$, the estimation is performed with 5 values of delay τ . While increasing τ_{max} , the estimation of the cyclic autocorrelation vector improves with a higher number of iterations, which results in a better decision on its symmetry. This is shown in Figure 4.18, where the detection performance of SPCAF detector improves with a larger τ_{max} .

4.6 Conclusion

In this chapter, we have described the real performance of a blind detector that employs the symmetry property of the cyclic autocorrelation function to perform signal detection. The algorithm is based on the application of compressed sensing to recover the sparse cyclic autocorrelation function (CAF) in the cyclic frequency domain. In this study, we have mainly focused on the real implementation of the proposed symmetry property of cyclic autocorrelation function based detector (SPCAF) sensing algorithm. Experimental tests were done to compare it with the classical energy detector. The implementation is carried out using GNU Radio and USRP N210 platforms. It has been shown through experimental results that the SPCAF does not only require less samples than the classical energy

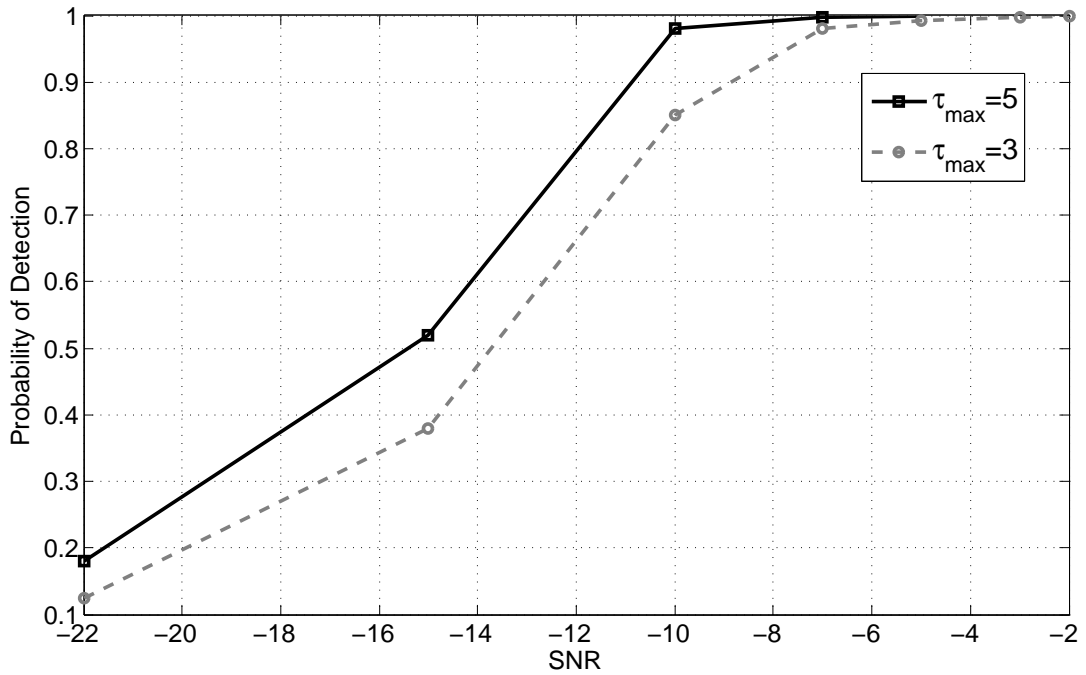


Figure 4.18: Effect of maximum value delay τ on detection performance of SP-CAF.

detector but also proves to be more efficient. Moreover, the SPCAF sensing algorithm is tested and validated with real 3G, DVB-T, and 802.11ac signals, and for different scenarios and in various frequency bands. The obtained results showed an enhanced and accurate performance of the reasonably-complex blind detector when used in real-world test-beds.

Chapter 5

RF Impairments Effects on Spectrum Sensing

5.1 Introduction

In all the theoretical formulations of CR detectors, the wireless data transfer between the transmitter and the receiver is assumed to be linear. However, several analog parts of the transceiver RF front-end exhibit impairments such as the analogue-to-digital (ADC) and digital-to-analogue (DAC) converters, the mixer, the local oscillator (LO) and the amplifiers, i.e. the power amplifier (PA) in the transmitter and the low-noise amplifier (LNA) in the receiver. At the receiver side, these imperfection generators become more and more efficacious with the increased dynamic range of the received signal. The challenge grows when the receiver operates over a wide bandwidth since nonlinear distortions will show up as unwanted signals in free bands and can hit the target band.

In fact, the nonlinear characteristics of the receiver analog front-end were proved to be a critical source of degradation of the sensing performance of a cognitive receiver. Unwanted frequency components resulting from such imperfections are clearly detected as real signals since they carry the special feature of the strong signal. Recently, many papers proposed analog improvement of the front-end stages to enhance the receiver performance [89–93]. Other researchers focused also on enhancing the antenna design for CR scenarios [94–100]. However, compensating the RF impairments via advanced DSP techniques, by benefiting from the software reconfigurability of the device, has not been efficiently studied. Since the design of a reconfigurable RF front-end is nowadays considered the bottleneck of the synthesis of a fully adaptive engine, linearizing the hardware in dynamic scenarios is currently beyond of the state-of-the-art in electronics. Thus, mitigation DSP techniques are urged not only to enhance the detection efficiency but also to relax the delicate conception of the cognitive hardware.

RF CR receivers are expected to process narrowband baseband signals

received over a wide frequency spectrum with reasonably low-complexity and low-power processors. In other words, the RF components such as antennas, amplifiers, mixers and oscillators are expected to operate over a wide range of frequencies. This necessitates the move towards reconfigurable and tunable RF CR front-end architectures. A tunable RF front-end receiver should function in the presence of an efficient software-defined engine. Software defined engines are not only expected to sense, process, learn and tune/control to guarantee an acceptable performance of the receiver, but are also required to account for RF impairments. This helps to avoid performance degradation due to the nonlinearity or phase noise of the spectrally-agile components in the RF receiver. The deterioration in a down-converted signal could be due to any of several factors, including: interference, nonlinearities, phase noise or mixing spurs. These always-present issues influence the level and quality of the down-converted signals, which dictate how the software defined engine performs its sense, process, learn, tune, and control tasks. As a result, it is crucial in a CR design to consider and account for RF impairments to efficiently sense the frequency spectrum.

Let's investigate a commercial tunable RF front-end sensing receiver for cognitive radio applications. It targets the WLAN IEEE 802.11g wireless standard key specifications. It incorporates a tunable filter-antenna, low-noise amplifier, tunable bandpass filter, single-ended balanced mixer, voltage-controlled oscillator, and variable gain IF amplifier. The reception of the tunable RF front-end sensing receiver is then tested to assess its performance. A typical block diagram of the proposed receiver, which incorporates crucial components for the reception, low-noise amplification, bandpass filtering, down-conversion, and proper detection of an RF signal in the 2.4-2.485 GHz frequency range, is shown in Figure 5.1. Each component has a unit number, ranging from (U1) to (U8). The role of each unit is discussed herein.

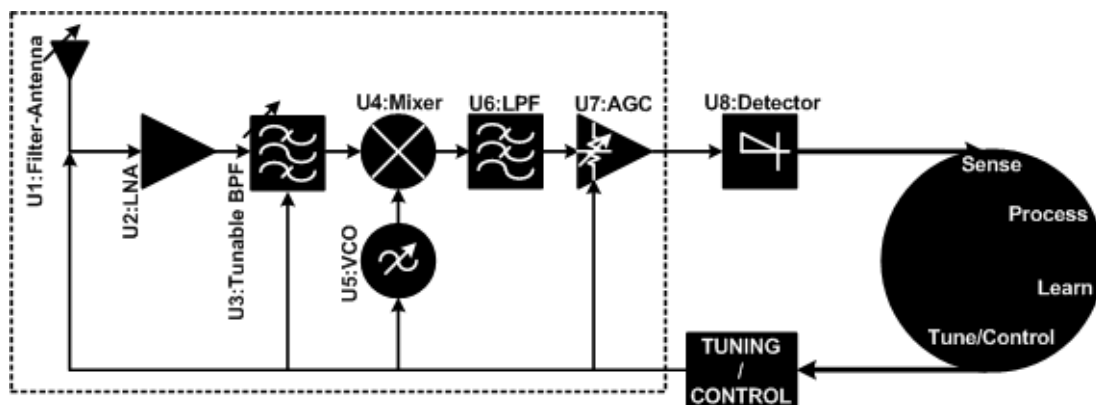


Figure 5.1: Block diagram of a commercial tunable RF front-end sensing receiver

Besides amplifying the signal received via (U1), the LNA unit (U2) is required to keep the receiver noise figure as small as possible, thus making the

receiver very sensitive. The tunable bandpass filter unit (U3) is required to reject all spurious-signal creating frequencies, including the image frequency, while simultaneously letting the desired RF bandwidth pass to the mixer. The mixer unit (U4) is required along with a tunable local oscillator (U5) for the down-conversion process to be successfully completed. The lowpass filter (U6) is required to suppress all the mixed output signals except the desired IF signal to detect. The AGC (Automatic Gain Control) unit (U7) is required to control the overall gain of the receiver. The AGC unit is followed by unit (U8), which detects the down-converted signals. The sense, process, learn, tune/control loop, which is driven by a specific sensing algorithm, is responsible for taking care of tuning the receiver's blocks operations. To synthesize the illustrated tunable RF front-end sensing receiver and analyze its performance, the key specifications of the adopted commercial wireless standard have to be targeted from the very beginning.

The reception of the tunable RF front-end sensing receiver is tested for two different carrier frequencies in the 2.4-2.485 GHz vicinity. Figure 5.2 illustrates two examples of down-converted signals in the megahertz vicinity. Compared to the 20-MHz one, the 19.22-MHz down-converted signal shows a higher noise level besides the frequency shift. This deterioration in the down-converted signal could be due to any of several factors, including interference, nonlinearities, phase noise or mixing spurs. These always-present issues influence the level and quality of the down-converted signals, which dictate how the software defined engine performs its sense, process, learn, tune and control tasks. As a result of this discussion, it is crucial in a CR design to consider and account for RF impairments to efficiently sense the frequency spectrum.

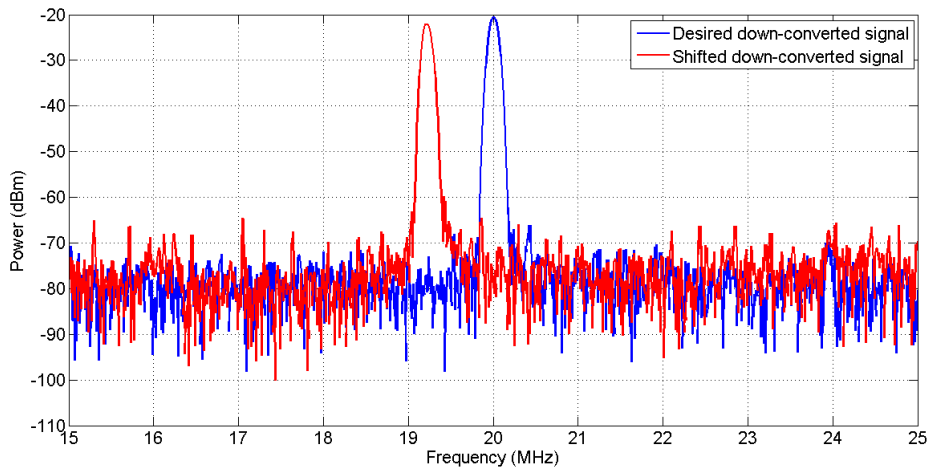


Figure 5.2: Down-converted Signals in the Megahertz Vicinity

In the sensing of a narrow-band signal, RF distortions could affect the

level and quality of the received signal which could vary the decision of the sensing scheme. The sensitivity against those signal distortions, also called in-band interferences, is a main characteristic of practical sensing techniques. The robustness of detectors could be enhanced by adding calibration and mitigation techniques that limit the signal degradation. However, sensing a wide band raises another challenge where impairments product could occupy the whole sensed band. This will affect the decisions of utilizing several narrow-bands affected by unwanted frequency components resulting from the hardware nonlinearities. The out-of-band interference is thus another major practical challenge that demands flexible solutions. For that, this chapter carefully discusses the RF impairments impact on sensing performance and recently proposed solutions are listed. This study was the main motivation behind devising a new sensing algorithm that take into account the RF limitation of CR receivers.

This chapter studies the RF impairments challenge in two different approaches. The in-band degradation of the sensing schemes performance is studied. It will be shown that the hardware imperfections could damage some detectors efficiency by altering the received signal. On the other hand, another issue could result from RF impairments when a wide band signal is sensed. In this case, the distorted signal will cause out-of-band interferences that could limit the cognitive transmission opportunities. To highlight these challenges, this chapter will be organized as follows. After an introduction in Section 5.1, a study of the sensitivity of the ED and the SPCAF detector is studied in Section 5.2. Proposed mitigation and calibration techniques to solve this in-band interference issue are listed in Section 5.3. Moreover, sensing in wide band scenarios while taking into consideration the hardware imperfection is thoroughly discussed in Section 5.4. A newly proposed solution is discussed in Section 5.5 followed by a conclusion section.

5.2 RF Impairments Impact on ED and SPCAF

In this section, the modeling and analysis of main RF impairments are highlighted and simulated results of the degradation of ED and SPCAF after the in-band distortions are shown and discussed. In communications systems, the most crucial RF impairments are the Carrier Frequency Offset CFO, Phase Noise, IQ Mismatch, and nonlinearities induced by the non-ideal stages of the RF front-end depicted in Figure 5.3. Let r be the received sequence taking into account the imperfections of the hardware, while y is the theoretically ideal received sequence. The goal of the following sections is to present the formulation of the main RF impairments and study their impact on the spectrum sensing techniques test statistics. For that, the amplitude of the distorted signal is formulated to observe the impact on the ED, since its test statistics is based on the calculation of the energy of the received signal. On the other hand, the distorted amplitude of

the CAF is investigated to highlight the impacts on the SPCAF detector.

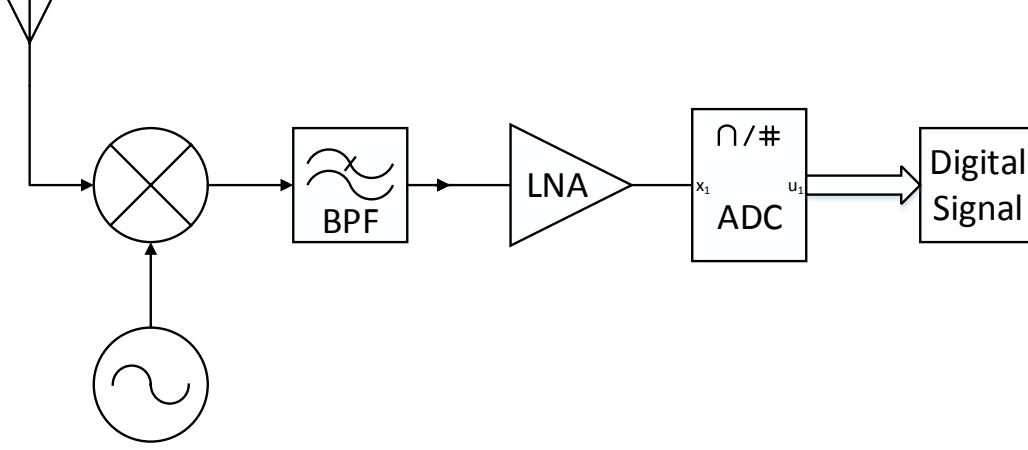


Figure 5.3: Stages of the RF Frontend of a receiver

5.2.1 Carrier Frequency Offset Impact

During the up and down conversion at the CR transceiver, the local oscillators should produce an ideal sine wave at the standard RF carrier frequency. In practice, the produced carrier frequency may differ from one to another LO, which causes CFO between the transmitter and receiver [101]. Let Δf be the carrier frequency offset between the transmitter and receiver and T_S is the sampling period. In this case, the baseband received signal could be written as:

$$\begin{cases} r(k) = y(k).e^{2\pi\Delta f k T_S} = w(k).e^{2\pi\Delta f k T_S} & H_0 \\ r(k) = y(k).e^{2\pi\Delta f k T_S} = w(k).e^{2\pi\Delta f k T_S} + s(k).e^{2\pi\Delta f k T_S} & H_1 \end{cases} \quad (5.1)$$

Obviously, since $|r(k)| = |y(k).e^{2\pi\Delta f k T_S}| = |y(k)|$, the test statistic of ED is not sensitive to the CFO. This is proved in Figure 5.4, where the unmodified ROC curve of the ED is plotted for several CFO $\epsilon = M\Delta f T_S$ values. In the case of the SPCAF, the discrete CAF of the distorted received signal yields to:

$$R_{rr}(\alpha, \tau) = \frac{1}{M} \sum_{k=1}^M r(k)r^*(k + \tau).e^{-j2\pi\alpha k} \quad (5.2)$$

$$R_{rr}(\alpha, \tau) = \frac{1}{M} \sum_{k=1}^M y(k).e^{2\pi\Delta f k T_S}.y^*(k + \tau).e^{-2\pi\Delta f(k+\tau)T_S}.e^{-j2\pi\alpha k} \quad (5.3)$$

$$R_{rr}(\alpha, \tau) = e^{-2\pi\Delta f\tau T_S} R_{yy}(\alpha, \tau) \quad (5.4)$$

This demonstrates that, after the CFO impact, $|R_{rr}(\alpha, \tau)| = |R_{yy}(\alpha, \tau)|$. The test statistic of the SPCAF based on the symmetry check of an estimation of the CAF is thus unaltered. To validate these conclusions, the ROC curves of the SPCAF for different values of CFO are simulated and plotted. Figure 5.5 shows that the SPCAF detector is not sensitive to the carrier frequency offset impact.

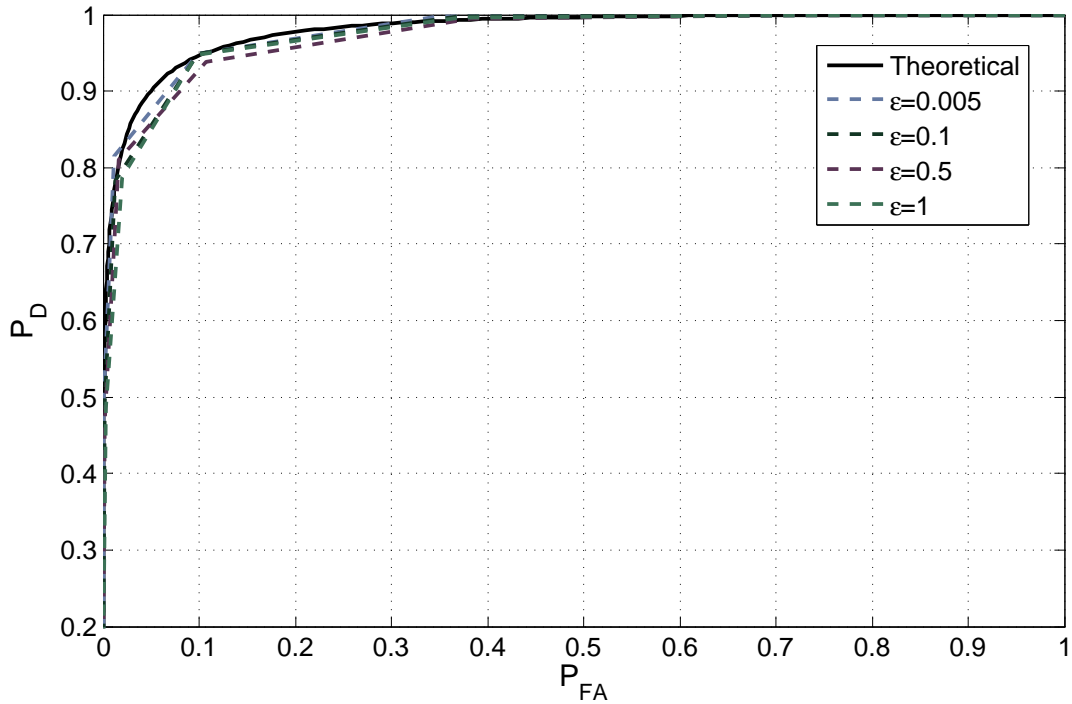


Figure 5.4: ROC of the ED for different values of CFO $\epsilon = M\Delta fT_S$

5.2.2 Phase Noise Impact

Phase noise is introduced by the local oscillator at both the transmitter and the receiver. It is a random process caused by the frequency fluctuation of the LO. Phase noise is the difference between the phase of the receiver oscillator and the phase of the carrier of the received signal [102]. The distortion could be modeled as:

$$r(k) = y(k).e^{j\varphi_k} \quad (5.5)$$

φ_k is the phase rotation of the received signal due to the phase noise. It is usually modeled as a Wiener random process or a wide-sense stationary (WSS) random process as:

$$\varphi_k = \varphi_{k-1} + \phi_k \quad (5.6)$$

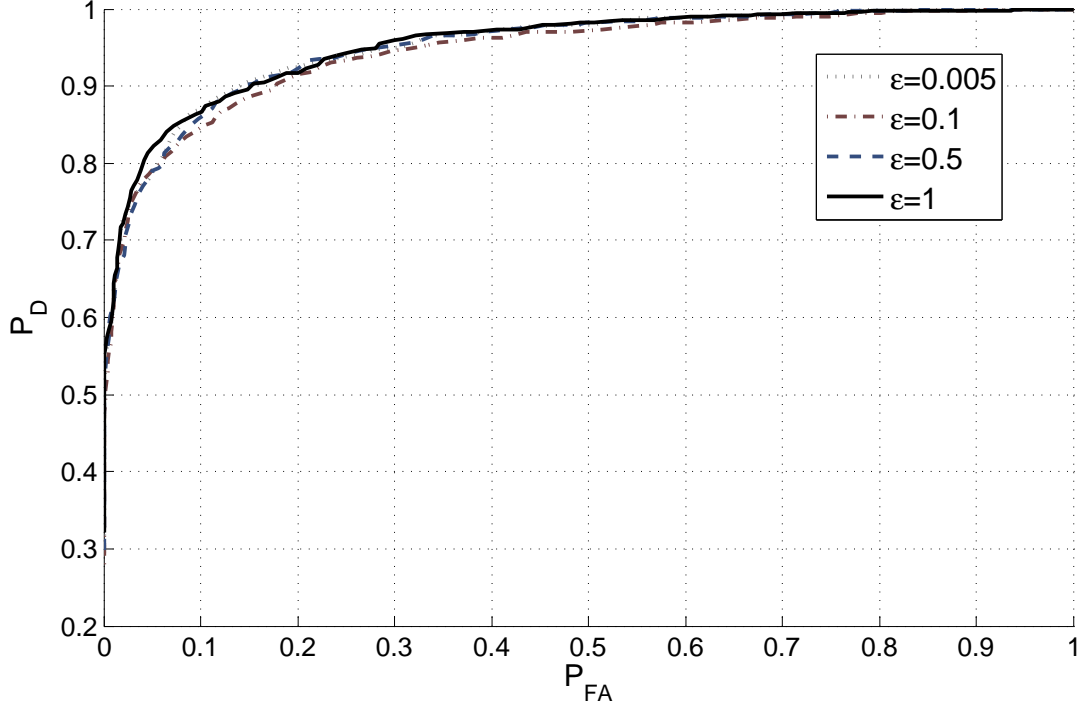


Figure 5.5: ROC of the SPCAF for different values of CFO $\epsilon = M\Delta f T_S$

ϕ_k is assumed to be an independent identically distributed real Gaussian process with zero mean and a variance of $\sigma_\phi^2 = 2\pi\beta T_S$, where β is called the Full-Width at Half-Maximum (FWHM) or the diffusion factor. The ED, being dependent on the calculation of the amplitude of the signal, is obviously robust against phase noise. For the SPCAF, the CAF will be affected as demonstrated below:

$$R_{rr}(\alpha, \tau) = \frac{1}{M} \sum_{k=1}^M y(k) \cdot e^{j\varphi_k} \cdot y^*(k + \tau) \cdot e^{-j\varphi_{k+\tau}} \cdot e^{-j2\pi\alpha k} \quad (5.7)$$

$$R_{rr}(\alpha, \tau) = \frac{1}{M} \sum_{k=1}^M y(k) \cdot y^*(k + \tau) \cdot e^{-j2\pi\alpha k} \cdot e^{j(\varphi_k - \varphi_{k+\tau})} \quad (5.8)$$

$$R_{rr}(\alpha, \tau) = \frac{1}{M} \sum_{k=1}^M y(k) \cdot y^*(k + \tau) \cdot e^{-j(2\pi\alpha k + \phi'_k)} \quad (5.9)$$

The CAF of the distorted signal $r(k)$ is clearly affected by a phase component ϕ'_k . To observe the impact of this phase factor on the test statistic and consequently on the detection performance, simulations are performed and results are shown below. In the simulations, the ROC curve is computed for the SPCAF while taking several values of the factor βT_S . As demonstrated in Figure

5.6, increasing βT_S dramatically degrades the performance of the SPCAF. For $\beta T_S = 5 \cdot 10^{-5}$, the probability of detection is almost equivalent to the probability of false alarm, which corresponds to the worst detector performance.

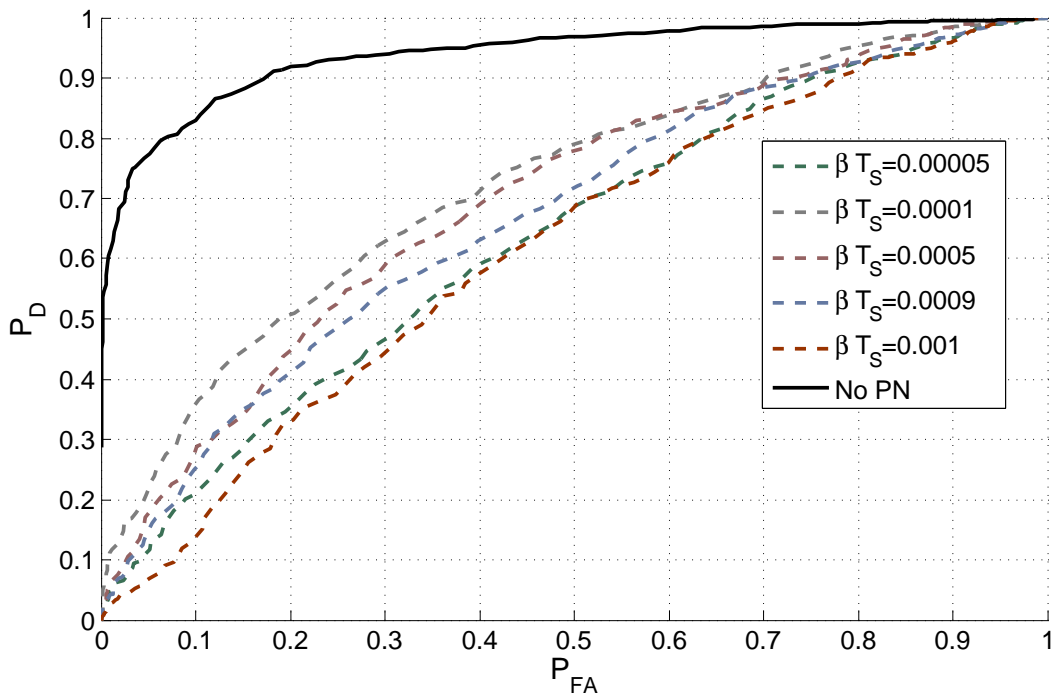


Figure 5.6: ROC of the SPCAF for different values of βT_S

5.2.3 I/Q Imbalance Impact

Another major source of impairments in wireless communications system is the mismatch between the I and Q branches or, equivalently between the real and imaginary parts of the complex signal at both the transmitter (during up-conversion) and receiver (during down-conversion). In reality, matching between the I and Q branches is not perfect, consequently the phase and the amplitude of the Q-path are altered. In this case, the baseband distorted received signal $r(k)$ could be written as a linear expression of the ideal signal $y(k)$ and its conjugate $y^*(k)$ as follows:

$$r(k) = \mu \cdot y(k) + \nu \cdot y^*(k) \quad (5.10)$$

The distortion parameters μ and ν depend on the mismatch amplitude g and phase θ between the I and Q branches in the analog stages. μ and ν could be formulated as:

$$\begin{cases} \mu = \cos(\frac{\theta}{2}) + jg \sin(\frac{\theta}{2}) \\ \nu = g \cos(\frac{\theta}{2}) - j \sin(\frac{\theta}{2}) \end{cases} \quad (5.11)$$

To analyze the impact of the I/Q imbalance on the energy detector, the distortion between $|r(k)|^2$ and $|y(k)|^2$ is observed.

$$|r(k)|^2 = |\mu.y(k) + \nu.y^*(k)|^2 \quad (5.12)$$

$$|r(k)|^2 = |\mu.y(k)|^2 + |\nu.y^*(k)|^2 + 2\Re(\mu.y(k).\nu^*.y(k)) \quad (5.13)$$

$$|r(k)|^2 = (1 + g^2).|y(k)|^2 + 2\Re(\mu.\nu^*.y(k)^2) \quad (5.14)$$

It is obvious that the mismatch amplitude g and phase θ could alter the performance of the ED. To observe this modification, the ROC of the radiometer is plotted for several values of g and θ in Figures 5.7 and 5.8. The degraded performance is obvious in the simulated results which demonstrated the high sensitivity of the ED to I/Q imbalance.

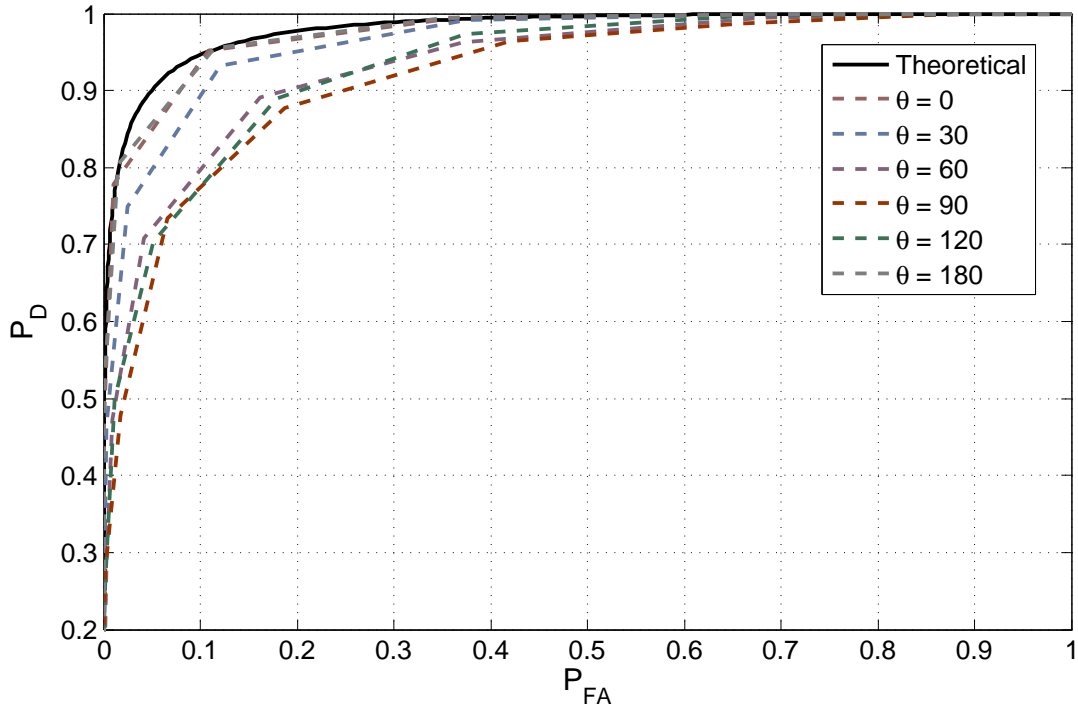


Figure 5.7: ROC of the ED for different values of θ

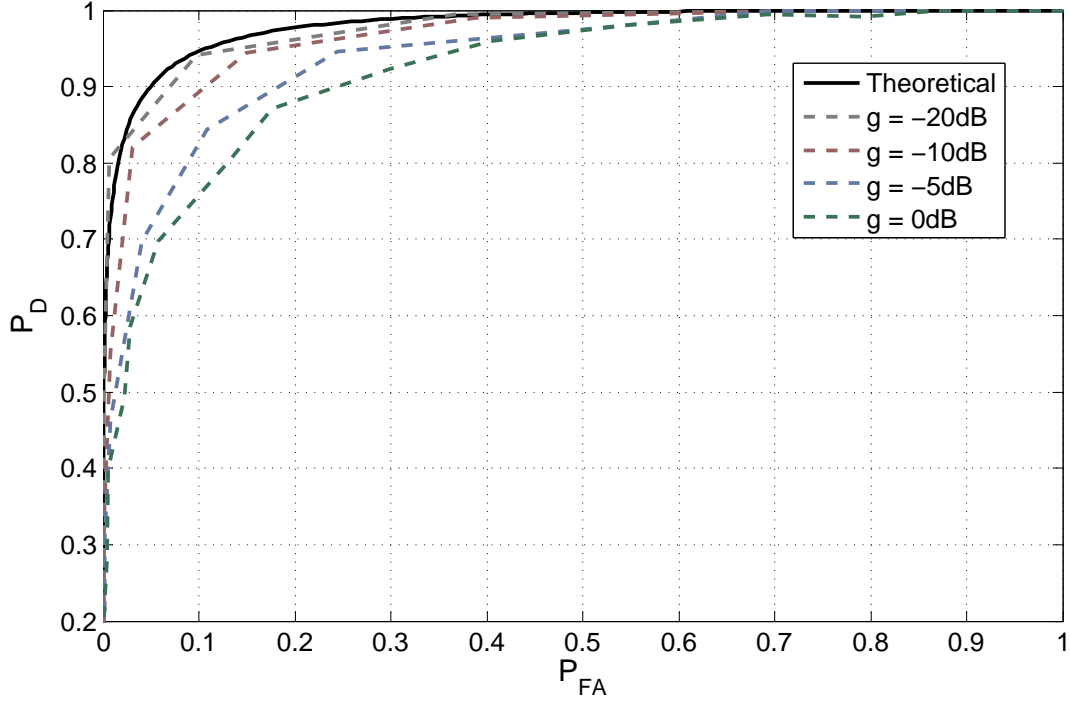


Figure 5.8: ROC of the ED for different values of g

The CAF is distorted due to I/Q imbalance as formulated below:

$$R_{rr}(\alpha, \tau) = \frac{1}{M} \sum_{k=1}^M [\mu \cdot y(k) + \nu \cdot y^*(k)] [\mu \cdot y(k + \tau) + \nu \cdot y^*(k + \tau)]^* \cdot e^{-j2\pi\alpha k} \quad (5.15)$$

$$R_{rr}(\alpha, \tau) = \frac{1}{M} \sum_{k=1}^M [\mu \cdot y(k) + \nu \cdot y^*(k)] [\mu^* \cdot y^*(k + \tau) + \nu^* \cdot y(k + \tau)] \cdot e^{-j2\pi\alpha k} \quad (5.16)$$

$$R_{rr}(\alpha, \tau) = (|\mu|^2 + |\nu|^2) \cdot R_{yy}(\alpha, \tau) + 2\Re(\mu \cdot \nu^* \cdot R'_{yy}(\alpha, \tau)) \quad (5.17)$$

$$\text{Where } R'_{yy}(\alpha, \tau) = \frac{1}{M} \sum_{k=1}^M y(k) y(k + \tau) \cdot e^{-j2\pi\alpha k}.$$

As concluded from the formulation above and as shown in [103], cyclostationarity based detectors are dramatically harmed by I/Q imbalance effects. However, this is not true for the SPCAF detector since it is sufficient to observe only the real part of the received signal (I branch) and estimate its CAF in order to decide on the presence of a PU. Results plotted in Figures 5.9 and 5.10 show the robustness on SPCAF against I/Q imbalance effects.

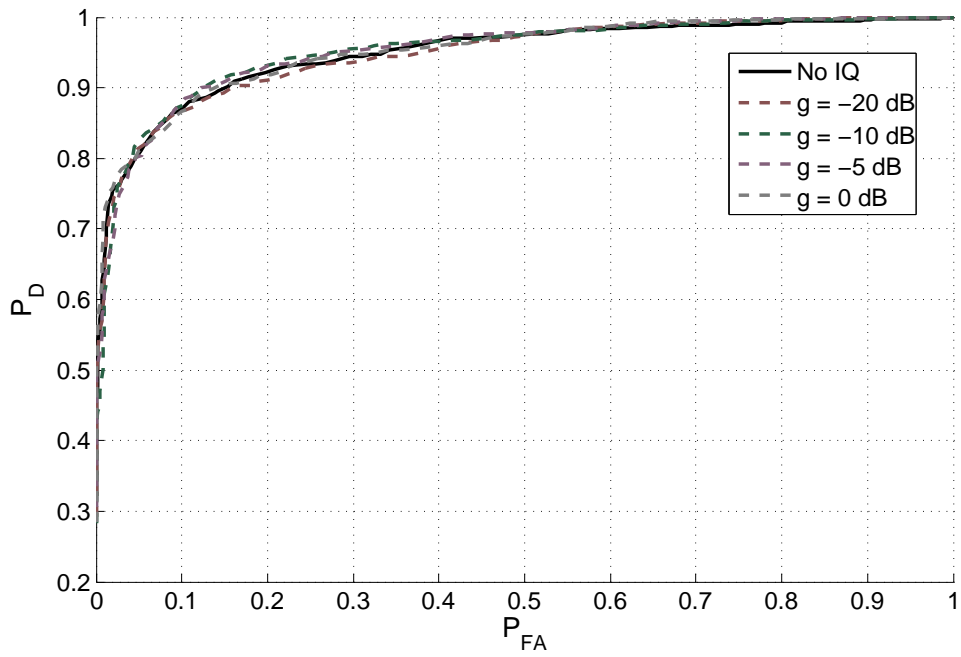


Figure 5.9: ROC of the SPCAF for different values of g

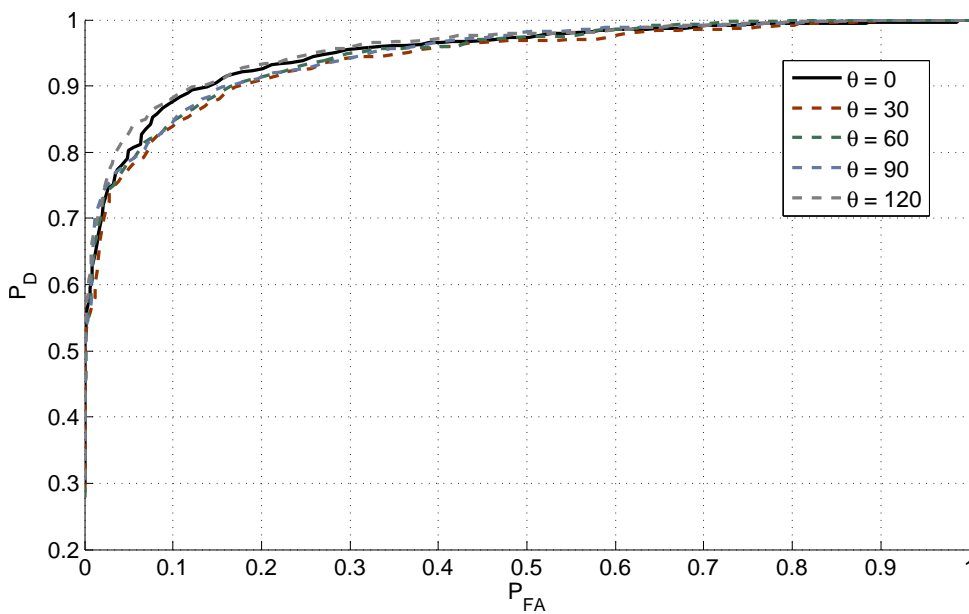


Figure 5.10: ROC of the SPCAF for different values of θ

5.2.4 Nonlinearities Impact

RF designers are struggling to design linear analog components for CR systems. However, the linearity constraint is becoming more and more challenging especially when building a dynamic and flexible receiver with tunable stages. Thus, RF nonlinearities are considered the most serious impairment caused by a reconfigurable hardware chain. In the case of nonlinearities, the distorted signal could be written as:

$$r(k) = \alpha_1 y(k) + \alpha_2 y(k)^2 + \alpha_3 y(k)^3 \quad (5.18)$$

where $\alpha_1 y(k)$, $\alpha_2 y(k)^2$, and $\alpha_3 y(k)^3$ represent the linear component, the second order nonlinear component, and the third order nonlinear component respectively. α_1 , α_2 , and α_3 , are real constants. Superior nonlinear components are omitted in this equation since it is only a proof of concept. An estimation of the nonlinear components induced by the WBX daughter board of a USRP N210 is conducted in [69] and results are: $\alpha_1 = 3.1623$, $\alpha_2 = 0.0114$, and $\alpha_3 = 1.7456$. Results depend on the hardware characteristics of the board such as the gain and the measured input-referred intercept points (IIP).

It is clear that the nonlinearities components will expand in the expression of $r(k) = w(k)$ in H_0 and $r(k) = y(k) + w(k)$ in H_1 . This will create the same (P_{FA}, P_D) couple but for higher threshold since the noise level is also increased by the nonlinear effect. Thus, the ROC curve of the ED will remain unmodified as illustrated in Figure 5.11.

Also for the SPCAF detector, the symmetry (cyclostationary feature) will be identically detected with or without nonlinearities since the symmetry is observed with low or high levels. In H_0 scenarios, inducing nonlinear components of the noise will not add a cyclostationary feature to its randomness. The ROC of the SPCAF simulated with the nonlinear components induced by a WBX board is shown in Figure 5.12.

The harmful effect of nonlinearly induced components is observed while sensing a wide band, since these unwanted harmonics can occupy free bands. This problem is described in Section 5.4 by showing real-world signals distorted by the nonlinear behavior of a USRP daughter board.

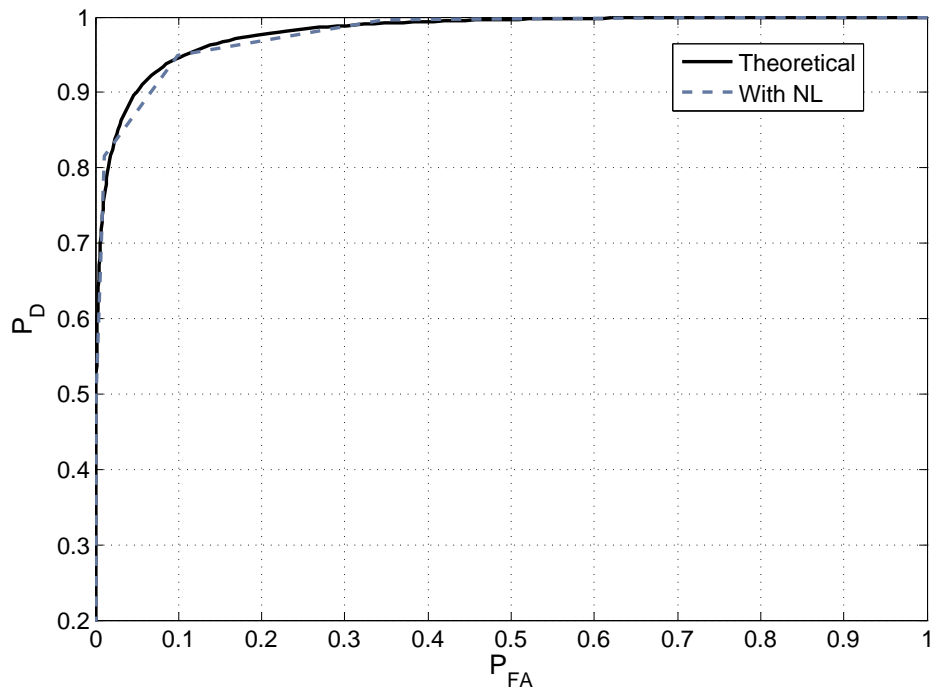


Figure 5.11: ROC of the ED with nonlinear components

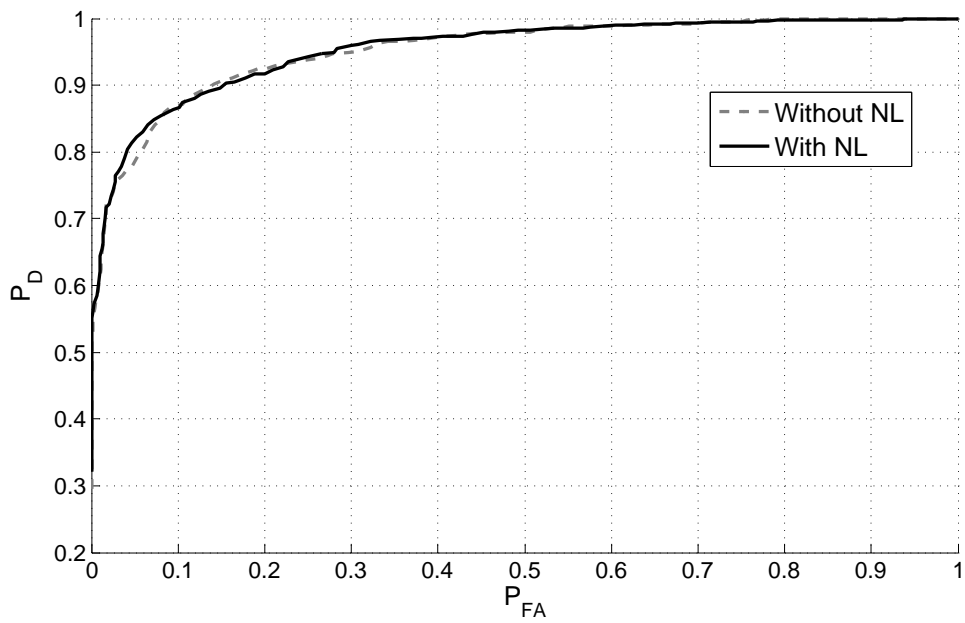


Figure 5.12: ROC of the SPCAF with nonlinear components

5.3 DSP Algorithms for In-Band RF Impairments Compensation

In Section 5.2, the SPCAF detector showed a high sensitivity to phase noise and the ED was dramatically changed by the I/Q Imbalance effect. As a software solution to this hardware issue, several pre-distortion techniques were proposed to mitigate these impairments on the transmitter side. However, in the critical design of a cognitive receiver, these DSP techniques should blindly compensate the main RF imperfections to guarantee a reliable sensing, thus a perfect functioning of the dynamic terminal. In this section, two adaptive compensation techniques, that address the main harmful impairments i.e. I/Q imbalance and phase noise, are described.

5.3.1 Phase Noise Impact Compensation

In the previous section, the destructive impact of the phase noise caused by LO is illustrated. It is shown that every second-order cyclostationarity-based sensing technique will lose its performance in the presence of such impairment. A blind compensation technique was reported in [104] to lower the noise effect. The blindness criteria of this scheme make it suitable for CR receivers since it conserves its flexibility feature. To combat the phase noise degradations, the algorithm estimates and compensates two major effects of phase noise, i.e. the inter-carrier interference (ICI) and the common phase error (CPE), while assuming an OFDM based signal. For that, the received signal is partitioned into sub-blocks and time-averages of the phase noise is calculated over each block. A reduction of the differences between obtained time-averages is applied as a first stage of the algorithm to mitigate the ICI resulting from phase noise. Then, an estimation of the CPE is applied by using the discrete Fourier transform of the corrected signal resulting from the ICI compensation stage. Finally, the CPE is compensated by computing the minimum mean square error (MMSE) filter coefficient of the one-tap equalizer. A block diagram of the algorithm is shown in Figure 5.13.

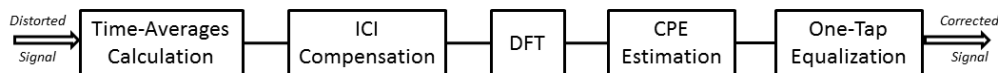


Figure 5.13: Block diagram of the blind phase noise compensator scheme

5.3.2 I/Q Imbalance Impact Compensation

Another RF impairment that harms the sensing efficiency of a cognitive terminal is the I/Q imbalance. For that, a blind compensation scheme should be added before the sensing part to protect the signal from damaging distortions. Such scheme was lately discussed in [105] by using 2-tap adaptive filters. Tap filters weights are computed using the constant modulus algorithm (CMA) and the algorithm is applied subcarrier by subcarrier in an OFDM based signal. To adaptively compute the weights of the compensator, CMA exploits the constant modularity of the transmitted signal. Since the CMA does not require any training signals, the algorithm is considered as blind and could be used for CR scenarios. The block diagram of this scheme is illustrated in Figure 5.14.

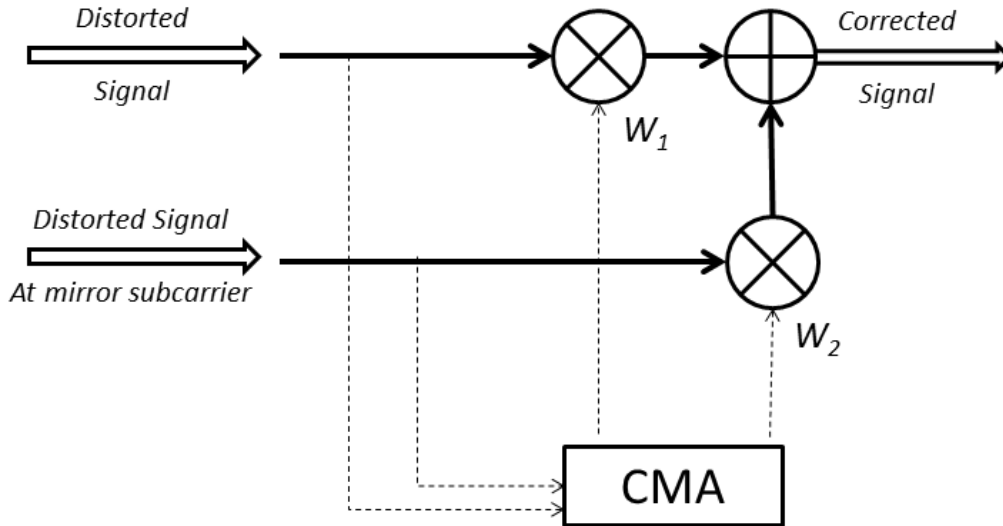


Figure 5.14: Block diagram of the blind I/Q Imbalance compensator scheme

5.4 RF Impairments Impact on Wide Band Sensing

5.4.1 RF Impairments Analysis in Wide Band Receivers

In practice, receivers are composed of several sources of hardware imperfections such as low noise amplifiers (LNA), mixers, local oscillators (LO), and analog to digital converters (ADC). CR receivers are required to operate with several standards, sense a wide band, and down-convert signals with variant levels. The

dynamic range of the captured frequency band could attain 100 dB [106]. This will result in the appearance of new frequency components in the received signal, classified in nonlinear distortions, I/Q imbalance, and oscillator phase noise. Consequently, strong primary users, also called blockers, could harm the performance of traditional spectrum sensing techniques by adding unwanted spectrum components via front-end's imperfections. When these components overlap with weak secondary users, a degradation in the reliability of SU transmissions occur. They can also virtually occupy the whole spectrum thus decreasing the opportunity to find a vacant transmission band. In both scenarios, the accuracy of any proposed algorithm will be deteriorated.

In Figure 5.15, RF front-end stages and baseband analog parts are illustrated with corresponding generated frequency components. In each stage, additional distortions are added to the sensed spectrum which will increase the probability of false alarm of the detection technique. First, the received signal $y(k)$ is affected by the nonlinearity of the RF front-end filter and LNA resulting in the distorted signal r_{RF} . The phase noise of the local oscillator increases the side lobes of the signal. Then, the mixer alters the spectrum by adding a mirror signal via I/Q imbalance. Finally, the signals at I and Q branches resulting from the mixer $r_{I,BB}$ and $r_{Q,BB}$ are also subject to the nonlinear behavior of the mixer, the filters, and the ADC. This baseband (BB) behavior is practically less severe than RF nonlinearities. As a result, potential white spaces could be masked if a strong PU is present in the sensed spectrum since the imperfection factors will be more significant.

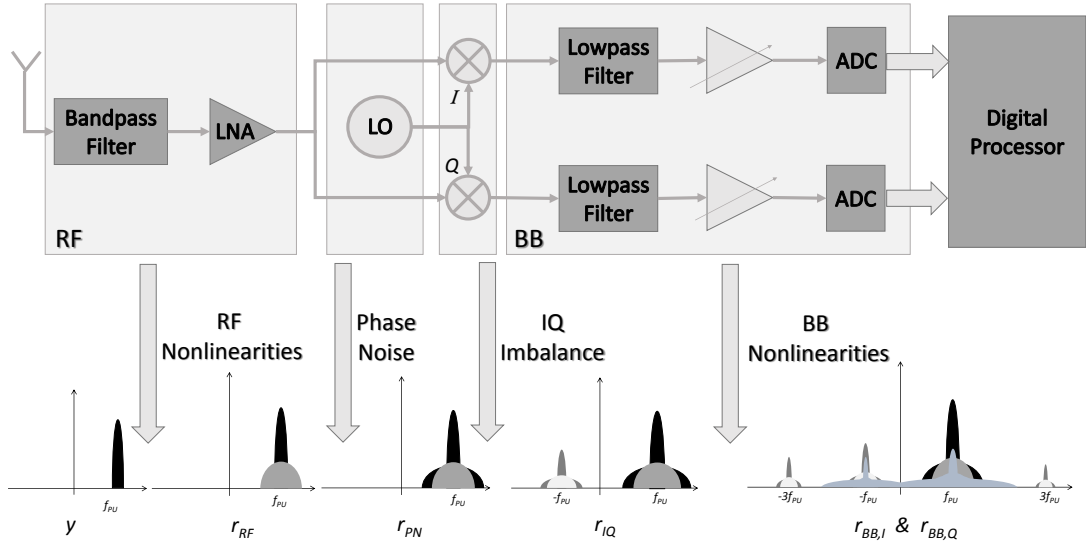


Figure 5.15: Wide band receiver stages and corresponding impairments

The distortions induced by the nonlinear behavior of the RF and BB

analog parts could be modeled using Equation 5.18. It is shown in [107] that second-order nonlinear components are usually not harmful since they appear only if the sensed signal is extremely wide band and full of strong PUs. According to [107], designed CR receivers have high second-order intercept point which will result in a very small α_2 and a negligible second-order component. Thus, a simplified RF nonlinearity model is:

$$r_{RF}(k) = \alpha_{RF1}.y(k) + \alpha_{RF3}.y(k)^3 \quad (5.19)$$

Similar to this model, the BB nonlinear behavior in the I/Q branches could be independently modeled as follows:

$$\begin{cases} r_{BB,I}(k) = \alpha_{BBI1}.r_{IQ}(k) + \alpha_{BBI3}.r_{IQ}(k)^3 \\ r_{BB,Q}(k) = \alpha_{BBQ1}.r_{IQ}(k) + \alpha_{BBQ3}.r_{IQ}(k)^3 \end{cases} \quad (5.20)$$

On the other hand, the outputs r_{IQ} and r_{PN} of the mixer and the local oscillator, respectively, are modeled as previously formulated in Section 5.2:

$$r_{PN}(k) = \mu.r_{RF}(k) + \nu.r_{RF}^*(k) \quad (5.21)$$

$$r_{IQ}(k) = r_{PN}(k).e^{j\varphi_k} \quad (5.22)$$

A summarized vision of the models of the above listed RF imperfections is illustrated in 5.16.

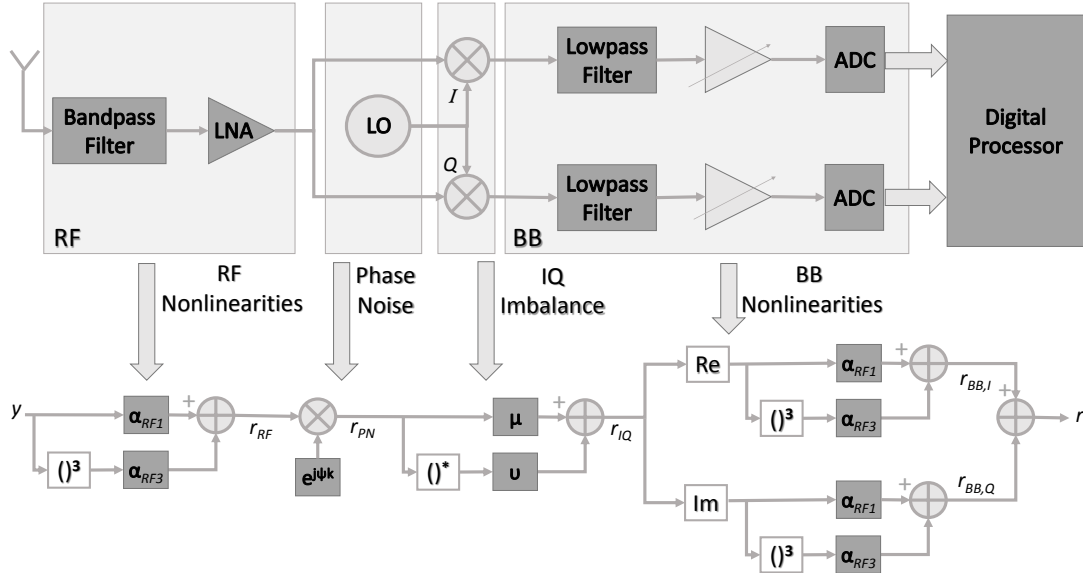


Figure 5.16: Wide band receiver stages and corresponding impairments

5.4.2 Analysis of the ED and SPCAF Degradation

To observe the degradation of the ED and SPCAF due to out-of-band added frequency components, a test-bed composed of two USRPs N210, acting as a primary transmitter and a wide band secondary receiver, is built. In the adopted scenario, the primary signal is a two-tone blocker signal with a power of -55 dBm and a 20 MHz band is sensed around the blocker. Figure 5.17 shows the occupation of the received signal with unwanted distortions due to the blocking effect. After partitioning the received spectrum into several narrow bands, the probability of false alarm is calculated using the ED and the SPCAF detectors to measure the harmful effect of the impairments. The ED decided H_1 for all the processed sub-bands and SPCAF delivered a very high probability of false alarm also, as shown in Figure 5.18. This increase in the value of P_{FA} was expected and inevitable for the SPCAF detector since the added frequency components are basically the inter-modulation factors of the signal. Consequently, they carry the feature of the signal and they are detectable as PUs by the SPCAF. For the ED, the result was obvious from the spectrum density of the received signal plotted in Figure 5.17. Thus, this virtual occupation of the spectrum can cancel many secondary transmission opportunities. As a result, this scenario demonstrated that mitigation techniques should be considered in the implementation of practical sensing schemes.

5.5 Mitigation algorithms for Wide Band Sensing

To mitigate the RF distortions in wide band sensing, a robust detector should be equipped with a compensation functionality to digitally reduce the effects of nonlinearities and I/Q imbalance. Possible compensation algorithms could be based on feed-forward techniques with reference nonlinearity, feed-back equalization, and training symbols based equalization. Recently, Grimm et al. proposed in [108] a mitigation algorithm to alleviate the RF distortions and nonlinearities produced by the RF front-end of direct conversion receiver. This algorithm is the enhanced version of the AIC algorithm proposed in [68]. We begin this section by introducing the AIC algorithm, and then we move to discuss the new mitigation algorithm.

5.5.1 The AIC Algorithm

In [68], Valkama et al. devised the adaptive interference cancellation (AIC) algorithm, which is a feed forward algorithm for the mitigation of second, third and fifth order inter-modulation distortions. The idea is to model the distortion caused by the interferer and then subtract them from the received signal. A

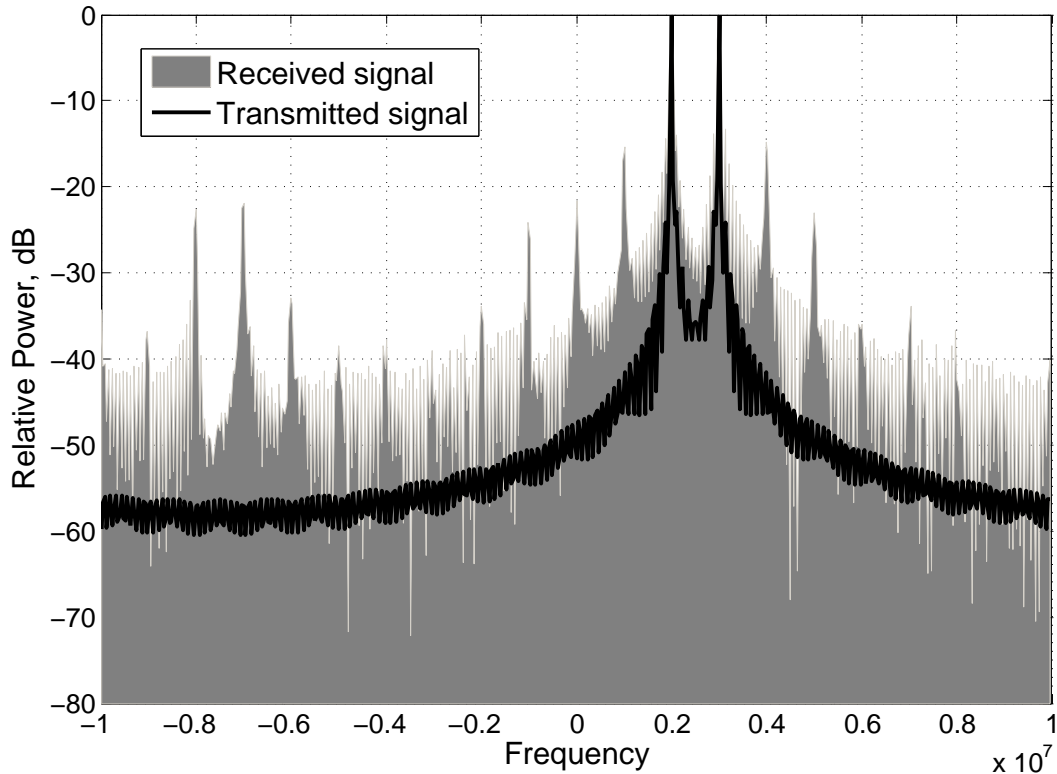


Figure 5.17: Spectrum Density of the transmitted and the received signals

mathematical formulation of the nonlinearity model and order is studied before implementing the algorithm. Then, an imitation of the distortion products and an adaptive adjustment of their levels is performed to compensate the distorted signal. The algorithm, illustrated in Figure 5.19 starts by splitting the band of the received signal in order to differentiate between the strong PU and other frequency components (SUs + distortions). The band splitting is accompanied by a coarse energy detector used to locate the strong interferer. Then a parallel block of reference non-linearities is used to extract potential distortion products from the strong interferer. An adaptive filter, the Least Mean Square (LMS), is used to adjust digitally-created distortions levels. The adaptive filter utilizes the distorted signal resulting from the band splitter as an input parameter and minimizes the common error signal $e(t)$. The adjusted non linearities are finally subtracted from the received signal to cleanse the band from non-linearity distortions. It is shown in [69] that the application of the AIC algorithm before the detector increases the detection reliability in CR devices.

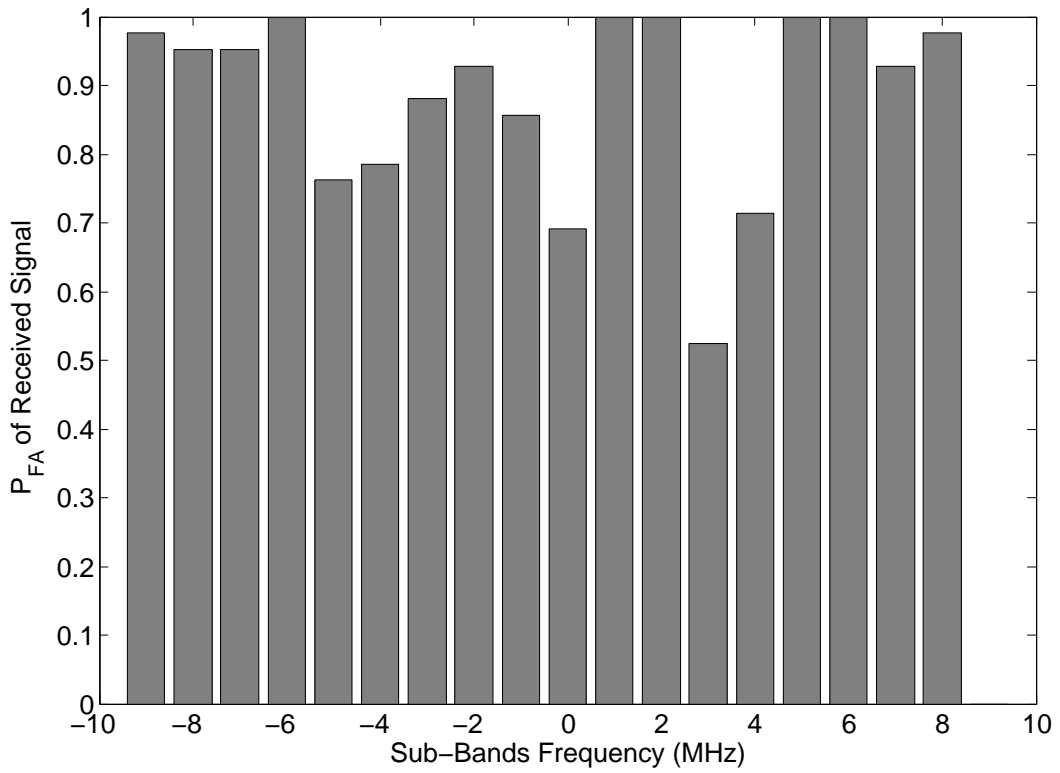


Figure 5.18: Probability of false alarm of the SPCAF for the transmitted and received signal

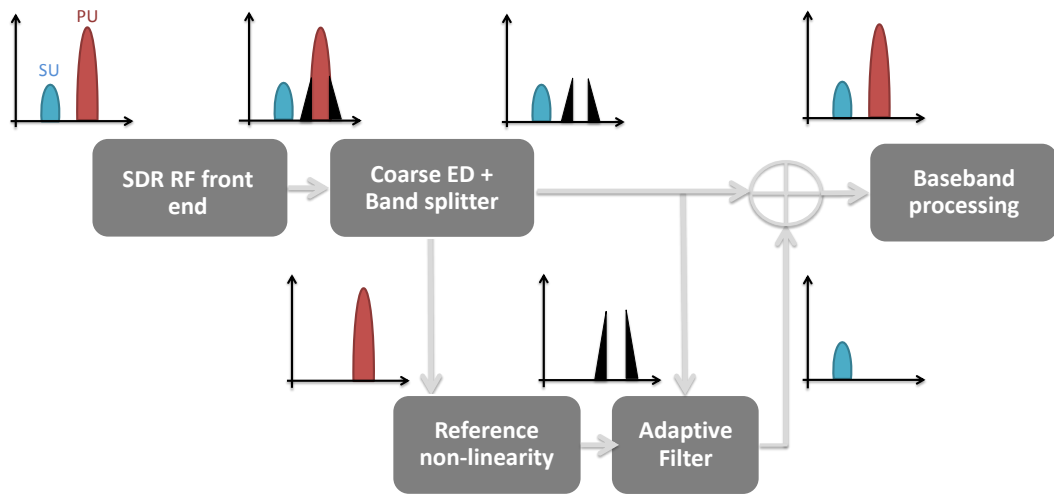


Figure 5.19: The AIC algorithm

5.5.2 The Improved Adaptive Mitigation Algorithm

As demonstrated by Valkama et al. in [68], inter modulation distortions could be digitally and adaptively detected and extracted from the received and digitized signal. The authors in [108] presented an adaptive mitigation algorithm to digitally alleviate the hardware imperfection impacts on practical cognitive communications. This technique, depicted in Figure 5.20, is based on an imitation of the mathematical models of the main hardware impairments, e.g. RF nonlinearities, baseband non-linearities, and I/Q imbalance. The strong licensed user is fed in three parallel stages to obtain several frequency components, then an adaptive calibration of their levels is performed by using the least mean square (LMS) method. In each iteration of the algorithm, the error between calculated distortions and the actual received signal is observed. Accordingly, an adaptive modification of the algorithm's weights is performed using the LMS rule. After the convergence of the scheme, the resulting distortions are subtracted from the received signal to obtain an impairments-free signal.

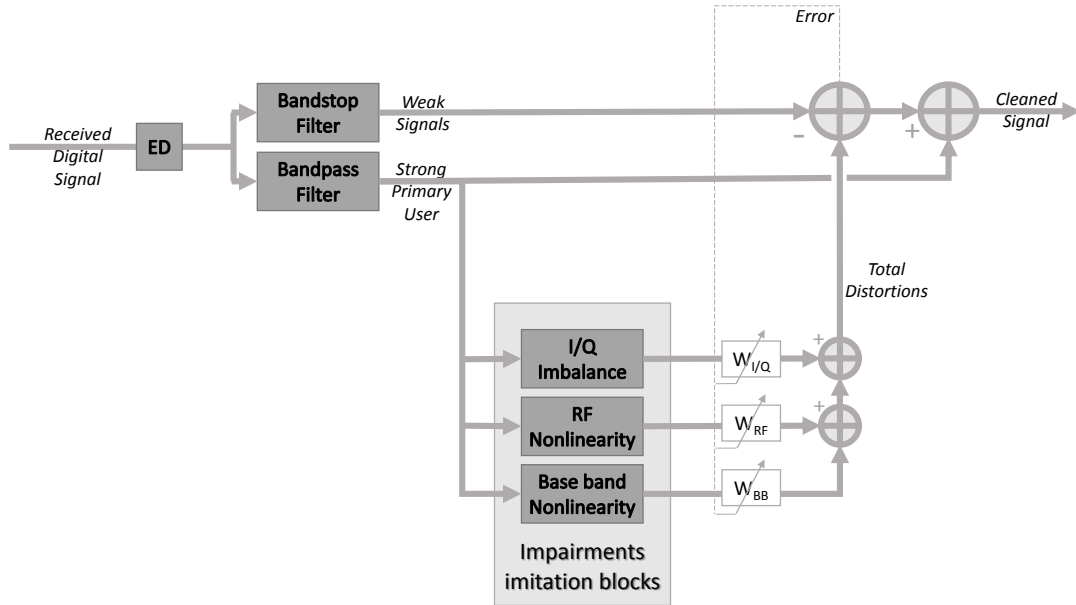


Figure 5.20: The improved adaptive mitigation algorithm

5.6 Conclusion

This chapter focused on one of the main targets of the dissertation: the hardware impairments in CR receivers. For that, the mathematical models of the main analog imperfections are presented. The sensitivity of the ED and the SPCAF

detector against these impairments in narrow band and wide band sensing is assessed. Moreover, several state-of-the-art mitigation techniques are discussed. All the results presented in this chapter affirm that a practical sensing scheme should be aware of all possible hardware imperfections. The degradation observed in the performance of the detectors was the motivation for devising a fast and blind sensing scheme aware of the hardware impairments to be perfectly deployable in real-world CR receivers.

Chapter 6

A Robust, Blind and Wide Band Sensing Algorithm for Practical CR Receivers

6.1 Introduction

As discussed in the previous chapters, the enabling step of the intelligent functionalities of a cognitive receiver is the capability to sense the environment. This necessitates unique signal processing challenges, especially in real-world implementations where fast and accurate techniques are needed. To address these challenges, the blind SPCAF detector was investigated since it does not require any a priori information of the PU. In fact, such information could not be always communicated to the receiver, especially in CR dynamic scenarios, which makes SPCAF a perfect candidate for real-world CR receivers. On the other hand, a practical sensing scheme should also consider the hardware imperfections, which does not appear in theoretical formulation and simulations. For that, the SPCAF should be assisted by a mitigation algorithm to be able to overcome the performance degradation highlighted in the last chapter.

First, a dual stage spectrum sensing algorithm is presented and tested. The first stage is the adaptive imperfections mitigation scheme that frees the unwanted frequency bands from results of the hardware imperfections of the receiver [108] while the second stage is the SPCAF. Being blind and robust, the resulting technique is adequate for practical implementation on real CR receivers. However, the computational complexity of this algorithm should be optimized to guarantee the flexible and dynamic behavior of CR systems. For that, a devised algorithm is proposed by combining the ED and SPCAF and optimizing the mitigation scheme. To demonstrate the efficiency of the devised technique, measurements were conducted using N210 USRPs and results validated the expected performance.

This chapter is organized as follows. The dual stage algorithm is discussed and tested in the first section. Then, a study of the proposed algorithm is presented in Section 6.3. All the proposed schemes are validated with USRP based test-beds and measured results are shown at the end of each section. A conclusion summarizes the devised techniques and its practical features.

6.2 The Dual Stage Algorithm

6.2.1 Stages of the Algorithm

To build a robust and blind detector, able to overcome the main limitations of practical communications, a dual stage technique is firstly proposed. In this approach, we suggest to perform a cleaning of the received band before searching for potential spectrum holes. For that, the digitized signal delivered by the ADC is fed into a coarse energy detector to locate the strong primary users that can cause non-negligible frequency distortions. The resulting location will be used as the center frequency of two complex filters, a bandpass filter that preserves the strong signal and a bandstop filter with an output composed of other weak signals and noise. To imitate and mitigate the latter signal, the strong PU enters the mitigation stage where frequency distortions are adaptively calculated using the LMS algorithm. Afterwards, the cleaned signal is divided into narrowbands signals using FFT and IFFT transformations and each resulting signal is processed by the SPCAF algorithm. It should be stated that digital filters could not be used to partition the signal since they induce repetitive feature in the signals and mislead the SPCAF detector. Finally, a binary decision on each sub-band of the received signal is generated, which will be used by the decision engine of the smart receiver to choose the adequate opportunity. A block diagram of the proposed algorithm is illustrated in Figure 6.1.

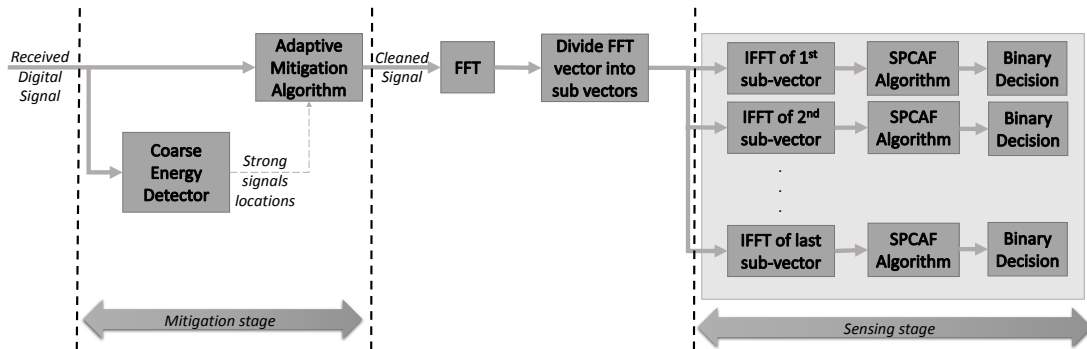


Figure 6.1: The proposed dual-stage algorithm

6.2.2 Results and Discussions

To demonstrate the performance of the proposed dual-stage algorithm with real-world signals and devices, a test-bed composed of two N210 USRPs, acting as primary transmitter and secondary receiver, is built. In the adopted scenario, the primary signal is a two-tone signal with an input power of -55 dBm sent over the 2.452 and 2.453 GHz carrier frequencies. At the receiver, a band of 20 MHz around 2.45 GHz is captured and digitized. For that, the daughter-board XCVR2450 operating in the bands 2.4-2.5 GHz and 4.9-5.9 GHz is inserted in the transmitting USRP, while the SBX with a range between 0.4 and 4.4 GHz is used at the receiver [84]. The daughter-boards analog gain at the transmitter and the receiver is set to 15 and 38 dB, respectively. A sketch of the measurement setup is illustrated in Figure 6.2.

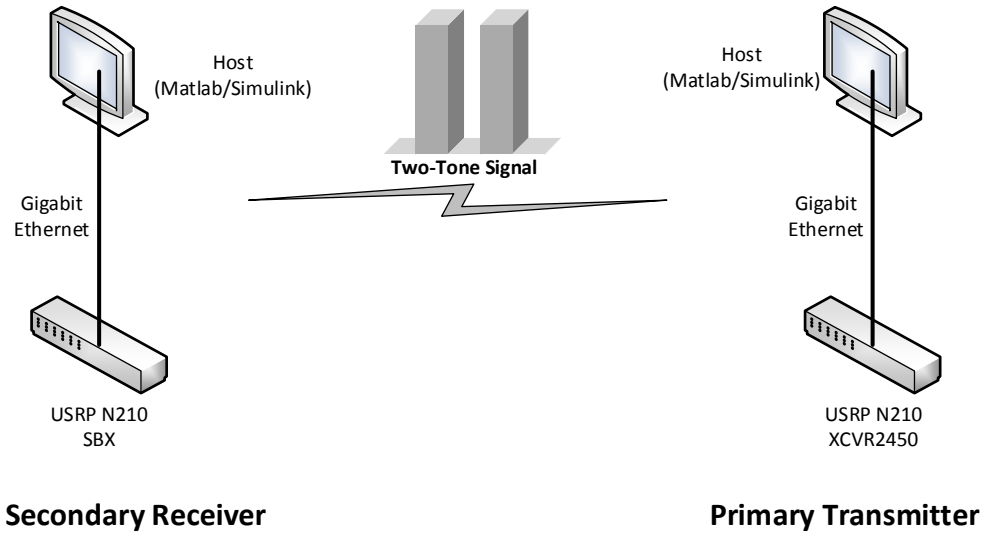


Figure 6.2: A sketch of the measurement setup

At the receiver, the captured signal spectrum is clearly filled with undesired frequency distortions induced by the RF impairments of the circuitry, as shown in Figure 6.3. In each sub-band of the received signal, an opportunity of finding a spectrum hole by the SPCAF detector is almost non-existing due to the received crowded spectrum. To highlight the enhanced performance of this blind detector, measurements are recorded with and without the mitigation stage. It is clear in Figure 6.3 that the mitigated signal is almost cleaned from RF unwanted components.

In addition to that, the binary decisions resulting the SPCAF for the available sub-bands are computed with and without mitigation. The probability

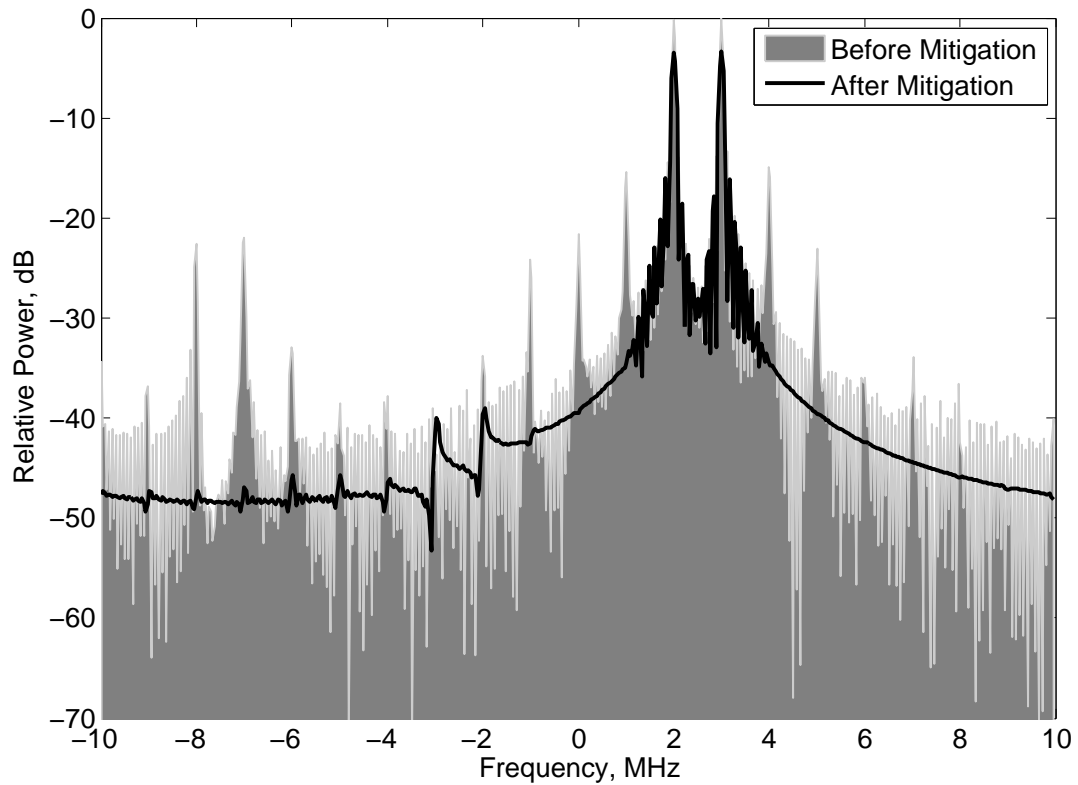


Figure 6.3: The spectra of the received signal before and after the mitigation stage.

of false alarm P_{FA} , which corresponds to a positive decision while no primary user is actually present, is observed. In Figure 6.4, plots of the P_{FA} with and without mitigation prove the improved performance. The percentage of the changed P_{FA} is illustrated in Figure 6.5 showing an average reduction of 35% in the probability of false alarm when adding the mitigation stage.

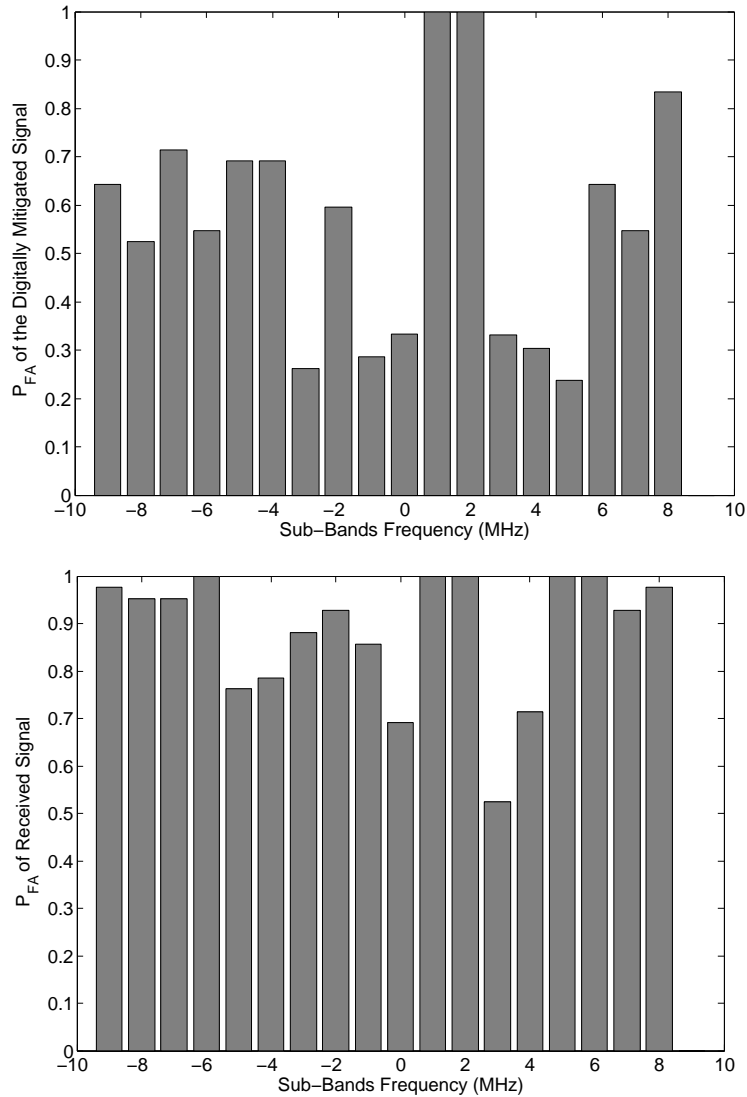


Figure 6.4: Measured P_{FA} (a) with and (b) without the mitigation stage

As shown above, the mitigation stage performs a digital cancellation of the undesired nonlinearities induced by RF front-end's impairments, while the sensing scheme is a blind technique that detects spectrum holes independently from any model estimation. Thus, the combined algorithm is blind and robust against model uncertainty and RF impairments and could be deployed in practical systems. Obtained results validated the theoretical performance of the detector by showing the enhancement in the spectrum of the received signal and the probability of false alarm. However, the only practical limitation that could arise with this dual stage algorithm is the computational complexity. In the coming section, combining and optimizing this algorithm is studied. A new blind, wide band, robust and flexible algorithm is devised to be a perfect candidate for real-

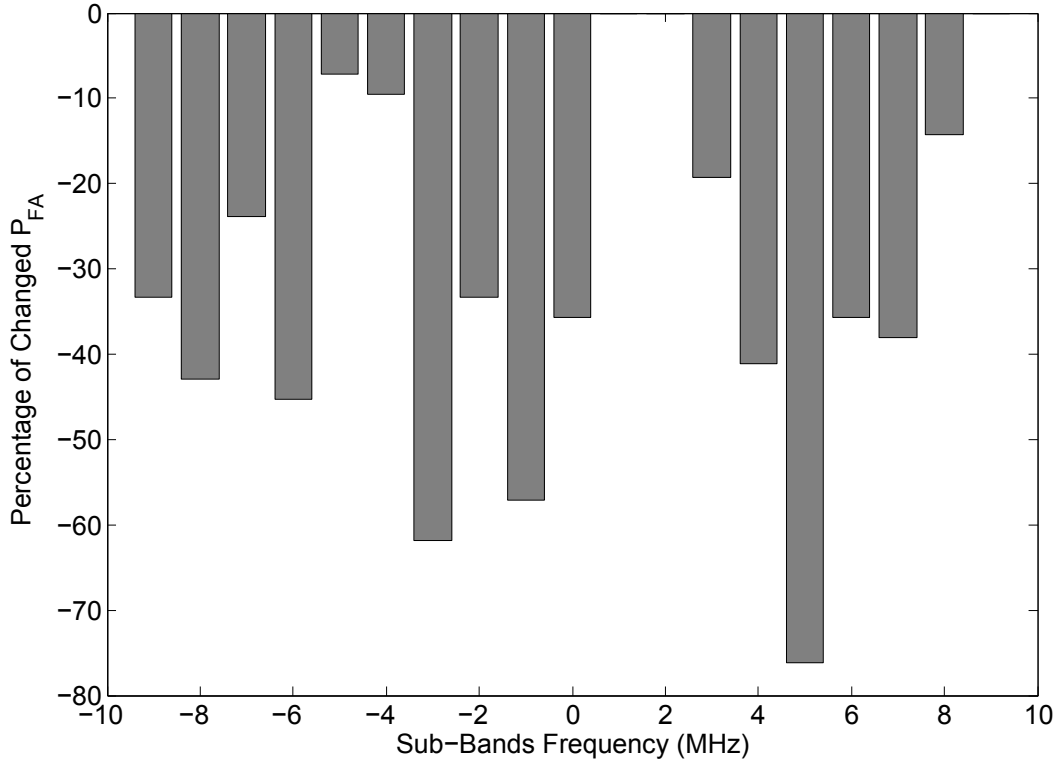


Figure 6.5: The percentage of changed P_{FA} after adding the mitigation stage.

world CR platforms.

6.3 The Proposed Algorithm

The major requirement of a practical CR sensing scheme is the flexibility and the fast computation. A secondary user should rapidly sense the spectrum and make decision of the available transmission opportunities. Any delay could lead to a harmful transmission on a newly occupied band. The efficiency, the robustness, and the blindness of the dual stage wide band detector proposed in the last section are essential characteristics of practical sensing techniques as discussed in the dissertation. In this section, all the previous work is combined to propose a new sensing scheme that takes into consideration all the practical limitations of real-world scenarios and deliver fast and accurate decisions.

6.3.1 Sensing Scheme

In the implementation of the new scheme, the SPCAF detector is selected based on its efficiency and blindness. Its complexity is obviously greater than the ED,

while the latter is less efficient and very sensitive to low SNR values as discussed in Chapter 4. On the other hand, a coarse energy detector is needed to locate the strong PU and mitigate the hardware imperfections, as proposed by [68]. This ED could be used to reduce the complexity of the algorithm by making decisions if a high energy is detected. Consequently, a hybrid sensing will be used to alleviate the complexity of SPCAF. A similar approach is studied in [109] where the cyclostationary based detector is assisted by the ED for uncertain energy levels.

In our proposed algorithm, the ED will be used not only to assist the SPCAF but also to locate strong PU. For that, three ED thresholds are introduced ξ_{min} , ξ_{max} and ξ_S . The calculation of these thresholds is based on the decision results of the proposed algorithm. As illustrated in Figure 6.6, ξ_{min} and ξ_{max} are the boundaries of the “uncertain zone” which corresponds to levels of the signal energy that could mislead the ED. ξ_S is the minimal signal energy that starts to introduce unwanted frequency components in the received wide band signal.

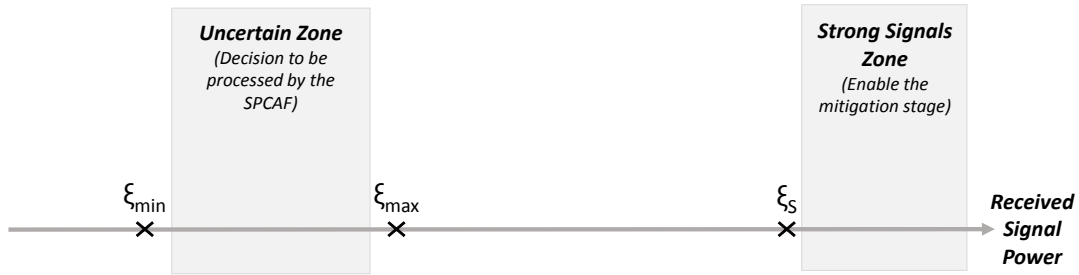


Figure 6.6: Thresholds of the hybrid energy detector

The calculation of the proposed thresholds will be based on averaging the signal levels already processed by the receiver. For example, the initial value of $\xi_{min} = 0$, then it is equal to the average of the past energy levels for which the SPCAF decided a vacant band. Also, the initial value of $\xi_{min} = 80dBm$ (which corresponds to maximum permissible RF power), then, it is equal to the average of the past energy levels for which the SPCAF decided a busy band. For ξ_S , the initial value is set according to the characteristics of the RF front-end (IIP3 and noise floor). A buffer recording the values of the collected energy is controlled by the weights of the adaptive algorithm in the mitigation process. Large weights corresponds to a significant mitigation process, while negligible weights indicate that the mitigation algorithm is not needed for such energy levels. Thus, the value of ξ_S could be modified according to the negligible weights observation. The adaptation of the thresholds is illustrated in the block diagram in Figure 6.7.

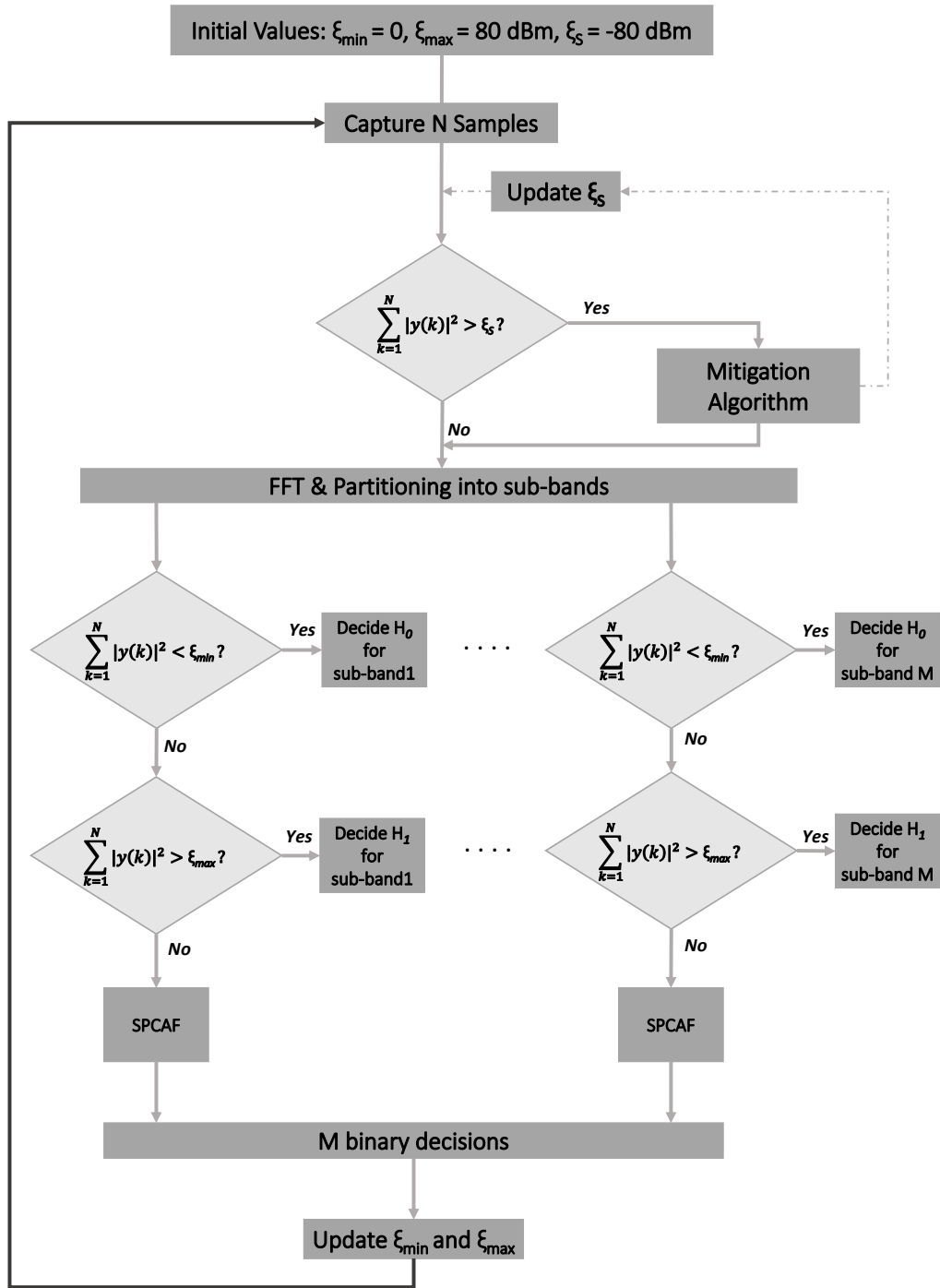


Figure 6.7: Block diagram of the sensing scheme

This hybrid approach for the spectrum sensing will relax the complexity of the SPCAF and will also disable the mitigation technique in the case of negligible distortions. The computational complexity is thus reduced while ensuring an accurate sensing via the SPCAF detector, a robustness to RF impairments via the mitigation algorithm and a blindness by computing adaptively the thresholds of the ED.

6.3.2 Mitigation Algorithm

Another major component of the devised algorithm is the mitigation stage which consists of parallel imitations of the RF impairments model, as depicted in Figure 6.8. The algorithm needs several complex and real filters to adequately partition the strong signal and imitate its distortions. Moreover, M filters are needed to extract the M narrow sub-bands. Since the filters are processed via FFT transformation, we propose to migrate the mitigation algorithm to the frequency domain and perform the mitigation and the LMS equalization on the FFT of the received wide band signal. It was shown in [110, 111] that the frequency-domain implementation of the LMS algorithm is attractive due to both the reduced computational complexity and the potential of faster convergence compared with the time domain implementation. The block diagram of a frequency-domain LMS filter, suggested by [112], is depicted in Figure 6.9. In this approach, the basic steps of the LMS algorithm are implemented with a time variant weights w while the input x , the desired signal d , and the error e are in the frequency domain.

Consequently, in our improved version of the mitigation algorithm, all the filters are replaced with FFT and IFFT transformations. Moreover, the imitation of the RF impairments is much easier in the frequency domain. The I/Q imbalance is imitated by flipping the FFT vector, while the nonlinearities are replaced by a convolution as shown in Figure 6.10. The new four-branch parallel structure is based on the study of the RF impairments presented in Section 5.4 where four unwanted components occupied the spectrum as depicted in Figure 6.11.

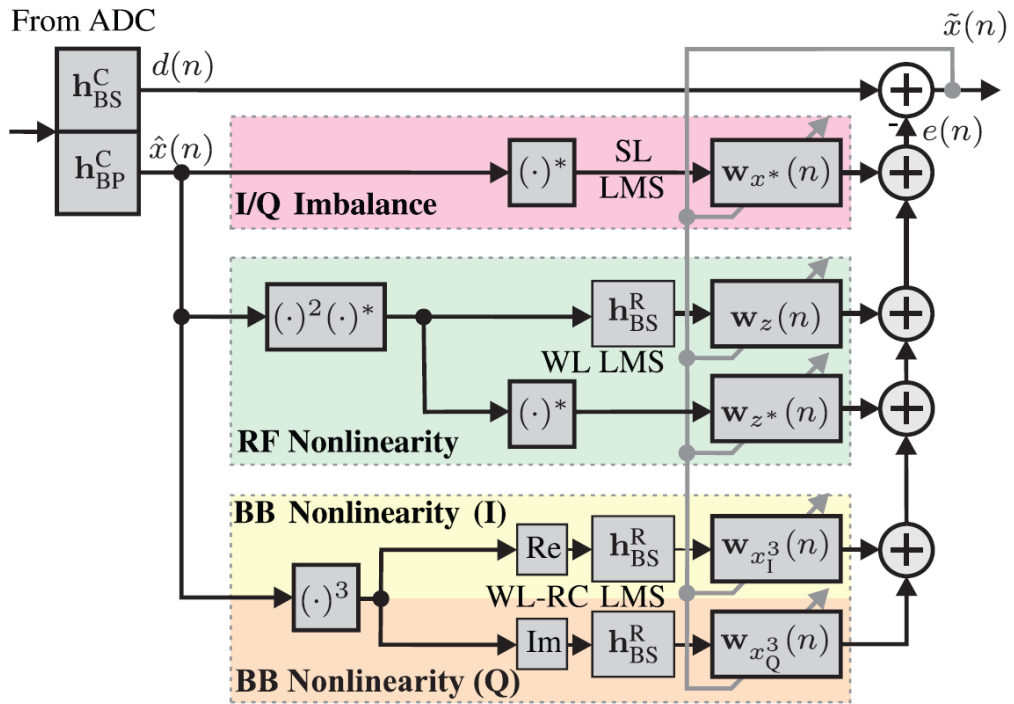


Figure 6.8: Block diagram of the mitigation algorithm proposed in [108]

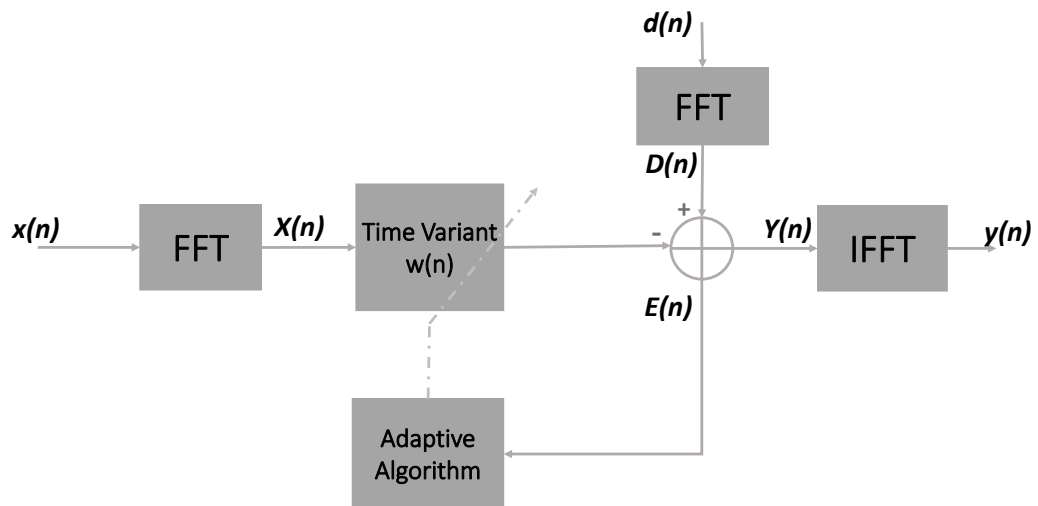


Figure 6.9: Block diagram of frequency-domain implementation of the LMS algorithm

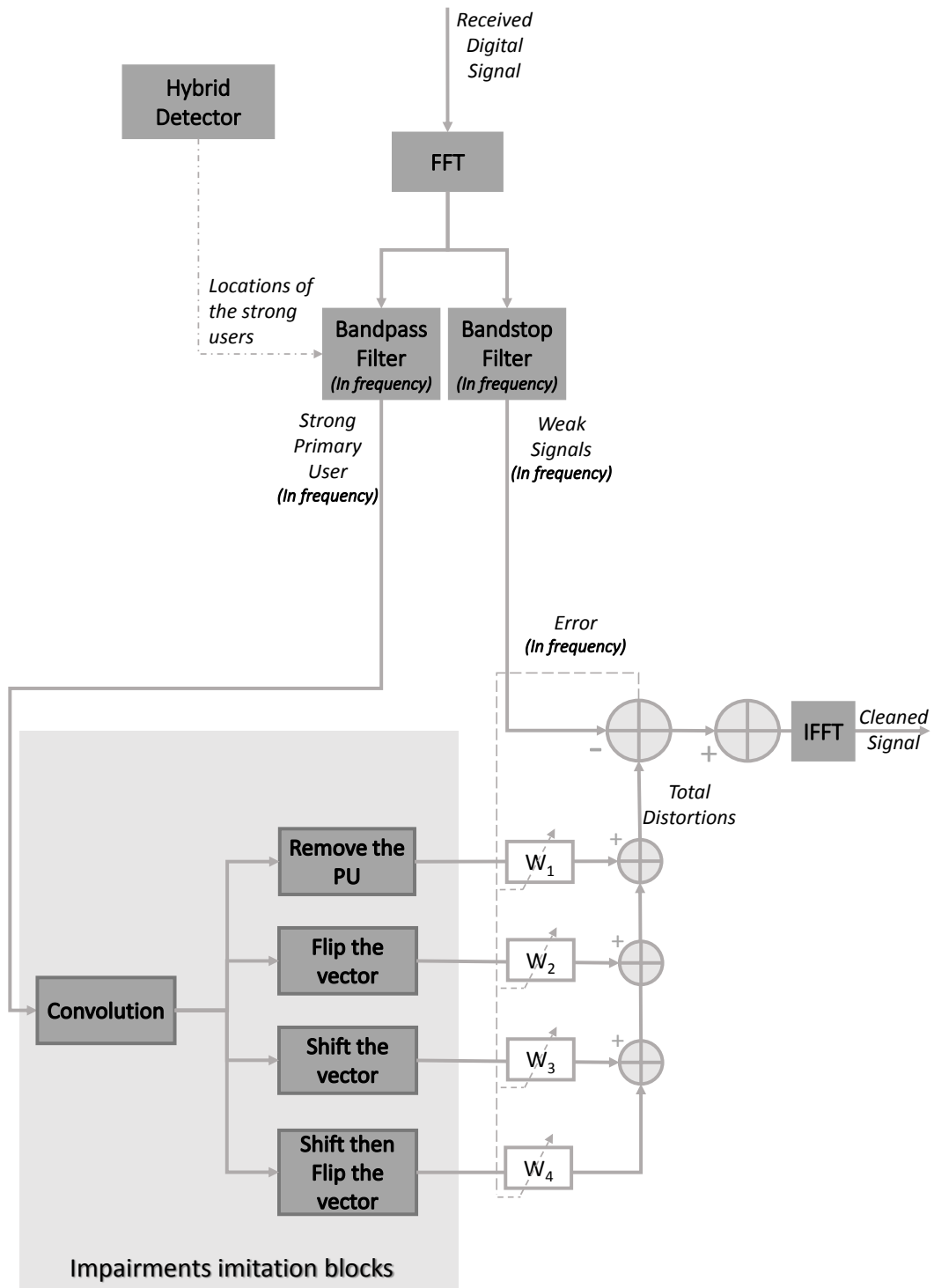


Figure 6.10: Block diagram of the proposed mitigation algorithm

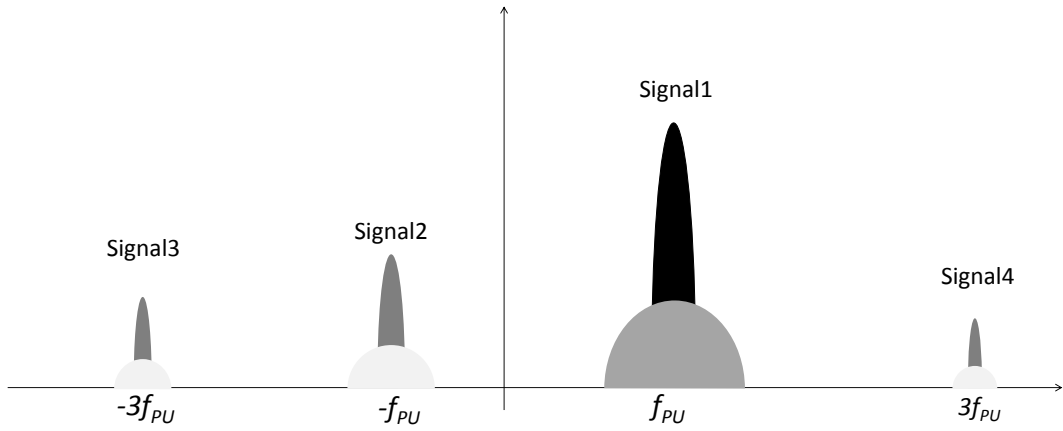


Figure 6.11: Main distortions appearing in the spectrum of the received wide band

6.3.3 The Combined Algorithm

As a result of the above improvements, the devised algorithm is based on a hybrid detection technique combining the SPCAF and the ED. Since the ED can process similar decision with time-domain or frequency-domain signals, the received wide band signal is directly transformed to the frequency domain after being digitized. The output of the FFT is partitioned into M sub-bands where the devised sensing scheme is required to deliver M accurate decisions on the vacancy of these bands. M outputs are fed into an energy detector responsible of three functions. The first function is to enable or not the mitigation algorithm proposed in the previous subsection. This decision depends on the signal power level collected in each of the studied sub-bands. The second function is to deliver a fast and certain binary decision on the occupancy of each sub-band. If the ED is not capable to deliver such decision, i.e. the received signal power is in the uncertain zone, the ED will perform its third function which is enabling the SPCAF detector for the uncertain band. A summarizing block diagram of the proposed algorithm is illustrated in Figure 6.12.

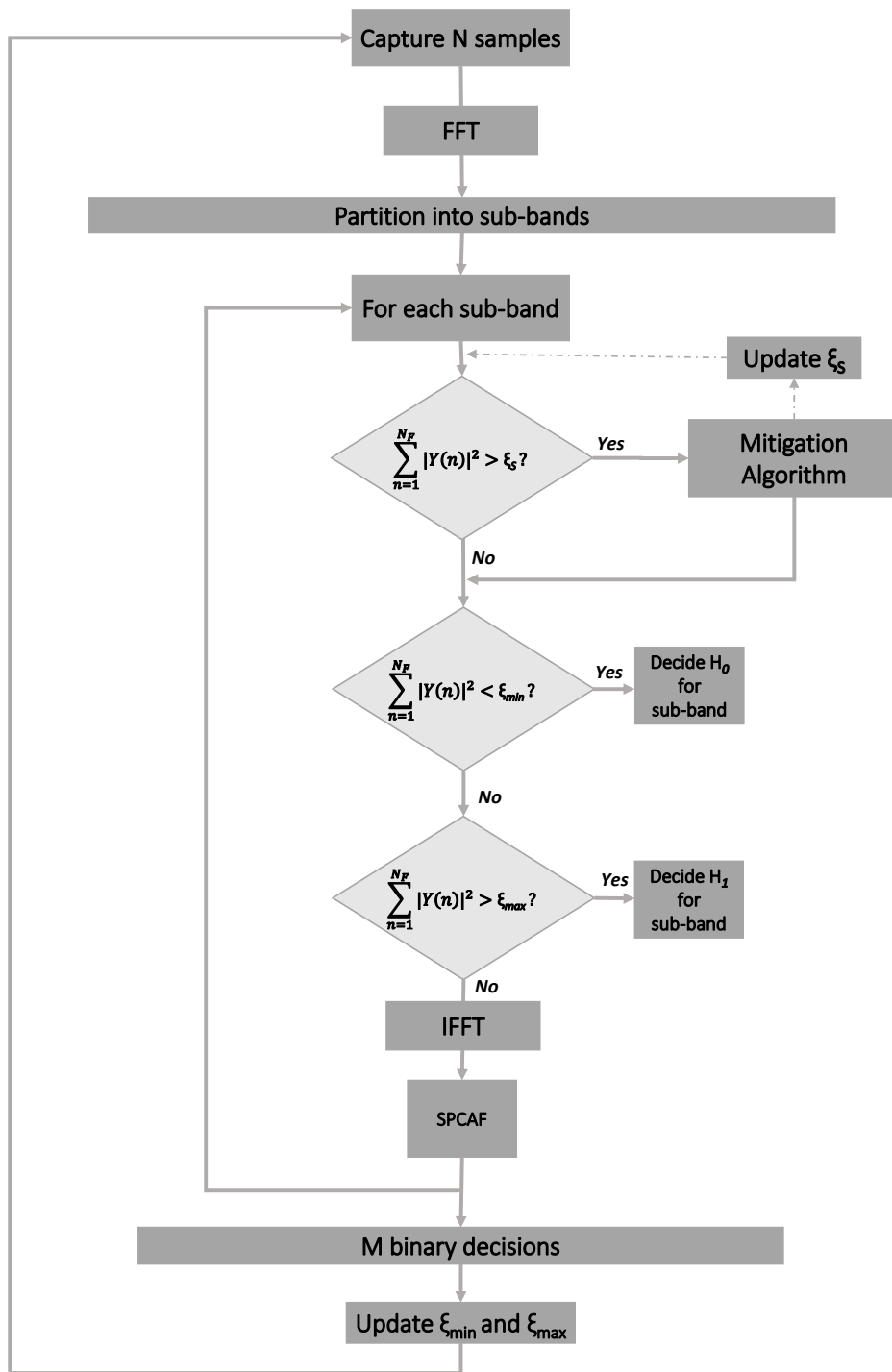


Figure 6.12: Block diagram of the devised algorithm

6.3.4 Results and Discussions

The same test-bed built in section 6.2.2 is considered to test the performance of the devised technique. In this case, the frequency domain output of the mitigation algorithm is illustrated in Figure 6.13. The decisions of the hybrid sensing scheme revealed a clear improvement compared to the results obtained using the dual stage algorithm. Figure 6.14 shows the probability of false alarm obtained without mitigation, with the dual stage algorithm, and with the proposed combined algorithm. The amelioration, shown in Figure 6.15, is obvious in the studied narrow bands. The dual stage algorithm was not able to decide correctly in these bands because of the usage of many filters that induce a cyclostationarity feature in the signal. Performing the mitigation in the frequency domain with a simple parallel structure and using a hybrid approach to sense the wide band spectrum are offering adequate decisions and cleaning the signal from RF distortions.

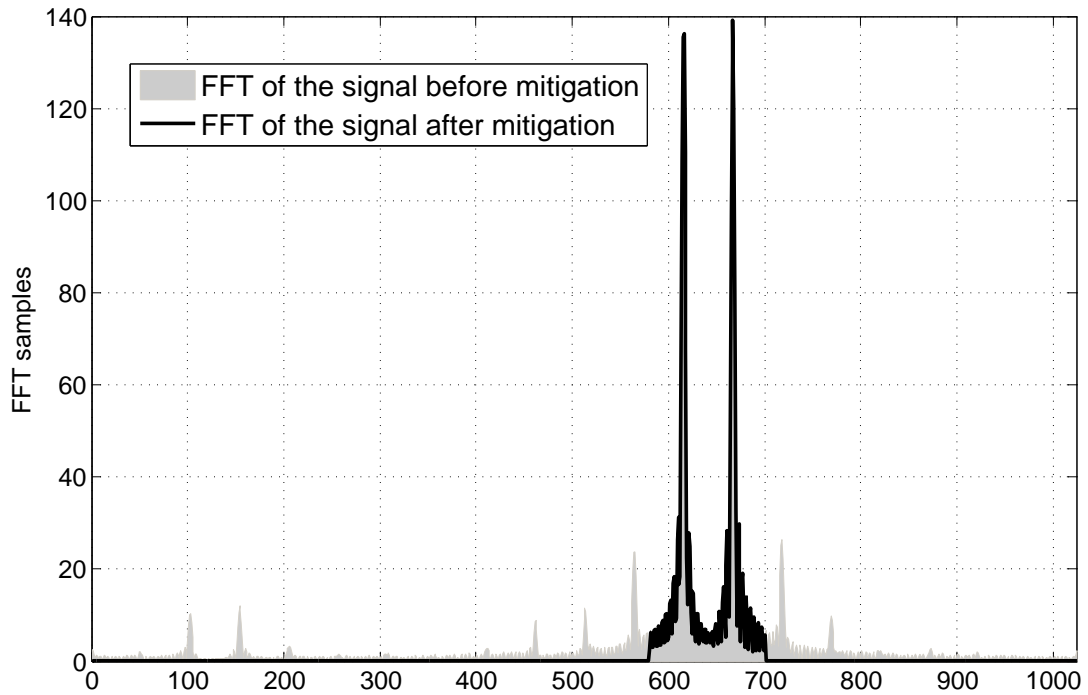


Figure 6.13: FFT of the wideband signal before and after the proposed mitigation stage

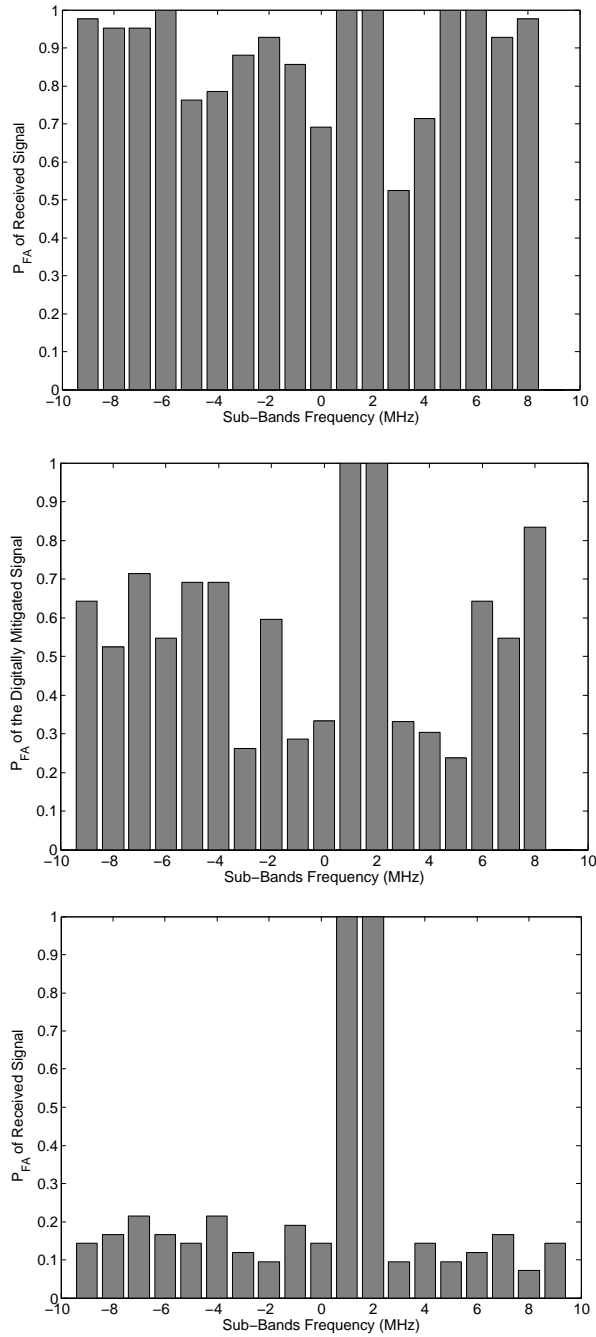


Figure 6.14: Measured P_{FA} (a) without the mitigation stage (b) with the dual stage algorithm (c) with the proposed algorithm

Another test-bed is built to observe the probability of detection provided by the proposed sensing scheme. In this scenario, three USRPs N210 are acting as strong primary transmitter, weak secondary transmitter, and a secondary re-

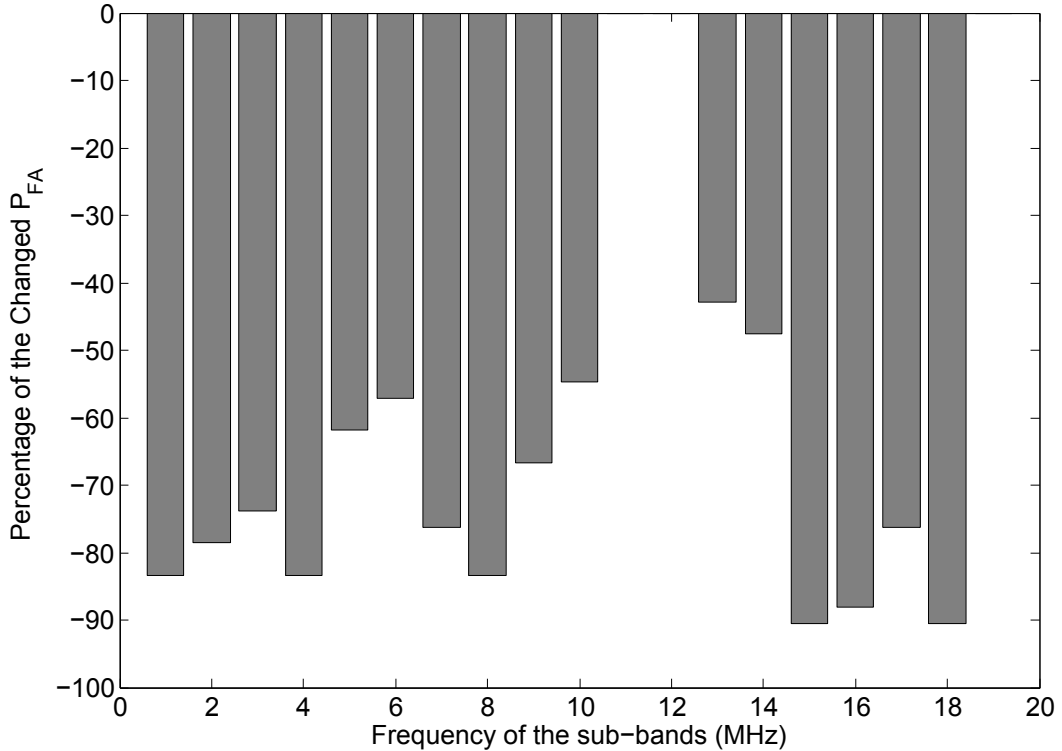


Figure 6.15: The percentage of changed P_{FA} after adding the mitigation stage.

ceiver. The primary signal is a two-tone signal with an input power of -55 dBm sent over the 2.452 and 2.453 GHz carrier frequencies. The secondary transmitter is a BPSK signal with an input power of -100 dBm centered on the 2.448 GHz. At the receiver, a band of 20 MHz around 2.45 GHz is captured and digitized. The daughter-boards analog gain at the transmitter and the receiver is set to 15 and 38 dB, respectively. A sketch of the measurement setup is illustrated in Figure 6.16. The measured probability of detection for the weak secondary transmitter sub-band is $P_D = 0.9745$ proving a good performance in low SNR scenarios.

6.3.5 Computational Complexity

In this section, the major improvement offered by the new sensing scheme is discussed. The computational complexity of the devised algorithm depends mainly on the complexity of the hybrid sensing algorithm and the proposed mitigation technique. In the hybrid technique, the SPCAF having a complexity of $O(N_{IDFT} * n * M * L)$ is assisted by the ED of complexity $O(n)$. In the scenarios conducted for measurements, the percentage of the usage of each of the algorithm is observed. Only 3.56% of the sub-bands are processed using SPCAF and all the other decisions are delivered by the ED since the collected signal power was

in the updated certain zone.

On the other hand, the mitigation technique proposed to compute the received signal in the frequency domain is less complex compared to the algorithm proposed in [108]. The filtering process was the heaviest load in the time-domain mitigation technique. Processing data in the frequency domain alleviated the complexity of the filter design and offered an accurate vector to be processed by the SPCAF without altering the cyclostationarity of the signal.

6.4 Conclusion

In this chapter, a new algorithm for practical spectrum sensing is proposed. The main features of the devised sensing scheme is the optimized computational complexity, the blindness, the robustness against RF impairments, and the efficiency in low SNR scenarios. The algorithm is suitable for wide band scenarios where a strong primary user can harm the efficiency of any sensing scheme by inducing unwanted spectrum components. Test-beds were built to show the cleaned wide band spectra in addition to the probabilities of false alarm and detection for the potential narrow bands. A hybrid sensing approach is used to benefit from the previously studied efficiency of SPCAF and the simplicity of the ED. A frequency-domain mitigation block based on parallel imitation branches is enabled if a strong PU is detected. The measured results affirmed the efficiency of the proposed technique in the presence of a strong PU and/or a weak secondary transmitter. The devised algorithm is thus suitable for practical CR receivers since it is aware of main real-world scenarios challenges.

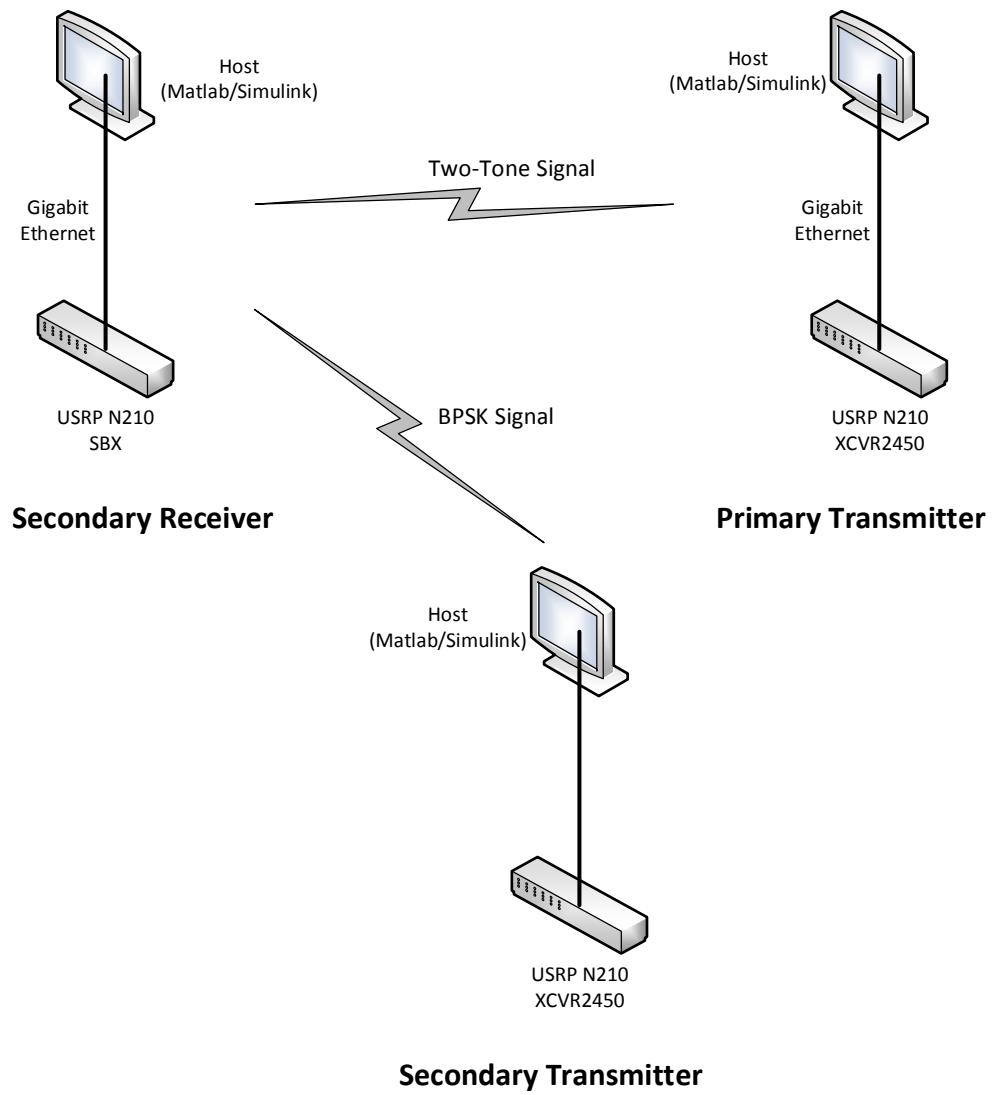


Figure 6.16: A sketch of the measurement setup

Chapter 7

Conclusion

In this chapter, we summarize the main contributions of this thesis and indicate future directions to investigate, which include direct extensions to the proposed work. A list of thesis related publications is also provided.

7.1 Contributions

In this dissertation, signal processing algorithms for building a highly adaptive, fully functional cognitive radio transceiver aware of practical challenges are investigated, implemented and conceived. For that, the contributions of this thesis could be divided into two different areas. The spectrum sculpting algorithms to be implemented in a CR transmitter and the proposed sensing scheme adequate for practical CR receivers. In summary, the main contribution of the thesis was to investigate all the hardware and practical limitations that were not considered in the implementation of DSP techniques, to highlight the resulting problems, and to propose adequate solutions.

Contribution 1: Spectrum sculpting

As discussed in the dissertation, unlicensed users are allowed to access spectrum bands licensed to primary users, while avoiding interference with them. This can be achieved by the use of adaptive UWB pulses characterized by the ability to form, in their spectral masks, nulls in the bands used by existing narrow-band wireless services. This is the concept of spectrum sculpting that can be achieved using two UWB signal design techniques: UWB pulse shaping filter design (hardware solution) and UWB waveform optimization (software solution). For that, spectrum sculpting techniques and hardware filter design were studied. Parks McClellan algorithm and Neural Networks-based algorithm were implemented and their performance was compared to the filter-based spectrum sculpting. It was shown that the hardware limitations accompanied by the filter design could be replaced by a software solution that benefits from the software-based architecture

of CR transceivers.

Contribution 2: Spectrum sensing

In the dissertation, we investigated and proposed signal processing algorithms to be implemented in a highly adaptive cognitive radio receiver. For that, several challenges were studied in depth to deliver a fast, robust, blind and wide band sensing scheme.

Blind spectrum sensing techniques:

As per regulation specifications, secondary users are required to detect very weak licensed users in order to protect primary transmissions. Any missed detection will enable an unlicensed transmission on a busy channel harming the incumbent primary signal. Unfortunately, many detectors reveal a performance degradation at low SNR due to inappropriate estimation of the signal or noise models. This phenomenon is known as SNR wall. For the classical energy detector, an estimation of the noise variance is required to select a suitable threshold. Imperfect knowledge of the noise model, especially in low SNR scenarios, will consequently deteriorate the efficiency of this algorithm. The SNR wall phenomenon also harms any detector based on the received signal's moments. Using cooperative spectrum sensing techniques or relying on calibration and compensation algorithms are possible solutions to the model uncertainty problem. However, using totally blind detectors, that detect the presence of a signal without any knowledge of signal or noise parameters, is considered the ideal alternative. A blind detector based on the symmetry property of the cyclic autocorrelation function (SPCAF) was implemented and tested in real experimental test-beds. A high efficiency of the SPCAF in low SNR scenarios was proved which affirms that such algorithm is suitable for real-world scenarios. To benefit from the simplicity of the energy detector and overcome its model uncertainty problem. A hybrid sensing scheme that combines the blindness of SPCAF and the fast computation of ED is proposed as a fast and blind detector.

Robust spectrum sensing techniques against RF impairments:

In conventional systems, the wireless data transfer between the transmitter and the receiver is assumed to be linear. However, several analog parts of the transceiver RF front-end exhibit impairments such as the analogue-to-digital (ADC) and digital-to-analogue (DAC) converters, the mixer, the local oscillator (LO) and the amplifiers, i.e. the power amplifier (PA) in the transmitter and the low-noise amplifier (LNA) in the receiver. At the receiver side, these imperfection generators become more and more efficacious with the increased dynamic range of the received signal. The challenge grows when the receiver operates over a wide bandwidth since nonlinear distortions will show up as unwanted signals in free bands and can hit the target band. The dissertation studied the RF impairments challenge in two different approaches. The in-band degradation of the sensing

schemes performance is studied. It was shown that the hardware imperfections could damage some detectors efficiency by altering the received signal. On the other hand, another issue could result from RF impairments when a wide band signal is sensed. In this case, the distorted signal will cause out-of-band interferences that could limit the cognitive transmission opportunities. For that, mitigation techniques should assist proposed sensing schemes to alleviate the hardware harmful effect.

As a result, a new sensing scheme is proposed to be deployed in adaptive and smart receivers. As carefully explained in this dissertation, the proposed scheme presents an optimized solution to the main challenges encountered in real-world scenarios.

Universal Software Radio Peripheral (USRP)

To prove the efficacy of the signal processing algorithms investigated and devised in this dissertation, the Universal Software Radio Peripheral (USRP N210) is used as a software defined radio transceiver where real RF signal could be transmitted/received and manipulated via a hosting computer. Hardware modules of the USRP accompanied with the daughter board and the antenna perform the RF and sampling processing. Their different functionalities include the RF filtering, amplifying, mixing and digitizing. On the other hand, the physical layer baseband operations, such as coding/decoding, interleaving, frequency hopping, equalization, and compression are software driven via an FPGA embedded in the USRP N210. To control the USRP transceiver and implement the proposed sensing technique, GNU Radio, an open source software toolkit for software defined radio, is used. GNU Radio offers a user-friendly and sophisticated graphical design environment, known as GNU Radio Companion (GRC), which allows users to create signal flow graphs with built-in communication blocks or out-of-tree modules. Various test-beds were built to present measured data and prove that the theoretically demonstrated algorithms are perfectly working in real scenarios where the hardware imperfections and the models uncertainty could degrade many sensing schemes.

7.2 Other Related Research Work

To ensure a clearer readability of the dissertation, some investigations and results were not described in the chapters of this manuscript. The two main omitted research projects are:

Reconfigurable Antennas:

Reconfigurable antennas are robust in their ability to adapt with changing system requirements or environmental conditions and their provision of additional

levels of functionality for communication systems. Frequency-reconfigurable antennas are designed and tested. The reconfiguration is attained through the use of switching components. Frequency-reconfigurable and notch-reconfigurable antennas are used for communicating in cognitive radio. The work on reconfigurable antennas is done as part of the work on cognitive radio and its hardware limitations.

Spectrum sensing in vehicular environments:

The Wireless Access in Vehicular Environments (WAVE) protocol stack has been recently defined to enable vehicular communication on the Dedicated Short Range Communication (DSRC) frequencies. Some recent studies have demonstrated that the WAVE technology might not provide sufficient spectrum for reliable exchange of safety information over congested urban scenarios. A blind detector is applied and tested on the cars level, to take advantage of their mobility to span a large area of the roads and deliver accurate decisions in vehicular changing environments. A fusion and decision algorithm is used by the Road Side Unit (RSU) to process the individual sensing data and decide on the vacancy of the bands. The performance of the sensing algorithm is evaluated and tested in various scenarios.

7.3 Future Research

Cognitive Radio is a swiftly evolving research area with most of the work still to be done. The following points summarize possible extensions of the dissertation's ideas.

Control of Reconfigurable Antennas:

Reconfigurable antennas employ switching devices such as RF MEMS, PIN diodes, and varactors, or motors to rotate some antenna parts. These devices should be driven, by controlling the voltage/current applied to them. The implementation of such control is a continuation of the dissertation focusing on calibrating the hardware using the software.

Control of RF Blocks in Cognitive Radios:

Any wireless communication system has, in addition to an antenna, RF blocks such as filters, low-noise amplifiers (LNAs), mixers, and oscillators. In CR systems, the RF front-end, which includes the antenna and the related RF blocks, should be agile. Digitally controlling the parameters of these RF blocks for CR is essential to the plan of producing a fully working CR system.

Machine learning in Spectrum Sensing:

To this date, most cognitive radio researchers have focused on smart radios that

obey to a list of rules on how the radio should behave in certain scenarios. At the level of the cognitive terminal, spectrum sensing algorithms are not benefiting from any past experience or decisions made by the radio. Since the RF impairments of the radio have static results and could be slowly changing within an acceptable range of time, reasoning and learning techniques could be added to the devised algorithms to enhance the fast response of the radio.

Adaptive Collaborative Sensing

After tackling the spectrum sensing at the terminal level, the study of an adaptive collaborative network of secondary users is important to measure the obtained improvement after adding sophisticated DSP techniques. Decision making algorithms will be studied and a fully functioning cognitive network could be implemented via USRPs to acquire real-time results.

7.4 Publications

7.4.1 Book Chapters

- [1] **L. Safatly**, A. Ramadan, M. Al-Husseini, Y. Nasser, K.Y. Kabalan and A. El-Hajj. “*Tunable RF Front-ends and Robust Sensing Algorithms for Cognitive Radio Receivers*“, in *Software-Defined and Cognitive Radio Technologies for Dynamic Spectrum Access and Management*, IGI Global, 2014, [In review].

7.4.2 Journal papers

- [1] K. Baraka, **L. Safatly**, H. Artail, A. Ghandour and A. El-Hajj. “*A Vehicle-Infrastructure Cooperative Spectrum Sensing Scheme for Vehicular Ad hoc Networks*“, *Ad Hoc Networks Elsevier*, Jan. 2014, [In review].
- [2] **L. Safatly**, M. Bkassiny, M. Al-Husseini and A. El-Hajj. “*Cognitive Radio Transceivers: RF, Spectrum Sensing and Learning Algorithms*“, Special Issue on Antennas and RF Front Ends for Cognitive Radio in *International Journal of Antennas and Propagation*, vol. 2014, Article ID 548473, 21 pages, 2014. doi:10.1155/2014/548473.
- [3] **L. Safatly**, B. Aziz, A. Nafkha, Y. Louet, Y. Nasser, A. El-Hajj, and K.Y. Kabalan. “*Blind Spectrum Sensing using Symmetry Property of Cyclic Autocorrelation Function: From Theory to Practice*“, *EURASIP Journal on Wireless Communications and Networking*, vol. 2014, no. 1, p. 26, 2014.

- [4] **L. Safatly**, M. Al-Husseini, A. El-Hajj and K. Y. Kabalan. “*Advanced Techniques and Antenna Design for Pulse Shaping in UWB Cognitive Radio*“, International Journal of Antennas and Propagation, vol. 2012, Article ID 390280, 8 pages, 2012.
- [5] M. Al-Husseini, **L. Safatly**, A. Ramadan, A. El-Hajj, K. Y. Kabalan, and C. G. Christodoulou. “*Reconfigurable Filter Antennas for Pulse Adaptation in UWB Cognitive Radio*“, Progress In Electromagnetics Research B, Vol. 37, 327-342, 2012.

7.4.3 Conference papers

- [1] **L. Safatly**, A. El-Hajj, K. Y. Kabalan, and H. Artail. “*Blind and Robust Spectrum Sensing Based on RF Impairments Mitigation for Cognitive Radio Receivers*“, The International Conference on High Performance Computing & Simulation (HPCS 2014), Bologna, Italy, July 2014. [In review]
- [2] **L. Safatly**, A. El-Hajj, and K. Y. Kabalan. “*A Practical Study of a Blind Spectrum Sensing Technique in Real Cognitive Radio Scenarios*“, National Wireless Research Collaboration Symposium (NWRCS2014), Idaho, USA, May 2014. [Accepted for Publication]
- [3] M. Haroun, H. Kobeissi, **L. Safatly**, H. Elmokdad, O. Bazzi, K. Y. Kabalan, and Y. Nasser. “*Effect of RF Impairments on Spectrum Sensing Techniques*“, Wireless Telecommunications Symposium 2014 (WTS 2014), Washington D.C., USA, Apr. 2014. [Accepted for Publication]
- [4] **L. Safatly**, M. Al-Husseini, A. El-Hajj, and K. Y. Kabalan. “*A Reduced-Size Antipodal Vivaldi Antenna with a Reconfigurable Band Notch*“, Progress in Electromagnetics Research Symposium (PIERS 2012), Moscow, Russia, Aug. 2012.

7.4.4 Presentations

- [1] **L. Safatly**, A. Ramadan, and K.Y. Kabalan. “*RF Energy Harvesting, Reconfigurable Antennas, Cognitive Radio, and EM Demining*“, The 3rd International Low Tech — High Tech Workshop, Beirut, Lebanon, Dec. 2013.
- [2] **L. Safatly**, A. El-Hajj, K.Y. Kabalan, and Y. Nasser. “*Dual Stage Spectrum Sensing Algorithm for RF Non-Linearity Mitigation in Wideband Cognitive Radio Receivers*“, CR summer school, London UK, July 2013.

- [3] **L. Safatly**, M. Al-Husseini, A. El-Hajj, and K. Y. Kabalan. “*Adaptive Pulses for UWB Cognitive Radio*“, Workshop on Antenna Design And Applications, Balqaa University, Jordan, May 2011.

Abbreviations

ADC	Analog-to-Digital Converter
AGC	Automatic Gain Controller
AIC	Adaptive Interference Cancellation
AWGN	Additive White Gaussian Noise
BB	Base Band
BPSK	Binary Phase Shift Keying
CAF	Cyclic Autocorrelation Function
CDMA	Code Division Multiple Access
CFO	Carrier Frequency Offset
CPO	Common Phase Error
CR	Cognitive Radio
CSD	Cyclostationary Spectrum Density
CSRR	Complementary Split-Ring Resonator
DAC	Digital-to-Analog Converter
DDC	Digital Down Converter
DFT	Discrete Fourier Transform
DSP	Digital Signal Processor
DUC	Digital Up Converter
DVB-T	Digital Video Broadcasting - Terrestrial
ED	Energy Detector
EIRP	Equivalent Isotropically Radiated Power
FA	False Alarm
FCC	Federal Communications Commission
FFT	Fast Fourier Transform
FPGA	Field Programmable Gate Array
GPP	General Purpose Processor
GRC	GNU Radio Companion
GSM	Global System for Mobile Communications
ICI	Intercarrier Interference
IDFT	Inverse Discrete Fourier Transform
ISM	Industrial, Scientific and Medical (radio band)
LMS	Least Mean Square
LNA	Low-Noise Amplifier

LO	Local Oscillator
MD	Missed Detection
NL	Non Linearities
NN	Neural Networks
OFDM	Orthogonal Frequency Division Multiplexing
OMP	Orthogonal Matching Pursuit
PA	Power Amplifier
PDF	Probability Density Function
PN	Phase Noise
PP	Parks-McClellan
PSD	Power Spectral Density
PU	Primary User
RBF	Radial Basis Function
RF	Radio Frequency
ROC	Receiver Operating Characteristic
SDR	Software-Defined Radio
SNR	Signal-to-Noise Ratio
SPCAF	Symmetry Property of the Cyclic Autocorrelation Function
SRR	Split-Ring Resonator
SU	Secondary User
UHD	Universal Hardware Driver
UHF	Ultra High Frequency
UHF	Ultra-High Frequency
U-NII	Unlicensed National Information Infrastructure (radio band)
USRp	Universal Software Radio Peripheral
UWB	Ultra-Wide Band
WAP	Wireless Access Point
WiMAX	Wireless Interoperability for Microwave Access
WLAN	Wireless Local Area Network
WRAN	Wireless Regional Area Network

Appendix A

Parks-McClellan Algorithm

The algorithm description

The Parks-McClellan algorithm is an efficient and fast procedure used for the design of finite-length impulse response filters with linear phase. It delivers the optimum Chebyshev approximation on separate intervals corresponding to passbands and/or stopbands. The ParksMcClellan algorithm is a variation of the Remez exchange algorithm to meet FIR filters design specifications. It has become a standard method for FIR filter design. A detailed description of the procedure is given in [29] for low-pass filters. Table 7.1 highlights the main steps of the algorithm.

In summary, the algorithm started with an initial setting of the positions of the extrema. Initially, they are evenly spaced in the pass and stop bands. In each iteration of the algorithm, a polynomial interpolation is performed to re-estimate the positions of the local extrema. After moving the extrema to new positions, the shift between the old and new position is calculated. A new iteration is enabled while a non-zero shift is observed.

The Matlab function

The MATLAB function *firpm* implements the Parks-McClellan algorithm. $b = \text{firpm}(n, f, a)$ returns row vector b containing the $n + 1$ coefficients of the order n FIR filter whose frequency-amplitude characteristics match those given by vectors f and a . *firpm* is used with *firpmord*, which finds the approximate order, normalized frequency band edges, frequency band amplitudes, and weights that meet the filter's specifications.

Table 7.1: Steps of the Parks McClellan Algorithm

Initialize: Choose an extremal set of frequencies $\{w_i^{(0)}\}$

For m iterations

- a) **Finite Set Approximation:** Calculate the best Chebyshev approximation on the present extremal set.
- b) Let $\delta^{(m)}$ be the value of the min-max error on the present extremal set.
- c) **Interpolation:** Calculate the error function $E(\omega)$ over the entire set of frequencies Ω using $\delta^{(m)}$.
- d) Find $|E^{(m)}(\omega)|$ the local maxima of the set Ω .
- e) **If** $\max_{\omega \in \Omega} |E^{(m)}(\omega)| > \delta^{(m)}$
 - ✓ Update the extremal set to $\{w_i^{(m+1)}\}$ by picking new frequencies where $|E^{(m)}(\omega)|$ has its local maxima.
 - ✓ Return to Step a and iterate.
- e) **Else**
 - ✓ Break

Algorithm Complete :

Use the set $\{w_i^{(m)}\}$ and the inverse discrete Fourier transform to obtain the filter coefficients.

List of Figures

1.1	Schematic block diagram of a digital radio	2
1.2	The universal software radio peripheral (USRP)	3
1.3	The US spectrum allocation chart [11]	4
1.4	Analog and digital blocks of a CR transceiver	5
1.5	Measurement of 0-6 GHz spectrum utilization [14]	6
1.6	RF/analog front-end architecture for CR receivers	7
2.1	The pulse generated by the PM algorithm	13
2.2	PSD of the pulse generated by the PM algorithm	14
2.3	RBF Neural Network model	14
2.4	PSD of the pulse generated by the neural network in Matlab . . .	15
2.5	PSD of the pulse generated by NeuroSolution	16
2.6	Photo of the designed dual stop-band filter	17
2.7	Configuration of the designed dual stop-band filter	17
2.8	Simulated and Measured S11	18
2.9	Simulated and Measured S21	18
2.10	Input Gaussian monocycle and corresponding output	20
2.11	Input Scholtz's monocycle and corresponding output	20
2.12	Antenna geometry	21
2.13	Antenna photo	22
2.14	Reflection coefficient when all switches are tuned OFF	22
2.15	Reflection coefficient when all switches are tuned ON	23
2.16	Radiation pattern at 4 or 6 GHz when switches are turned ON or OFF	23
3.1	Possible scenarios of detection	26
3.2	ROC of the energy detector	27
3.3	Block diagram of the energy detector	28
3.4	Simulated and theoretical ROC of the ED for $n = 80$ and $SNR =$ $-7dB$	30
3.5	Theoretical 3D plot of a CAF	31
3.6	Theoretical 3D plot of a CSD	32
3.7	Block diagram of the cyclostationarity feature based detector . . .	33

3.8	ROC Curves for comparison between spectrum sensing algorithms	34
3.9	A wideband spectrum seen as a train of narrowband signals and presenting frequency irregularities	38
3.10	Block diagram of Wavelet transform based technique.	39
4.1	ROC of the SPCAF detector for a BPSK signal at SNR = 0dB . .	46
4.2	Theoretical plot of the norm of the CAF of a BPSK signal	47
4.3	Estimated plot of the norm of the CAF of a BPSK signal	47
4.4	Block Diagram of the SPCAF algorithm	48
4.5	GNU Radio interface through SWIG	49
4.6	A snapshot of the GNU radio receiver model with ED and SPCAF detectors blocks.	50
4.7	Hardware/Software platform	51
4.8	Photo of the implemented testbed to test the performance of SPCAF	51
4.9	Sketch of scenario 1: USRP Signals	53
4.10	Sketch of scenario 2: 3G Network	54
4.11	Sketch of scenario 3: 802.11ac indoor channel	55
4.12	Probability of Detection versus SNR for scenario 1	56
4.13	Probability of detection of the SPCAF detector in DVB-T scenarios.	57
4.14	Probability of false alarm of the SPCAF detector in DVB-T scenarios.	58
4.15	Probability of Detection versus SNR for scenario 3	59
4.16	Effect of number of received samples on detection performance of SPCAF.	60
4.17	Effect of FFT length on the detection performance of SPCAF. . .	61
4.18	Effect of maximum value delay τ on detection performance of SPCAF.	62
5.1	Block diagram of a commercial tunable RF front-end sensing receiver	64
5.2	Down-converted Signals in the Megahertz Vicinity	65
5.3	Stages of the RF Frontend of a receiver	67
5.4	ROC of the ED for different values of CFO $\epsilon = M\Delta fT_S$	68
5.5	ROC of the SPCAF for different values of CFO $\epsilon = M\Delta fT_S$. . .	69
5.6	ROC of the SPCAF for different values of βT_S	70
5.7	ROC of the ED for different values of θ	71
5.8	ROC of the ED for different values of g	72
5.9	ROC of the SPCAF for different values of g	73
5.10	ROC of the SPCAF for different values of θ	73
5.11	ROC of the ED with nonlinear components	75
5.12	ROC of the SPCAF with nonlinear components	75
5.13	Block diagram of the blind phase noise compensator scheme . . .	76
5.14	Block diagram of the blind I/Q Imbalance compensator scheme .	77
5.15	Wide band receiver stages and corresponding impairments	78

5.16	Wide band receiver stages and corresponding impairments	79
5.17	Spectrum Density of the transmitted and the received signals . . .	81
5.18	Probability of false alarm of the SPCAF for the transmitted and received signal	82
5.19	The AIC algorithm	82
5.20	The improved adaptive mitigation algorithm	83
6.1	The proposed dual-stage algorithm	86
6.2	A sketch of the measurement setup	87
6.3	The spectra of the received signal before and after the mitigation stage.	88
6.4	Measured P_{FA} (a) with and (b) without the mitigation stage . . .	89
6.5	The percentage of changed P_{FA} after adding the mitigation stage.	90
6.6	Thresholds of the hybrid energy detector	91
6.7	Block diagram of the sensing scheme	92
6.8	Block diagram of the mitigation algorithm proposed in [108] . . .	94
6.9	Block diagram of frequency-domain implementation of the LMS algorithm	94
6.10	Block diagram of the proposed mitigation algorithm	95
6.11	Main distortions appearing in the spectrum of the received wide band	96
6.12	Block diagram of the devised algorithm	97
6.13	FFT of the wideband signal before and after the proposed mitiga- tion stage	98
6.14	Measured P_{FA} (a) without the mitigation stage (b) with the dual stage algorithm (c) with the proposed algorithm	99
6.15	The percentage of changed P_{FA} after adding the mitigation stage.	100
6.16	A sketch of the measurement setup	102

List of Tables

3.1	Steps of the MME detector	36
4.1	Steps of the SPCAF detector	45
4.2	Parameters of the experiments at 802.11ac indoor channel	54
7.1	Steps of the Parks McClellan Algorithm	113

Bibliography

- [1] F. K. Jondral, “Software-Defined Radio: Basics and Evolution to Cognitive Radio,” *EURASIP Journal on Wireless Communications and Networking*, vol. 2005, no. 3, pp. 275–283, August 2005.
- [2] J. Mitola III, “Cognitive Radio for Flexible Mobile Multimedia Communications,” in *Proceedings of the 1999 IEEE International Workshop on Mobile Multimedia Communications (MoMuC’99)*, (San Diego, CA, USA), pp. 3–10, November 1999.
- [3] M. Nekovee, “Dynamic Spectrum Access - Concepts and Future Architectures,” *BT Technology Journal*, vol. 24, no. 2, pp. 111–116, April 2006.
- [4] J. Mitola, “Cognitive Radio: An Integrated Agent Architecture for Software Defined Radio,” PhD Thesis, Royal Institute of Technology (KTH), Stockholm, Sweden, May 2000.
- [5] S. Haykin, “Cognitive Radio: Brain-Empowered Wireless Communications,” *IEEE Journal on Selected Areas in Communications*, vol. 23, no. 2, pp. 201–220, February 2005.
- [6] FCC, “Spectrum Policy Task Force Report,” tech. rep., 2002.
- [7] M. McHenry, D. McCloskey, and G. Lane-Roberts, “Spectrum Occupancy Measurements, Location 4 of 6: Republican National Convention, New York City, NY, Aug. 30, 2004-Sept. 3, 2004, revision 2,” tech. rep., Shared Spectrum Company, August 2005.
- [8] A.J. Petrin, “Maximizing the Utility of Radio Spectrum: Broadband Spectrum Measurements and Occupancy Model for Use by Cognitive Radio,” PhD Thesis, Georgia Institute of Technology, Atlanta, GA, USA, August 2005.
- [9] D.A. Roberson, C.S. Hood, J.L. LoCicero, and J.T. MacDonald, “Spectral Occupancy and Interference Studies in Support of Cognitive Radio Technology Deployment,” in *Proceedings of the First IEEE Workshop on Network Technologies for Software-Defined Radio Networks*, (Reston, USA), pp. 26–35, September 2006.

- [10] M. Wellens, A. de Baynast, and P. Mahonen, "Exploiting Historical Spectrum Occupancy Information for Adaptive Spectrum Sensing," in *Proceedings of the 2008 IEEE Wireless Communications and Network Conference (WCNC 2008)*, (Las Vegas, NV, USA), pp. 717–722, March 2008.
- [11] NTIA, "U.S. Frequency Allocation Chart," tech. rep., <http://www.ntia.doc.gov/osmhome/allochrt.pdf>, 2003.
- [12] J. Ma, G.Y. Li, and B.H. Juang, "Signal Processing in Cognitive Radio," *Proceedings of the IEEE*, vol. 97, no. 5, pp. 805–823, May 2009.
- [13] D. Cabric, S.M. Mishra, and R.W. Brodersen, "Implementation Issues in Spectrum Sensing for Cognitive Radios," in *Proceedings of 38th Asilomar Conference on Signals, Systems and Computers*, (Asilomar, CA, USA), pp. 772–776, November 2004.
- [14] J. Yang, "Spatial Channel Characterization for Cognitive Radios," MS Thesis, UC Berkeley, January 2004.
- [15] M. Kitsunezuka, K. Kunihiro, and M. Fukaishi, "Efficient Use of the Spectrum," *IEEE Microwave Magazine*, vol. 13, no. 1, pp. 55–63, Jan-Feb., 2012.
- [16] H. Darabi, A. Mirzaei, and M. Mikhemar, "Highly Integrated and Tunable RF Front Ends for Reconfigurable Multiband Transceivers: A Tutorial," *IEEE Transactions on Circuits and Systems I: Regular Papers*, vol. 58, pp. 2038–2050, Sept 2011.
- [17] H. Harada, "A Small-Size Software Defined Cognitive Radio Prototype," in *IEEE 19th International Symposium on Personal, Indoor and Mobile Radio Communications, 2008 (PIMRC 2008)*, pp. 1–5, Sept 2008.
- [18] H. Harada, "A Feasibility Study on Software Defined Cognitive Radio Equipment," in *3rd IEEE Symposium on New Frontiers in Dynamic Spectrum Access Networks, 2008 (DySPAN 2008)*, pp. 1–12, Oct 2008.
- [19] A. Tyagi and R.V. Rajakumar, "A Wideband RF Frontend Architecture for Software Defined Radio," *Circuits, Systems, and Signal Processing*, vol. 30, no. 4, pp. 689–704, 2011.
- [20] S. Balasubramanian, S. Boumaiza, H. Sarbishaei, T. Quach, P. Orlando, J. Volakis, G. Creech, J. Wilson, and W. Khalil, "Ultimate Transmission," *IEEE Microwave Magazine*, vol. 13, pp. 64–82, Jan 2012.
- [21] Z. Zhou, B. Li, and Q. Song, "Open Spectrum and UWB Research in China: Spectrum Reform and Radio Revolution," in *Proceedings of 2010*

- IEEE International Conference on Ultra-Wideband (ICUWB 2010)*, (Nanjing, China), pp. 1–5, September 2010.
- [22] H. Arslan and M. Sahin, “UWB-Based Cognitive Radio Networks,” in *Cognitive Wireless Communication Networks* (E. Hossain and V.K. Bhargava, ed.), pp. 213–230, Springer US, 2007.
- [23] S. Nag, M.A. Barnes, and T. Payment, “An Ultra-Wideband Through-Wall Radar for Detecting the Motion of People in Real Time,” in *Proceedings of the international society for optics and photonics (SPIE)*, (Orlando, FL, USA), pp. 48–57, July 2002.
- [24] D.S. Zeng, A. Annamalai Jr., and A.I. Zaghloul, “Pulse Shaping Filter Design in UWB System,” in *Proceedings of the 2003 IEEE Conference on Ultra-Wideband Systems and Technologies (ICUWB-ST 2003)*, (Reston, Virginia, USA), pp. 66–70, November 2003.
- [25] S.H. Liao, M.H. Ho, C.H. Chen, C.C. Chiu, and W.C. Chung, “A Novel DS-UWB Pulses Design Using Genetic Algorithm,” in *Proceedings of the International Conference on Future Computer and Communication*, (Kuala Lumpur, Malaysia), pp. 296–300, April 2009.
- [26] M.P. Wylie-Green, “Adjacent Frequency Coding Technique for Decreasing MB-OFDM Ultra-WideBand Interference to Other Radio Services,” in *Proceedings of the 2006 IEEE Sarnoff Symposium (SARNOF 2006)*, (Princeton, NJ, USA), pp. 1–4, March 2006.
- [27] R.M. Yang, Z. Zhou, and L.Y. Zhang, “Detection and Avoidance Scheme for DS-UWB System: a Step Towards Cognitive Radio,” *IET Communications*, vol. 2, no. 8, pp. 1043–1050, September 2008.
- [28] T. Dissanayake and K.P. Esselle, “Prediction of the Notch Frequency of Slot Loaded Printed UWB Antennas,” *IEEE Transactions on Antennas and Propagation*, vol. 55, no. 11, pp. 3320–3325, November 2007.
- [29] J. McClellan and T.W. Parks, “A Personal History of the Parks-McClellan Algorithm,” *IEEE Signal Processing Magazine*, vol. 22, no. 2, pp. 82–86, March 2005.
- [30] X. Shi, “Adaptive UWB Pulse Design Method for Multiple Narrowband Interference Suppression,” in *Proceedings of the Intelligent Computing and Intelligent Systems (ICIS) IEEE International Conference*, (Missouri, USA), pp. 545–548, October 2010.
- [31] J.J. Hopfield, “Neural Networks and Physical Systems with Emergent Collective Computational Abilities,” in *Proceedings of the National Academy of Sciences of USA*, vol. 79, (USA), pp. 2554–2558, 1982.

- [32] J. D. Powell, *Radial Basis Function Approximations to Polynomials*. Dundee UK: Numerical Analysis, 1987.
- [33] L. Bin, Z. Zheng, and Z. Weixia, "A Novel Spectrum Adaptive UWB Pulse: Application in Cognitive Radio," in *Proceedings of the 2009 IEEE Vehicular Technology Conference (VTC 2009-Fall)*, (Anchorage, AK), pp. 1–5, September 2009.
- [34] J. B. Pendry, A.J. Holden, D.J. Robbins, and W.J. Stewart, "Magnetism from Conductors and Enhanced Nonlinear Phenomena," *IEEE Transactions on Microwave Theory and Techniques*, vol. 47, no. 11, pp. 2075–2084, November 1999.
- [35] Y. Zhang, W. Hong, C. Yu, Z. Kuai, Y. Don and J. Zhou, "Planar Ultra WideBand Antennas with Multiple Notched Bands Based on Etched Slots on the Patch and/or Split Ring Resonators on the Feed Line," *IEEE Transactions on Antennas and Propagation*, vol. 56, no. 9, pp. 3063–3068, September 2008.
- [36] M. Al-Husseini, A. Ramadan, Y. Tawk, C.G. Christodoulou, K.Y. Kabalan, and A. El-Hajj, "A Planar Ultra WideBand Antenna with Multiple Controllable Band Notches for UWB Cognitive Radio Applications," in *Proceedings of the 5th European Conference on Antennas and Propagation (EuCAP 2011)*, (Rome, Italy), pp. 375–377, April 2011.
- [37] Ansoft HFSS, "Pittsburg, PA 15219."
- [38] B. Parr, C. ByungLok Cho, K. Wallace, and D. Zhi, "A Novel Ultra-WideBand Pulse Design Algorithm," *IEEE Communications Letters*, vol. 7, no. 5, pp. 219–221, May 2003.
- [39] P. Withington, "Impulse Radio Overview," Time Domain Corporation, <http://user.it.uu.se/~carle/Notes/UWB.pdf>.
- [40] X. Chen and S. Kiaei, "Monocycle Shapes for Ultra WideBand System," in *Proceedings of the 2002 IEEE International Symposium on Circuits and Systems*, vol. 1, (Scottsdale, Arizona, USA), pp. 597–600, August 2002.
- [41] T. Yucek and H. Arslan, "A Survey of Spectrum Sensing Algorithms for Cognitive Radio Applications," *Communications Surveys and Tutorials*, vol. 11, no. 1, pp. 116–130, 2009.
- [42] E. Axell, G. Leus, E. Larsson, and H. Poor, "Spectrum Sensing for Cognitive Radio : State-of-the-Art and Recent Advances," *IEEE Signal Processing Magazine*, vol. 29, no. 3, pp. 101–116, May 2012.

- [43] Y. Zeng, Y.-C. Liang, A. T. Hoang, and R. Zhang, “A Review on Spectrum Sensing for Cognitive Radio: Challenges and Solutions,” *EURASIP J. Adv. Signal Process*, vol. 2010, p. 15, Jan. 2010.
- [44] A. Sonnenschein and P. M. Fishman, “Radiometric Detection of Spread-spectrum Signals in Noise of Uncertainty Power,” *IEEE Transactions on Aerospace and Electronic Systems*, vol. 28, no. 3, pp. 654–660, 1992.
- [45] S. M. Kay, *Fundamentals of Statistical Signal Processing: Detection Theory*. Prentice Hall, Upper Saddle River, NJ, USA, 1998.
- [46] Z. Ye, G. Memik, and J. Grosspietsch, “Energy Detection Using Estimated Noise Variance for Spectrum Sensing in Cognitive Radio Networks,” in *Proceedings of 2008 IEEE Wireless Communications and Networking Conference (WCNC 2008)*, (Las Vegas, NV, USA), pp. 711–716, March 2008.
- [47] H. S. Chen, W. Gao, and D. G. Daut, “Signature Based Spectrum Sensing Algorithms for IEEE 802.22 WRAN,” in *IEEE International Conference on Communications (ICC '07)*, (Glasgow, Scotland), pp. 6487–6492, June 2007.
- [48] S. Xu, Z. Zhao, and J. Shang, “Spectrum Sensing Based on Cyclostationarity,” in *IEEE Workshop on Power Electronics and Intelligent Transportation System (PEITS '08)*, (Guangzhou, China), pp. 171–174, August 2008.
- [49] W.A. Gardner, “Exploitation of Spectral Redundancy in Cyclostationary Signals,” *IEEE Signal Processing Magazine*, vol. 8, no. 2, pp. 14–36, April 1991.
- [50] W.A. Gardner, A. Napolitano, and L. Paura, “Cyclostationarity: Half a Century of Research,” *Signal Processing*, vol. 86, no. 4, pp. 639–697, April 2006.
- [51] W.A. Gardner, “Spectral Correlation of Modulated Signals Part I: Analog Modulation,” *IEEE Transactions on Communications*, vol. 35, no. 6, pp. 584–595, 1987.
- [52] W.A. Gardner, W.A. Brown III, and C.K. Chen, “Spectral Correlation of Modulated Signals Part II: Digital Modulation,” *IEEE Transactions on Communications*, vol. 35, no. 6, pp. 595–601, 1987.
- [53] Y. H. Zeng and Y.C. Liang, “Covariance Based Signal Detections for Cognitive Radio,” in *IEEE International Symposium on New Frontiers in Dynamic Spectrum Access Networks (DySPAN '07)*, (Dublin, Ireland), pp. 202–207, April 2007.

- [54] Y.H. Zeng and Y.C. Liang, "Spectrum-Sensing Algorithms for Cognitive Radio Based on Statistical Covariances," *IEEE Transactions on Vehicular Technology*, vol. 58, no. 4, pp. 1804–1815, 2009.
- [55] Y. H. Zeng and Y.C. Liang, "Eigenvalue Based Sensing Algorithms," *IEEE 802.22-06/0118r0*, p. , July 2006.
- [56] Y.H. Zeng and Y.C. Liang, "Maximum-Minimum Eigenvalue Detection for Cognitive Radio," in *The 18th International Symposium on Personal, Indoor and Mobile Radio Communications (PIMRC '07)*, (Athens, Greece), p. , September 2007.
- [57] Y. H. Zeng and Y.C. Liang, "Eigenvalue-Based Spectrum Sensing Algorithms for Cognitive Radio," *IEEE Transactions on Communications*, vol. 57, no. 6, pp. 1784–1793, 2009.
- [58] A.M. Wyglinski, M. Nekovee, and Y.T. Hou, *Cognitive Radio Communications and Networks*. Academic Press, 2010.
- [59] D. Bhargavi and C.R. Murthy, "Performance Comparison of Energy, Matched-Filter and Cyclostationarity-Based Spectrum Sensing," in *IEEE Eleventh International Workshop on Signal Processing Advances in Wireless Communications (SPAWC 2010)*, (Marrakech, Morocco), pp. 1–5, June 2010.
- [60] R. Tandra and A. Sahai, "SNR Walls for Signal Detection," *IEEE Journal of Selected Topics in Signal Processing*, vol. 2, no. 1, pp. 4–17, February 2008.
- [61] R.W. Heath Jr and G.B. Giannakis, "Exploiting Input Cyclostationarity for Blind Channel Identification in OFDM Systems," *IEEE Transactions on Signal Processing*, vol. 47, no. 3, pp. 848–856, March 1999.
- [62] H. Hsieh, H.K. Chang, and M.L. Ku, "Higher-order Statistics Based Sequential Spectrum Sensing for Cognitive Radio," in *2011 11th International Conference on ITS Telecommunications (ITST)*, pp. 696–701, Aug. 2011.
- [63] D. Cabric, A. Tkachenko, and R.W. Brodersen, "Experimental Study of Spectrum Sensing Based on Energy Detection and Network Cooperation," in *Proceedings of the first international workshop on Technology and policy for accessing spectrum*, TAPAS '06, (New York, NY, USA), ACM, 2006.
- [64] W. Jouini, "Energy Detection Limits Under Log-Normal Approximated Noise Uncertainty," *Signal Processing Letters, IEEE*, vol. 18, no. 7, pp. 423–426, July 2011.

- [65] S. Bahamou and A. Nafkha, “Noise Uncertainty Analysis of Energy Detector: Bounded and Unbounded Approximation Relationship,” in *21st European Signal Processing Conference 2013 (EUSIPCO 2013)*, (Marrakech, Morocco), Sep. 2013.
- [66] S.M. Mishra, S. Ten Brink, R. Mahadevappa, and R.W. Brodersen, “Cognitive Technology for Ultra-WideBand/WiMax Coexistence,” in *Proceedings of the 2nd IEEE International Symposium on New Frontiers in Dynamic Spectrum Access Networks (DySDAN 2007)*, (Dublin, Ireland), pp. 179–186, April 2007.
- [67] G. Fettweis, M. Lohning, D. Petrovic, M. Windisch, P. Zillmann, and W. Rave, “Dirty RF: a New Paradigm,” in *IEEE 16th International Symposium on Personal, Indoor and Mobile Radio Communications (PIMRC)*, vol. 4, (Berlin, Germany), pp. 2347–2355, Sept. 2005.
- [68] M. Valkama, A. Shahed Hagh Ghadam, L. Anttila, and M. Renfors, “Advanced Digital Signal Processing Techniques for Compensation of Nonlinear Distortion in Wideband Multicarrier Radio Receivers,” *IEEE Transactions on Microwave Theory and Techniques*, vol. 54, pp. 2356–2366, 2006.
- [69] M. Grimm, R.K. Sharma, M.A. Hein, and R.S. Thomas, “DSP-Based Mitigation of RF Front-End Non-Linearity in Cognitive Wideband Receivers,” *IEEE Transactions on Microwave Theory and Techniques*, vol. 6, no. 9-10, pp. 303–310, 2012.
- [70] Z. Quan, S. Cui, A.H. Sayed, and H.V. Poor, “Optimal Multiband Joint Detection for Spectrum Sensing in Cognitive Radio Networks,” *IEEE Transactions on Signal Processing*, vol. 57, pp. 1128–1140, Mar. 2009.
- [71] Z. Tian and G. Giannakis, “A Wavelet Approach to Wideband Spectrum Sensing for Cognitive Radios,” in *IEEE Cognitive Radio Oriented Wireless Networks and Communications (CROWNCOM’06)*, (Mykonos Island, Greece), pp. 1–5, June 2006.
- [72] B. Farhang-Boroujeny, “Filter Bank Spectrum Sensing for Cognitive Radios,” *IEEE Transactions on Signal Processing*, vol. 56, pp. 1801–1811, Apr. 2007.
- [73] Z. Tian and G. Giannakis, “Compressive Sensing for Wideband Cognitive Radios,” in *IEEE International Conference on Acoustics, Speech, and Signal Processing*, (Honolulu, HI), pp. 1357–1360, Apr. 2007.
- [74] E. G. Larsson and M. Skoglund, “Cognitive Radio in a Frequency-Planned Environment: Some Basic Limits,” *IEEE Transactions on Wireless Communications*, vol. 7, pp. 4800–4806, Dec. 2008.

- [75] A. Sahai and D. Cabric, “Spectrum Sensing: Fundamental Limits and Practical Challenges,” in *IEEE International Symposium on New Frontiers in Dynamic Spectrum Access Networks (DySPAN)*, 2005.
- [76] E. G. Larsson and G. Regnoli, “Primary System Detection for Cognitive Radio: Does Small-Scale Fading Help?,” *IEEE Communications Letters*, vol. 11, no. 10, pp. 799–801, 2007.
- [77] I. M. Johnstone, “On the Distribution of the Largest Eigenvalue in Principle Components Analysis,” *Annals Statistics*, vol. 29, no. 2, pp. 295–327, 2001.
- [78] Z. Khalaf, A. Nafkha, and J. Palicot, “Blind Spectrum Detector for Cognitive Radio using Compressed Sensing and Symmetry Property of the Second Order Cyclic Autocorrelation,” in *The 7th International ICST Conference on Cognitive Radio Oriented Wireless Networks and Communications (CROWNCOM)*, (Stockholm, Sweden), pp. 291–296, June 2012.
- [79] S. Chantaraskul and K. Moessner, “Implementation of Wavelet Analysis for Spectrum Opportunity Detection,” in *IEEE 20th International Symposium on Personal, Indoor and Mobile Radio Communications*, pp. 2310–2314, Sep. 2009.
- [80] Y.L. Polo, Y. Wang, A. Pandharipande, and G. Leus, “Compressive Wide-Band Spectrum Sensing,” in *IEEE International Conference on Acoustics, Speech and Signal Processing (ICASSP)*, pp. 2337–2340, Apr. 2009.
- [81] S. Mallat and Z. Zhang, “Matching Pursuit in a Time-Frequency Dictionary,” *IEEE Transactions on Signal Processing*, pp. 3397–3415, 1993.
- [82] G. Davis, S. Mallat, and M. Avellaneda, “Adaptive Greedy Approximations,” *Constructive Approximation*, vol. 13, no. 1, pp. 57–98, 1997.
- [83] A. Sahai, N. Hoven, and R. Tandra, “Some Fundamental Limits on Cognitive Radio,” in *The 42nd Annu. Allerton Conf. Communication, Control, and Computing*, (Monticello, IL), pp. 1662–1671, Oct. 2004.
- [84] Ettus Research: USRP N210, Ettus Research LLC, National Instruments, “USRP N210,” 2014.
- [85] GNU Radio, “<http://gnuradio.org/redmine/projects/gnuradio/wiki>,” 2014.
- [86] WAP Access Points, “<http://www.linksys.com/en-eu/products/accesspoints/WAP300N>,” 2014.
- [87] Samsung Galaxy S4, “<http://www.samsung.com/global/microsite/galaxy>,” 2014.

- [88] D. Danev, E. Axell, and E.G.D. Larsson, "Spectrum Sensing Methods for Detection of DVB-T Signals in AWGN and Fading Channels," in *Proceedings of 38th Asilomar Conference on Signals, Systems and Computers*, (Asilomar, CA, USA), pp. 772–776, November 2004.
- [89] J. Arias, L. Quintanilla, J. Segundo, L. Enríquez, J. Vicente, and J.M. Hernández-Mangas, "Parallel continuous-time $\Delta\Sigma$ ADC for OFDM UWB receivers," *IEEE Transactions on Circuits and Systems I*, vol. 56, no. 7, pp. 1478–1487, 2009.
- [90] C. Lelandais-Perrault, T. Petrescu, D. Poulton, P. Duhamel, and J. Oksman, "Wideband, bandpass, and versatile hybrid filter bank A/D conversion for software radio," *IEEE Transactions on Circuits and Systems I*, vol. 56, no. 8, pp. 1772–1782, 2009.
- [91] A. Gruget, M. Roger, V. T. Nguyen, C. Lelandais-Perrault, P. Benabes, and P. Loumeau, "Optimization of Bandpass Charge Sampling Filters in Hybrid Filter Banks Converters for Cognitive Radio Applications," in *The 20th European Conference on Circuit Theory and Design (ECCTD 2011)*, (Linpöping, Sweden), pp. 785–788, 2011.
- [92] A. Gruget, M. Roger, V. T. Nguyen, C. Lelandais-Perrault, P. Benabes, and P. Loumeau, "Wide-Band Multipath A to D Converter for Cognitive Radio Applications," in *The IEEE International Microwave Workshop Series on RF Front-Ends for Software Defined and Cognitive Radio Solutions (IMWS 2010)*, (Aveiro, Portugal), pp. 73–76, 2010.
- [93] V. Nguyen, F. Villain, and Y. Le Guillou, "Cognitive radio RF: Overview and challenges," *VLSI Design*, Feb. 2012.
- [94] M. Al-Husseini, K. Y. Kabalan, A. El-Hajj, and C. G. Christodoulou, "Reconfigurable Microstrip Antennas for Cognitive Radio," in *Advancement in Microstrip Antennas with Recent Applications* (A. Kishk, ed.), ch. 14, pp. 337–362, InTech, 2013.
- [95] Y. Li, W. Li, and Q. Ye, "A Reconfigurable Triple-Notch-Band Antenna Integrated with Defected Microstrip Structure Band-Stop Filter for Ultra-Wideband Cognitive Radio Applications," *International Journal of Antennas and Propagation*, vol. 2013, 2013.
- [96] T. Aboufoul, A. Alomainy, and C. Parini, "Reconfigured and Notched Tapered Slot UWB Antenna for Cognitive Radio Applications," *International Journal of Antennas and Propagation*, vol. 2012, 2012.

- [97] J. Perruisseau-Carrier, P. Pardo-Carrera, and P. Miskovsky, "Modeling, Design and Characterization of a Very Wideband Slot Antenna with Reconfigurable Band Rejection," *IEEE Transactions on Antennas and Propagation*, vol. 58, no. 7, pp. 2218–2226, 2010.
- [98] M. Al-Husseini, J. Costantine, C. Christodoulou, S. Barbin, A. El-Hajj, and K. Kabalan, "A Reconfigurable Frequency-notched UWB Antenna with Split-ring Resonators," in *The 2010 Asia-Pacific Microwave Conference (APMC 2010)*, (Yokohama, Japan), Dec. 2010.
- [99] C. Sim, W. Chung, and C. Lee, "Planar UWB Antenna with 5 GHz Band Rejection Switching Function at Ground Plane," *Progress In Electromagnetics Research*, vol. 106, pp. 321–333, 2010.
- [100] M. Al-Husseini, A. Ramadan, Y. Tawk, C. Christodoulou, A. El-Hajj, and K. Kabalan, "Design Based on Complementary Split-ring Resonators of an Antenna with Controllable Band Notches for UWB Cognitive Radio Applications," in *The 2011 IEEE AP-S International Symposium on Antennas and Propagation (IEEE AP-S 2011)*, (Spokane, Washington, USA), Jul. 2011.
- [101] D. Tandur and M. Moonen, "Joint Adaptive Compensation of Transmitter and Receiver IQ Imbalance Under Carrier Frequency Offset in OFDM Based Systems," *IEEE Transactions on Signal Processing*, vol. 55, no. 11, pp. 5246–5252, November 2007.
- [102] D. Petrovic, W. Rave, and G. Fettweis, "Effects of Phase Noise on OFDM Systems With and Without PLL: Characterization and Compensation," *IEEE Transactions on Communications*, vol. 55, no. 5, pp. 1607–1616, August 2007.
- [103] M. Haroun, H. Kobeissi, L. Safatly, H. Elmokdad, O. Bazzi, K. Y. Kabalan, and Y. Nasser, "Effect of RF Impairments on Spectrum Sensing Techniques," in *Wireless Telecommunications Symposium 2014 (WTS 2014)*, (Washington D.C., USA), pp. 73–76, Apr. 2014.
- [104] M.K. Lee, S.C. Lim, and K. Yang, "Blind Compensation for Phase Noise in OFDM Systems over Constant Modulus Modulation," *IEEE Transactions on Communications*, vol. 60, no. 3, pp. 620–625, 2012.
- [105] M. Matsui, T. Nakagawa, R. Kudo, K. Ishihara, and M. Mizoguchi, "Blind Frequency-Dependent IQ Imbalance Compensation Scheme using CMA for OFDM System," in *IEEE 22nd International Symposium on Personal, Indoor and Mobile Radio Communications (PIMRC)*, (Washington D.C., USA), pp. 1386–1390, 2011.

- [106] B. Razavi, "Design Considerations for Direct-Conversion Receivers," *IEEE Transactions on Circuits Systems II, Analog Digital Signal Processing*, vol. 62, pp. 428–435, Jun 1997.
- [107] B. Razavi, "Cognitive Radio Design Challenges and Techniques," *IEEE Journal on Solid-State Circuits*, vol. 45, p. 15421553, Aug 2010.
- [108] M. Grimm, M. Allen, J. Marttila, M. Valkama, and R. Thoma, "Joint Mitigation of Nonlinear RF and Baseband Distortions in Wideband Direct-Conversion Receivers," *IEEE Transactions on Microwave Theory and Techniques*, vol. 62, pp. 166–182, Jan 2014.
- [109] Z. Khalaf, A. Nafkha, J. alicot, and M. Ghozzi, "Hybrid Spectrum Sensing Architecture for Cognitive Radio Equipment," in *Telecommunications (AICT), 2010 Sixth Advanced International Conference on*, pp. 46–51, IEEE, 2010.
- [110] J. Lee and C.K. Un, "Performance Analysis of Frequency-Domain Block LMS Adaptive Digital Filters," *Circuits and Systems, IEEE Transactions on*, vol. 36, pp. 173–189, Feb 1989.
- [111] A.O. Ogunfunmi and A. Peterson, "On the Implementation of the Frequency-Domain LMS Adaptive Filter," *Circuits and Systems II: Analog and Digital Signal Processing, IEEE Transactions on*, vol. 39, pp. 318–322, May 1992.
- [112] J. Shynk, "Frequency-Domain and Multirate Adaptive Filtering," *Signal Processing Magazine, IEEE*, vol. 9, pp. 14–37, Jan 1992.